AD-A283 260

REPORT DOCUMENTATION PAGE

Form Approved
OMB No. 0704-0188

1. AGENCY USE ONLY (Leave blank)	2. REPORT DATE	3. REPORT TYPE AND DATES COVERED

4. TITLE AND SUBTITLE
Nowcasting convective storm evolution in East-Central Florida Using Satellite And Doppler Radar Data

5. FUNDING NUMBERS

6. AUTHOR(S)
Marvin H. Treu

7. PERFORMING ORGANIZATION NAME(S) AND ADDRESS(ES)
Colorado State University

8. PERFORMING ORGANIZATION REPORT NUMBER
94-109

9. SPONSORING/MONITORING AGENCY NAME(S) AND ADDRESS(ES)
DEPARTMENT OF THE AIR FORCE
AFIT/CI
2950 P STREET
WRIGHT-PATTERSON AFB OH 45433-7765

10. SPONSORING/MONITORING AGENCY REPORT NUMBER

11. SUPPLEMENTARY NOTES

12a. DISTRIBUTION/AVAILABILITY STATEMENT
Approved for Public Release IAW 190-1
Distribution Unlimited
MICHEAL M. BRICKER, SMSgt, USAF
Cheif Administration

12b. DISTRIBUTION CODE

13. ABSTRACT (Maximum 200 words)

14. SUBJECT TERMS

15. NUMBER OF PAGES
143

16. PRICE CODE

17. SECURITY CLASSIFICATION OF REPORT	18. SECURITY CLASSIFICATION OF THIS PAGE	19. SECURITY CLASSIFICATION OF ABSTRACT	20. LIMITATION OF ABSTRACT

NSN 7540-01-280-5500

Standard Form 298 (Rev. 2-89)

94-109

THESIS

NOWCASTING CONVECTIVE STORM EVOLUTION IN EAST-CENTRAL FLORIDA USING SATELLITE AND DOPPLER RADAR DATA

Submitted by

Marvin H. Treu

Department of Atmospheric Science

In partial fulfillment of the requirements
for the Degree of Master of Science
Colorado State University
Fort Collins, Colorado
Summer 1994

COLORADO STATE UNIVERSITY

May 10, 1994

WE HEREBY RECOMMEND THAT THE THESIS PREPARED UNDER OUR SUPERVISION BY MARVIN H. TREU ENTITLED NOWCASTING CONVECTIVE STORM EVOLUTION IN EAST-CENTRAL FLORIDA USING SATELLITE AND DOPPLER RADAR DATA BE ACCEPTED AS FULFILLING IN PART REQUIREMENTS FOR THE DEGREE OF MASTER OF SCIENCE.

Committee on Graduate Work

_____

_____

_____

_____
Adviser

_____
Department Head

ABSTRACT OF THESIS

NOWCASTING CONVECTIVE STORM EVOLUTION IN EAST-CENTRAL FLORIDA USING SATELLITE AND DOPPLER RADAR DATA

The relationship between infrared cloud top temperatures from the Geostationary Operational Environmental Satellite's (GOES) Visible and Infrared Spin Scan Radiometer (VISSR) and radar reflectivity returns from NCAR's CP-4 C-band Doppler radar is examined for nine thunderstorm cells over east central Florida. The cell data are from three case study days during the summer 1991 Convective and Precipitation/ Electrification (CaPE) Experiment. Rapid scan satellite data available during the selected case study days provide a high frequency of image times (Δ t = 5-15 min.) for better temporal resolution in the data comparisons.

A method was developed to graphically combine GOES visible and infrared images with universal format Doppler radar reflectivity and velocity scans for display on a PC workstation. Previous studies by others, my personal forecasting experience, and the present study illustrate a need to combine meteorological data sources in order to improve operational nowcasting capabilities.

The analyses showed that development of most cells as viewed via cloud top temperature (CTT) area, are found to lag the corresponding defined radar echo area from 5-30 minutes. This is an important finding for local area nowcasting. Similarly, the maximum time averaged rate-of-change of radar echo area precedes the time averaged rate-of-change of CTT area growth. Cloud top temperature changes being a better

indicator of convective storm dissipation. The results are specific to thunderstorm development in the summer subtropical humid climate of east-central Florida.

The combined satellite/radar product, utilizing the strengths of each source, is noted to be beneficial to forecasters for improving nowcasting skills.

Marvin H. Treu
Department of Atmospheric Science
Colorado State University
Fort Collins, CO 80523
Summer 1994

ACKNOWLEDGEMENTS

Without the guidance and advice from so many helpful people, the experience of writing a thesis and earning a Master's Degree would not have been nearly as enjoyable or rewarding. From the very beginning of my work Mr. Patrick Dills and Mr. David Brunkow (CHILL radar software engineer) provided a great deal of assistance, helping me understand and rewrite essential FORTRAN code. Mr. Kenneth Eis and Dr. David Randel taught me the power of the PC. Their donation of time and help not only saved me from many hours of directionless pursuits, but also helped me to produce better quality graphs and figures to properly display my results. I also owe thanks to Ken Eis for taking the time to review my first draft and make many insightful comments and suggestions.

My advisor, Professor Thomas H. Vonder Haar, gave me the freedom and encouragement to pursue this topic of personal interest. I am grateful to Dr. Vonder Haar and my committee members: Professors Richard Johnson and V.N. Bringi, and Dr. James F.W. Purdom for their comments and suggestions for improving this thesis.

I owe thanks to many CIRA personel. Kelly Dean, Nan McClurg, Debra Molenar, Dale Reinke, and Kevin Schrab were especially helpful. They allowed me to interrupt them countless times with questions or to request assistance when problems arose. Loretta Wilson has been extremely patient and helpful in assembling the thesis text and figures.

I am grateful to Steve Williams (NCAR/OFPS) and Bob Rilling (NCAR/RDP) for providing me with the necessary data. I also owe thanks to Dennis Buechler from Marshall Space Flight Center for sending me a program which got me started with this project. Thanks to Capt. Dean Hazen and Capt. Patrick Barrett for providing me with the 45th Weather Squadron information and statistics.

Nothing I've ever accomplished in life would have been possible without the support of a strong, loving family. I am therefore thankful to my parents, brothers, and sister. I am especially thankful to my father for his professional guidance and advice.

And finally, I am most thankful to my wife, Kristi, for her support, encouragement, and patience to put up with me and my long hours of work during the first four months of our marriage.

This research was supported by the United States Air Force, Air Force Institute of Technology. Additional support of computer facilities, photo processing and thesis preparation was provided by the Cooperative Institute for Research in the Atmosphere at Colorado State University through its cooperative agreement with the National Oceanic and Atmospheric Administration under contract NA37RJ0202.

TABLE OF CONTENTS

LIST OF TABLES

LIST OF FIGURES

Chapter 1

INTRODUCTION

Since 1975 the National Center for Atmospheric Research (NCAR) has operated portable Doppler radars in research field programs (Wilson et al., 1980) including: SESAME, CINDE, and CaPE. These experiments have revealed the value of Doppler radar data to the forecaster by allowing them to monitor boundary-layer convergence lines evident in the reflectivity and Doppler velocity displays.

During the summers of 1989 and 1990 NCAR issued and collected data on nowcasts of thunderstorm initiation, evolution, and movement for a region in northeast Colorado. These forecasts were based primarily on Doppler radar observations (Wilson and Mueller, 1993). Wilson and Mueller (1993) found forecasters had even more difficulty nowcasting the evolution of storms than determining the when and where of convective initiation. Some of the reasons given include a deficiency in knowledge of the details of storm initiation and evolution, a need for more detailed boundary-layer and cumulus cloud observations, and the manually intensive nature of the forecaster duties.

Satellite research has previously addressed these same concerns. In order to better understand convective development, the National Earth Satellite Service (NESS) investigated the dynamics and thermodynamics of arc clouds using research aircraft and GOES rapid scan imagery. Based upon this data, a life cycle of arc cloud lines has been developed (Purdom and Sinclair, 1988). To satisfy the need for more detailed boundary-

layer and cumulus cloud observations, GOES rapid scan imagery was found to provide observations of convective behavior at temporal and spatial resolutions compatible with the scale of the physical mechanisms responsible for triggering deep and intense convective storms (Sinclair and Purdom, 1982). Addressing the problem of manually intensive forecaster duties, through digitally compositing satellite and radar data Reynolds and Smith (1979) offered a method by which a forecaster could reduce the amount of information needed to be assimilated.

Both present and past research using satellite and radar data have produced positive results in the nowcasting of convective storms. One of the many areas of study of the Cooperative Institute of Research in the Atmosphere (CIRA) at Colorado State University is to combine satellite data with other data sets in order to gain a better understanding of mesoscale atmospheric processes (Purdom and Parker, 1982).

1.1 Nowcasting: Current Status

Nowcasting is defined as a detailed description of the current weather along with forecasts obtained by extrapolation up to two hours ahead (Browning, 1982). Improving the quality of these very short-range forecasts remains a challenge today even with advances in technology. This is due to a variety of factors including sparse data for the area of coverage and not enough processing capability of the data available in the time required to make a nowcast. Traditional forecasts are based on widely spaced observational data which yield general forecasts. Numerical weather prediction models have helped forecasts extending out a day or more, but do not do provide much assistance

for forecasts on the mesoscale up to 12 hours ahead due to the poor resolution of data on this scale (Browning and Collier, 1990) (Figure 1).

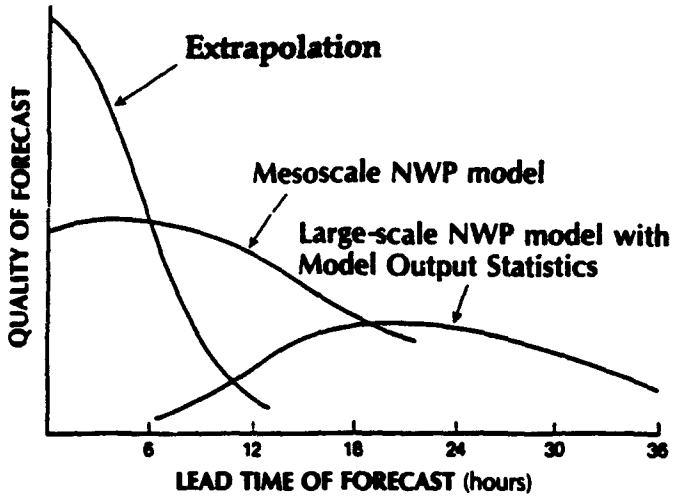

Figure 1. Schematic diagram illustrating forecast quality as a function of lead time for three different forecasting methods. (from Browning and Collier 1990).

Nowcasting and the very short-range forecasting of mesoscale weather is one of the most challenging problems in meteorology today. The reason for this is that the mesoscale is ill-defined and poorly understood (Purdom, 1982). To improve operational capabilities, empirical information must be incorporated into new procedures for nowcasting. What is required is immediate display capability for current data (satellite, radar, surface observations, etc.) and derived products in a readily comprehensible form for use by operational meteorologists (Purdom, 1982).

This is the mission of NOAA's Prototype Regional Observing and Forecasting Service Program (PROFS) in Boulder, Colorado. A PROFS interactive workstation such as the Denver Advanced Weather Interactive Processing System (AWIPS) Risk

Reduction and Requirements Evaluation (DARRRE) collects, combines, and displays real-time data in a format readily available and understandable to a forecaster. An NCAR nowcasting experiment in the Denver area during the 1989 and 1990 summers successfully used the DARRRE workstation to assist forecasters in preparing nowcasts (Wilson and Mueller, 1993). The available data and displays in this system are shown in Figure 2.

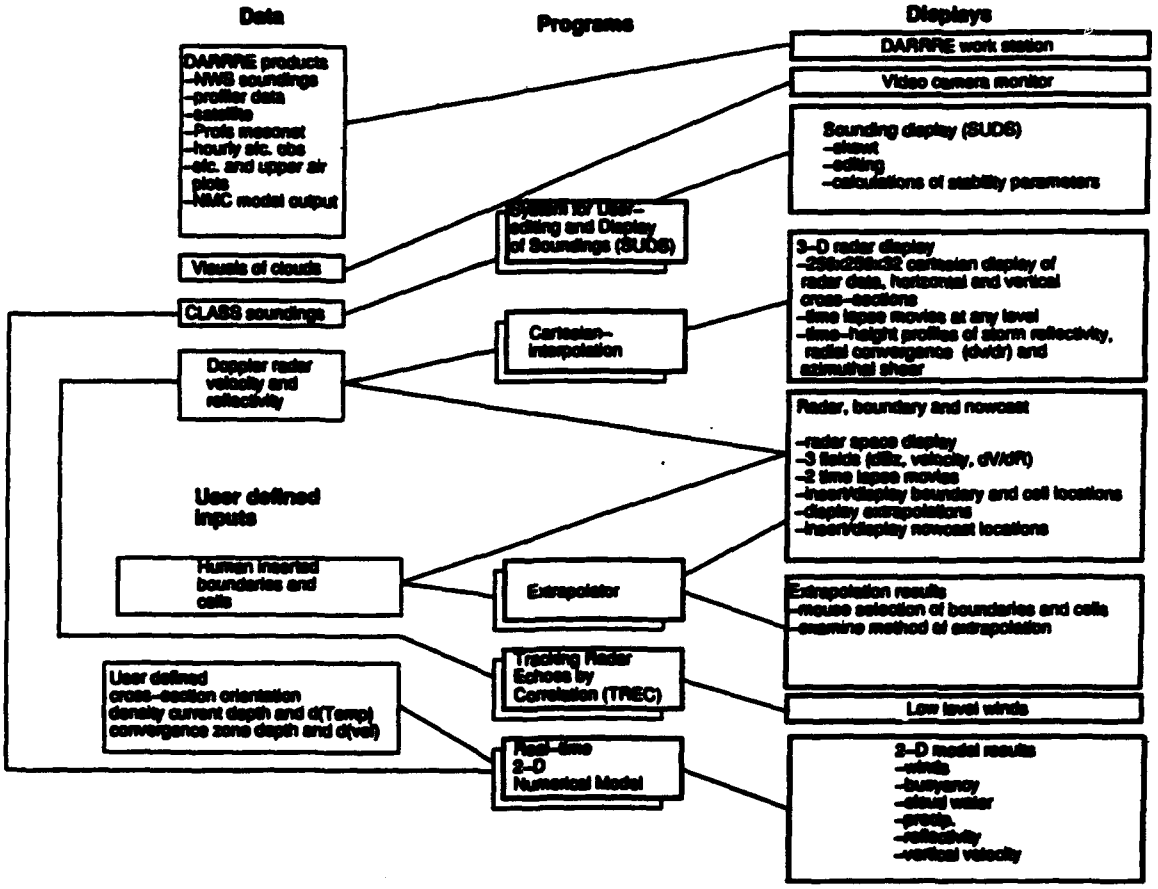

Figure 2. Diagram of the multiple data sources and their integration into various displays available during the NCAR 1989/1990 nowcast experiments (from Wilson and Mueller, 1993).

Another example of a forecaster weather data display system is the Forecast Systems Laboratory's (NOAA Research Laboratory, Boulder, CO) Local Analysis and Prediction System (LAPS). The purpose of LAPS is to provide the weather service with help to cope with large data sets and meet a goal of improved forecast services in the 0 to 6 hour time period (McGinley et al., 1992). This system collects data from a variety of sources including GOES and TIROS satellites, Doppler radar, wind profilers, surface mesonet data, and aircraft reports (Figure 3). LAPS objectively analyzes this data on a high-resolution (10 km), three-dimensional grid, and produces products which include quantitative gridded fields of meteorological quantities. Following a 1989 warm season convective precipitation experiment using LAPS, McGinley et al. (1992) concluded that if the weather services are to benefit fully from the advanced data sets to be operational by the mid-1990s, local assimilation and analysis systems must be available concurrently.

The importance of nowcasting along with the improvement in the automation of derived data sets is a conceptual need shared by most operational meteorologists. The most significant weather affecting human activity has time scales on the order of one to six hours (McGinley et al., 1992), therefore there is a need for operational short-range forecasts or nowcasts for areally limited domains. The NWS and USAF Air Weather Service (AWS) are embarking on plans to significantly upgrade services within this range. The goal is to rapidly update and display unprecedented amounts of data on systems such as the NWS' AWIPS (Advanced Weather Information Processing System) and the AWS' AWDS (Automated Weather Distribution System).

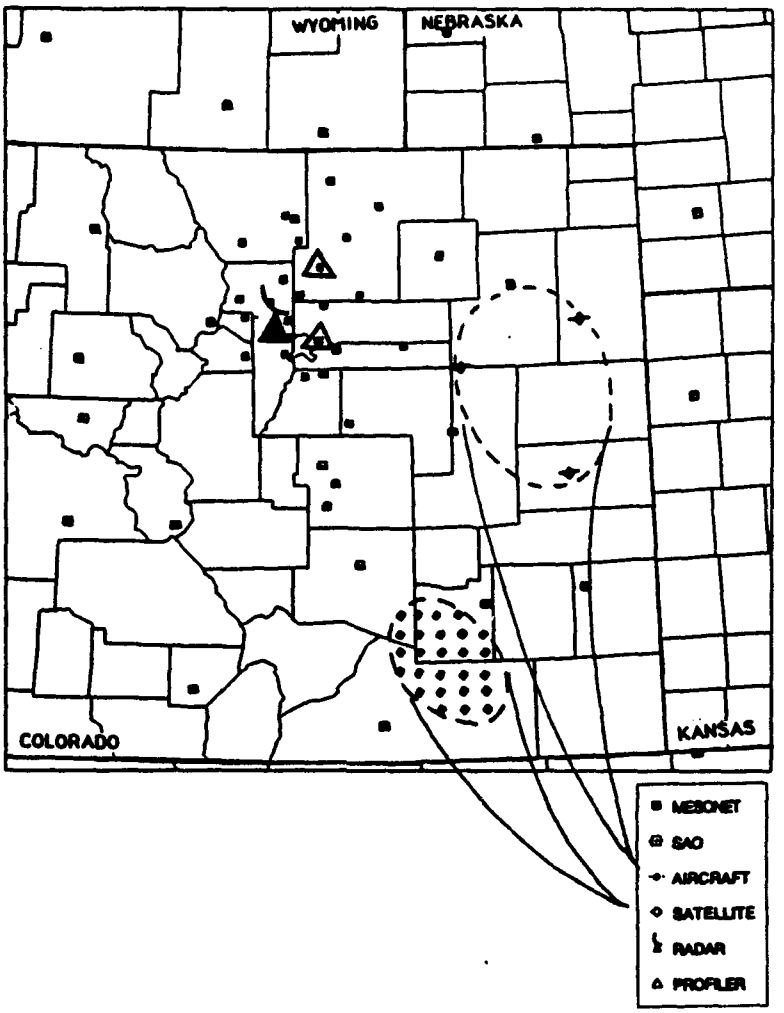

Figure 3. LAPS data available in northeastern Colorado. Inset shows typical data densities extended over the domain for aircraft and GOES satellite data during an average 90 minute period (from McGinley et al., 1992).

1.1.1 Nowcasting Challenge of the U.S. Air Force's 45th Weather Squadron

The mission challenges of the U.S. Air Force's 45th Weather Squadron (Patrick Air Force Base, Florida) illustrates the importance of nowcasting and the need for capability improvement. The 45th Weather Squadron provides weather forecasting support for the nation's Eastern Launch Range. The Range consists of Cape Canaveral

Air Force Station (CCAFS), Kennedy Space Center (KSC), Patrick Air Force Base (PAFB) and other downrange sites and support locations (JDMTA, and Antigua Air Station). The areas of primary responsibility, however, are Cape Canaveral AFS and KSC. The 45th provides Range users with weather forecasts to support space vehicle launch operations as well as day-to-day ground processing operations. The goal is to provide timely and accurate forecasts to these users in order to protect Range assets both human and material) from potentially destructive weather. This goal is to be achieved while simultaneously maintaining a low false alarm rate, preventing an unnecessary shutdown of the Range — costing Range users more money.

The cost of human injury or loss of life due to poor forecasts is clearly unacceptable. The cost of scrubs or delays in pre-launch processing or during launch countdowns is perhaps less obvious and difficult to quantify. Weather-sensitive ground operations such as transporting and erecting launch vehicles and their payloads, fueling operations, performance tests, or moving or stacking solid rocket boosters occur on a daily basis, around the clock. Weather warnings and advisories curtail and restrict processing which directly impact launch schedules and subsequently increase budget requirements (Madura et al., 1992).

The customer at the Titan Integrate, Transfer and Launch (ITL) area near Complex 40/41 (Figure 4) have assessed the cost of downtime due to a specific weather advisory. The most commonly issued weather advisory which disrupts the tasks of the Range users (and specifically the ITL area) is one which forecasts the occurrence of lightning within 5 nm of an operations area. In 1990, this advisory was issued for the ITL

area 98 times, accounting for a total of 380 work force hours lost (Wicklund and Youngren, 1993). Martin Marietta, the primary Titan contractor, estimates the cost of manpower in this area to be $57,000/day (Wyatt and Kintigh, 1989). At this rate, 380 hours lost translates to 1 million/year in manpower losses alone. This figure increases after factoring in time spent evacuating and re-manning launch pads and platforms before and after the advisory period and considering the time loss due to reinitiating interrupted procedural tests.

Excessive costs can also be accrued by launch programs when launch countdowns are impacted by adverse weather or by violations of one or more of the strict weather launch constraint rules (Appendix A). Scrubbing a launch after entering the countdown can also be costly. At worst, catastrophic damage could occur to the launch vehicle and payload if exposed to unexpected high winds, lightning, or precipitation while in the final stages of a launch countdown (at which time the vehicle is not shielded by its protective gantry). At best, there are wasted costs of manpower and configuring the Range for support of the launch attempt. The Atlas booster program estimates this cost to be at least 1/4 million dollars (Weems, 1994). A scrub after entering the terminal count costs the Shuttle program even more: over 1/2 million dollars if the vehicle has already been through the tanking procedure (Weems, 1994). Although weather is not the primary cause for aborted launch attempts, it certainly has a major impact on both Expendable Launch Vehicles (ELVs) and the Shuttle program (Tables 1 and 2).

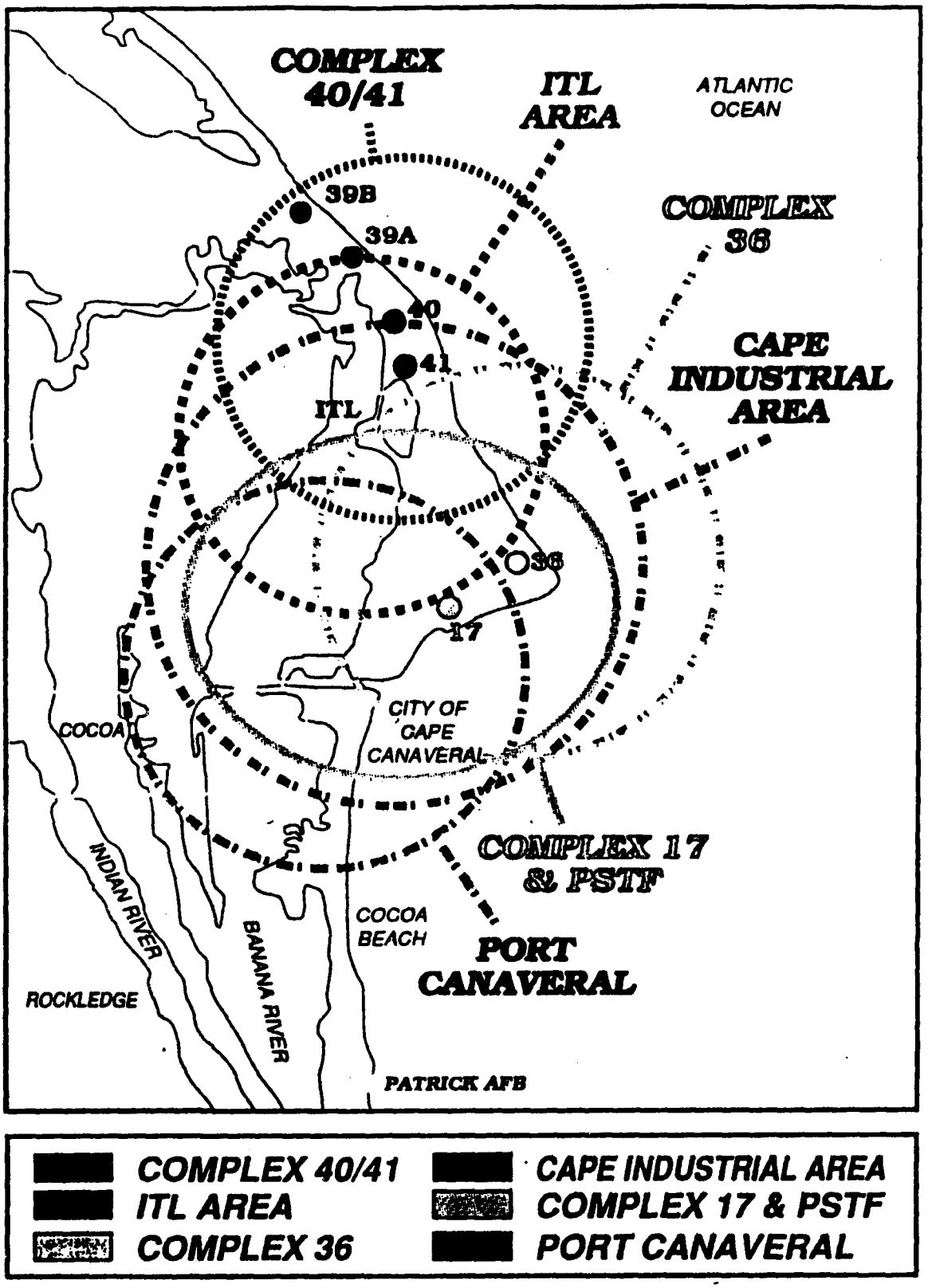

Figure 4. Map of Cape Canaveral AFS launch complexes (courtesy of USAF/45th Weather Squadron).

WEATHER IMPACT STATS

ELVs 1987-94; STS 1981-86 AND 1988-94

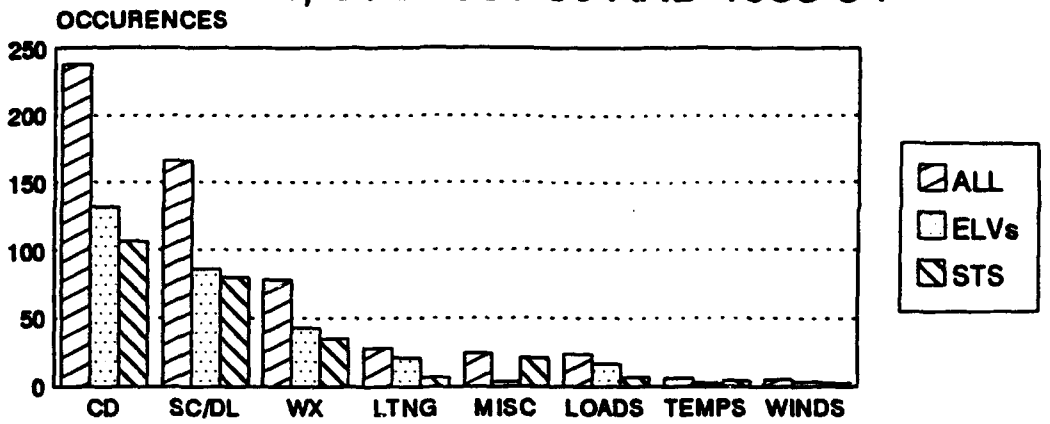

	CD	SC/DL	WX	LTNG	MISC	LOADS	TEMPS	WINDS
ALL	238	166	78	28	24	23	6	5
ELVs	132	86	43	21	3	16	2	3
STS	106	80	35	7	21	7	4	2

CD - COUNTDOWNS; SC/DL - SCRUBS/DELAYS; WX - WX SCRUBS/DELAYS; STS MISC - RTLS/TAL/RANGE

Table 1: Weather Impact Statistics - Total Countdowns, Nov 87 - Mar 94. Weather affects (scrubs/delays) approximately 1 in 3 countdowns (courtesy of USAF/45th Weather Squadron).

WEATHER IMPACT STATS

ELVs 1987-94; STS 1981-86 AND 1988-94

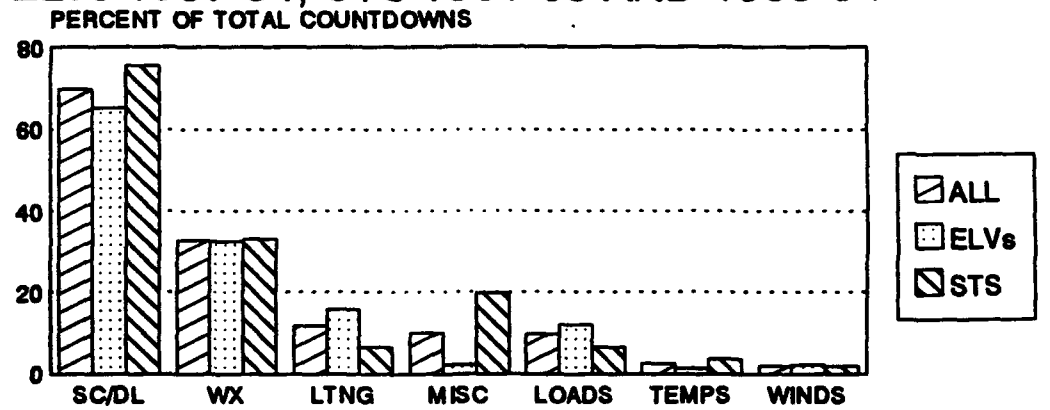

	SC/DL	WX	LTNG	MISC	LOADS	TEMPS	WINDS
ALL	69.7	32.8	11.8	10.1	9.7	2.5	2.1
ELVs	65.2	32.6	15.9	2.3	12.1	1.5	2.3
STS	75.5	33	6.6	19.8	6.6	3.8	1.9

ELV - 132; STS - 106 COUNTDOWNS; STS MISC - RTLS/TAL/RANGE

Table 2: Weather Impact Statistics - Scrub/Delay Percentage, Nov 87 - Mar 94. Weather accounts for nearly half of all launch scrubs/delays (courtesy of USAF/45th Weather Squadron).

Specific to the Shuttle program are the landing and ferry flight operations. By completing a mission by landing the orbiter at Kennedy Space Center, Florida rather than Edwards AFB, CA, NASA saves 1 million dollars in costs by avoiding at least five days of additional vehicle processing by "ferrying" it across the country atop a Boeing 747. In addition to the shorter Shuttle Landing Facility (SLF) runway at KSC, NASA is hesitant to use KSC as the primary landing site due to the dynamic, hard-to-forecast weather conditions of central Florida. The shuttle requires a 90-minute forecast to support the time it takes to descend from its orbit to the selected landing site.

Launch operations at the Eastern Range are impacted daily by the forces of weather. The 45th Weather Squadron is responsible to provide forecasting services to a multitude of customers, each with different needs or requirements. Inaccurate forecasts are capable of causing Range managers/directors to make decisions costing a launch program hundreds of thousands or millions of dollars. Improvement of nowcasting capabilities is needed and strongly desired.

1.1.2 45th Weather Sqdn. Forecaster Performance and Proposed Improvements

Forecasters at the Cape Canaveral Forecast Facility (CCFF) are challenged with a difficult mission. Although they are tasked with supporting a relatively small region, the requirements demand high-resolution weather support coverage over the primary areas of CCAFS and KSC. Within the CCAFS and KSC locations, forecasts are tailored for each launch complex or area. For example, CCAFS alone has six specific regions in which to advise of the threat/occurrence of lightning within 5 nm (Figure 4). Similarly, KSC is

subdivided into four different advisory areas (Appendix B). Appendix C lists all the separate forecast criteria for the 45th Weather Squadron's areas of responsibility. The more specific the forecast, the less likely Range operations in a given area will be shut down needlessly due to a false alarm. These more stringent requirements, however, are quickly outdistancing the capabilities of the forecaster.

In 1992 Madura, et al. (1992) reported forecasters issued warnings and advisories at a 40% false-alarm rate while 10% are issued with zero lead time. False alarms degrade productivity and waste valuable budget dollars, while issuing with zero lead time endangers lives and billion dollar assets (Madura et al., 1992). Current statistics reveal little improvement during 1993 and early 1994. Desired lead times on warnings (Figure 5) and advisories (Figure 6) remain below standard for most months, while false alarm rates continue to be wastefully high (Figures 5 and 6).

The challenge to improve forecasting performance requires an increase in data density (especially in the boundary layer to resolve the many small-scale features which drive CCAFS and KSC weather) and improvements in data assimilation (including expert systems and mesoscale models) to help the forecaster digest the sometimes overwhelming amount of critical data needed to meet stringent space program requirements (Madura et al., 1992).

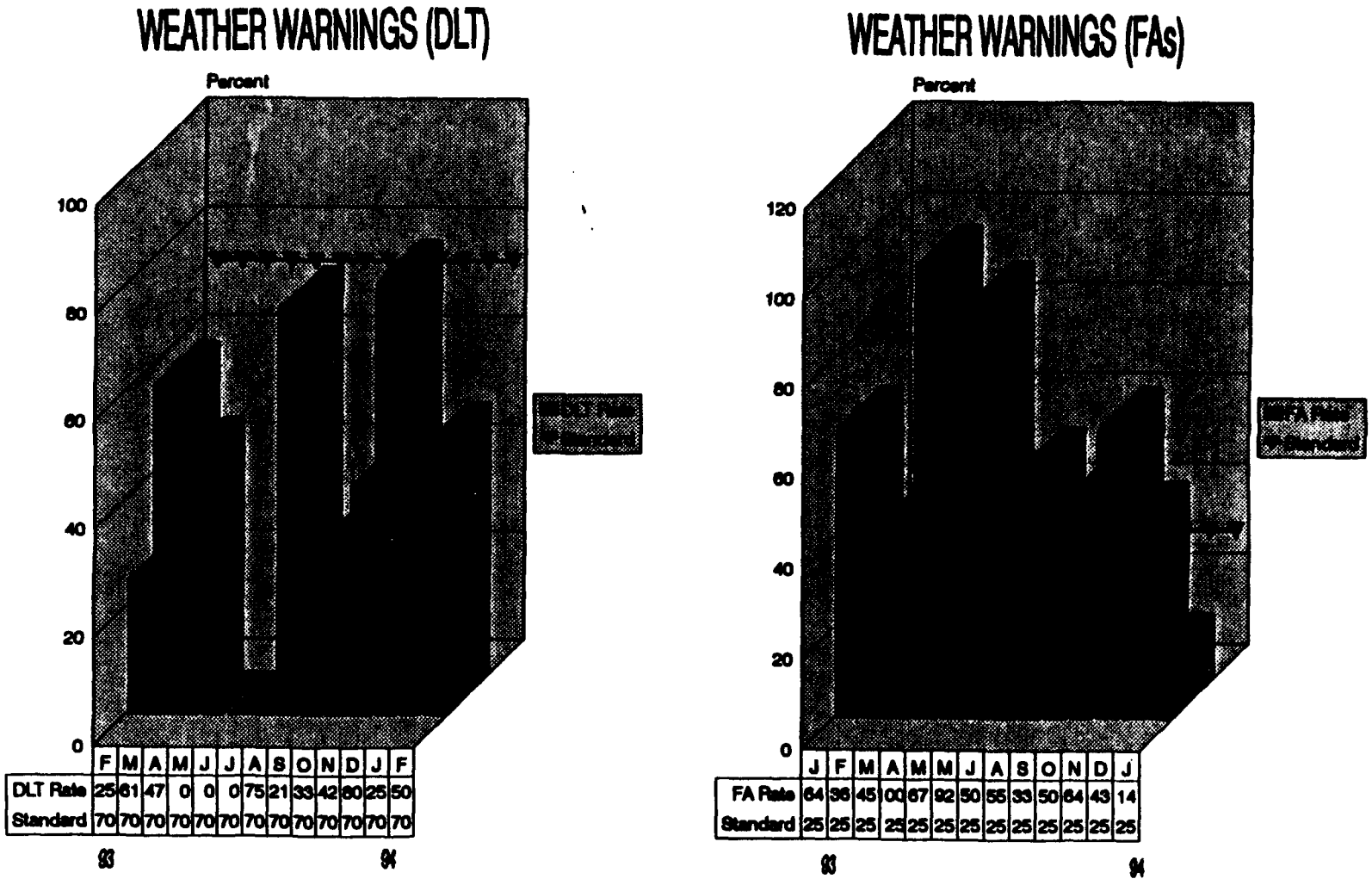

Figure 5. 45th Weather Squadron Weather Warning desired lead times and false alarm rates. The May-July 93 DLT rates of 0% indicate no weather warnings issued (courtesy of USAF/45th Weather Squadron).

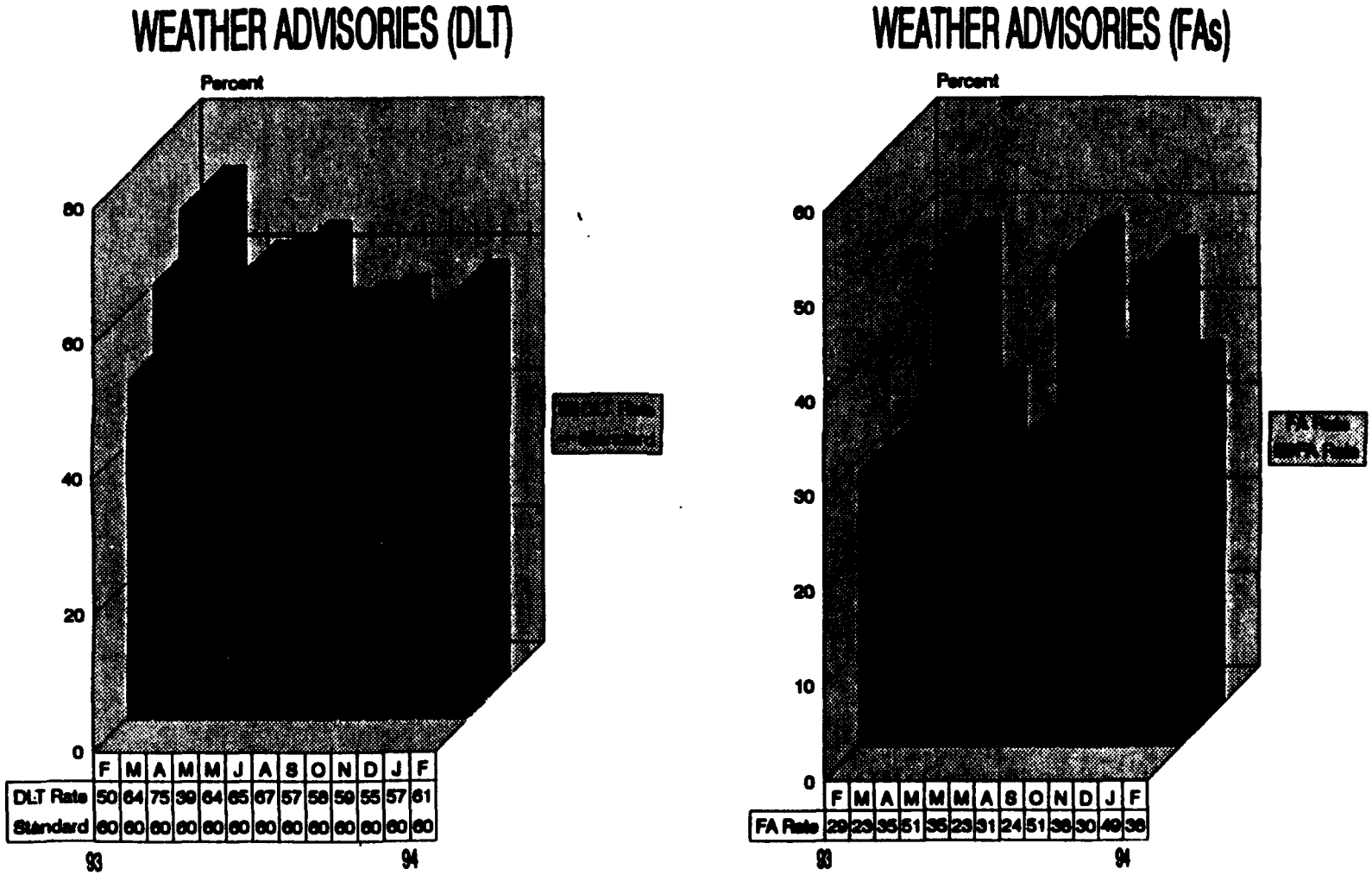

Figure 6. 45th Weather Squadron Weather Advisory desired lead times and false alarm rates (courtesy of USAF/45th Weather Squadron).

1.2 Background Information

Many studies using GOES data or Doppler radar data exist for investigating convective storm evolution. Few, however, deal with combining these data sources even though researchers and operational meteorologists acknowledge the value of such a product.

1.2.1 Personal Experience

As an Air Force Launch Weather Officer (LWO) at the Cape Canaveral Air Force Station, I supported space launch operations on a daily basis. The job of the LWO is to provide weather support for sensitive operational testing, processing and launch of all Kennedy Space Center/Eastern Range Shuttle, Titan, Atlas-Centaur, and Delta launch vehicles, in addition to Trident and Poseidon ballistic missiles. The LWO is also responsible for researching meteorological requirements for ground preparations and launch operations.

The most challenging aspect of the job is attempting to forecast the rapidly changing, convective Florida weather. Although the Cape Canaveral Forecast Facility is equipped with a wide array of instrumentation (Appendix D), the task of assimilating the information still resides in the hands of the forecaster.

Observing various forecasting methods of the fellow LWOs and forecasters (both experienced and inexperienced), I recognized a common trait. Each individual tends to rely on, or strongly favor one primary tool to develop their nowcast. Some will depend almost exclusively on radar (McGill volumetric scans or Doppler), some satellite, and

others will even attempt to discount observational data, faithfully trusting model output to support a nowcast decision. This pattern is even more evident when there is convection imminent or approaching and time is unavailable for methodical consideration of a variety of data sources.

The most successful forecasters realize there is valuable information in all data sources, however they have the ability to discriminate between them and quickly filter out the nonessential information. They realize the day-to-day differences in the initial conditions and utilize the data sources accordingly. The better forecaster also has a good understanding of the strengths and weaknesses of the data sources. Most forecasters are trained on what a sensor/information source can do, but are frequently ill-informed on its limitations or weaknesses.

Even the most educated, experienced, capable forecaster has a limit to the amount of information they can mentally assimilate in order to make a forecast. Advances made by adding instrumentation and upgrading equipment will be of limited benefit unless methods of combining data from a variety of sources into useful products are developed and provided to the forecaster in a routine, timely manner.

1.2.2 Use of Satellite Data for Nowcasting

The geostationary satellite is valuable to nowcasting because it has the unique ability to provide frequent, uniformly calibrated observations of the atmosphere and its cloud cover from a single sensor over a broad range of scales (Purdom, 1982). Visible

and infrared imagery reveal synoptic-scale patterns down to single cell storms of the mesoscale where nowcasting interest is concentrated.

A key to short-range forecasting is understanding the mechanisms which lead to convection and the evolution of storms. Geostationary satellite loops assist in this understanding by representing the integrated effect of ongoing dynamic and thermodynamic processes in the atmosphere (Purdom, 1982). GOES imagery provides a forecaster with routine observations of features often unobserved with a conventional surface observation network. Smith and Purdom (1993) describe a method to improve data resolution in the Surface Airways Observation Network (SAO) by using geostationary satellite data in regions of strong surface gradients. In these regions, severe storm triggering mechanisms such as outflow boundaries and dry lines are often misanalyzed with the insufficient information provided by the surface network (Smith and Purdom, 1993).

Many mesoscale phenomena associated with thunderstorm initiation and development are easily identified in GOES imagery (Purdom, 1982). Even benign features such as fog and stratus viewed from satellite can provide clues to the time and location of future convection. Purdom (1982) also presents the use of GOES in aiding surface temperature analysis, cloud and rainshower development forecasts, and identifying convective initiation features. Features with potential for triggering strong convection are generally organized convergence lines including: fronts, pre-frontal squall lines, gust fronts (outflow boundaries), and sea/lake breezes. All of these mechanisms can be found in satellite imagery prior to development of deep convection and before

detection by radar (Purdom, 1976). Monitoring outflow boundaries and sea breeze fronts are important because of the frequency at which they generate convection or interact to generate convection, especially in the late afternoon hours (Figure 7).

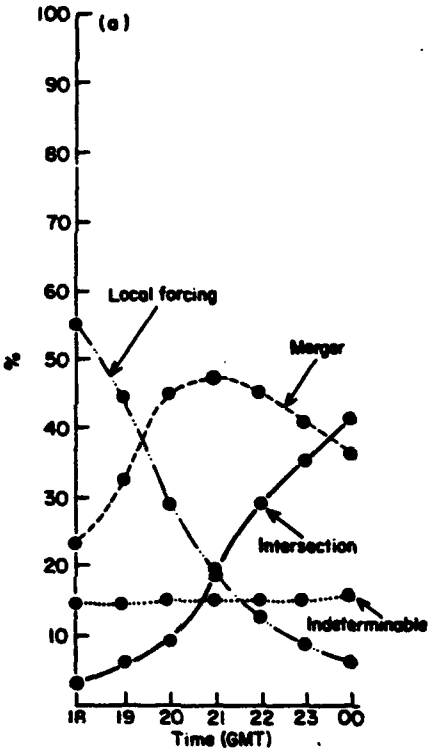

Figure 7. Distribution of convective generation mechanisms for all storms with tops colder than -20 C versus time for a sample of over 9850 storms during the summer of 1979 over the southeast U.S. (from Purdom, 1982).

Using a conceptual model of Convective Scale Interaction (CSI), Purdom and Sinclair (1990) explain the development and evolution of deep convection along arc cloud lines observed with GOES imagery. The potential of a gust front to initiate new convection depends on the parent storm (strength, stage of growth) and the stability of the environment where it is advancing (Purdom and Sinclair, 1990). With atmospheric sounding data in the area and time of interest, the amount of vertical motion required to

overcome the negative buoyancy in the boundary layer to initiate convective growth can be estimated (Figure 8) (Purdom and Sinclair, 1990). GOES/VAS soundings are preferred for this application as opposed to rawinsonde data, because it provides near instantaneous observations through a column in the atmosphere with moderate vertical resolution and high spatial resolution (hourly intervals) all from a uniformly calibrated sensor (Purdom, 1986).

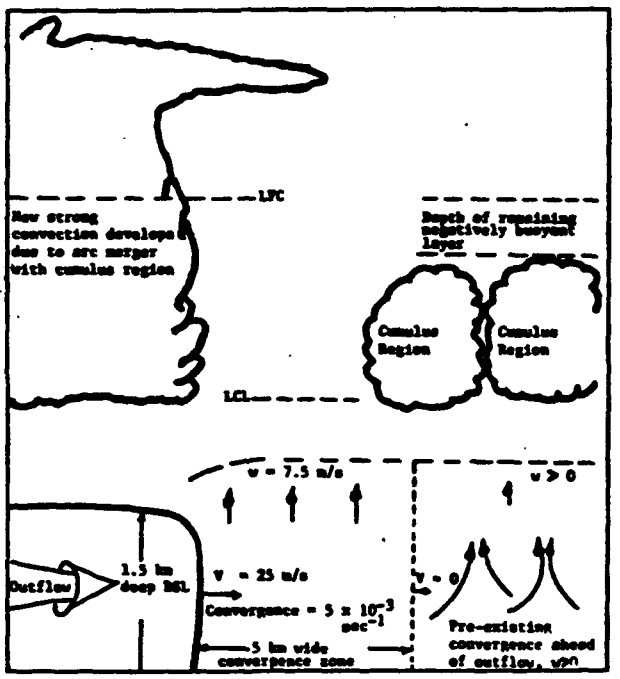

Figure 8. Schematic showing an arc cloud line approaching a cumulus region where some remaining negative buoyancy prevents deep convective development. The vertical motion generated in the convergence zone ahead of the arc cloud line's DSL may provide the additional forcing required to initiate convection (from Purdom and Sinclair, 1990).

Although GOES infrared images have poorer resolution than the visible, they are still useful in forecasting mesoscale weather. Adler and Fenn (1979) used GOES/IR data to study thunderstorm vertical growth rates and cloud top structure to try to find a correlation with the occurrence of severe weather on the ground. They found areal

expansion of cold cloud top areas, delineated by blackbody temperature isotherms to be useful in monitoring growth rates. Tornadoes were found to take place during, or just after, rapid expansion of the satellite-observed thunderstorm top (Figure 9). Furthermore, expansion rate and minimum cloud top temperature parameters reach a critical level soon enough to provide a potential 30-minute lead-time for issuing a weather warning (Adler and Fenn, 1979).

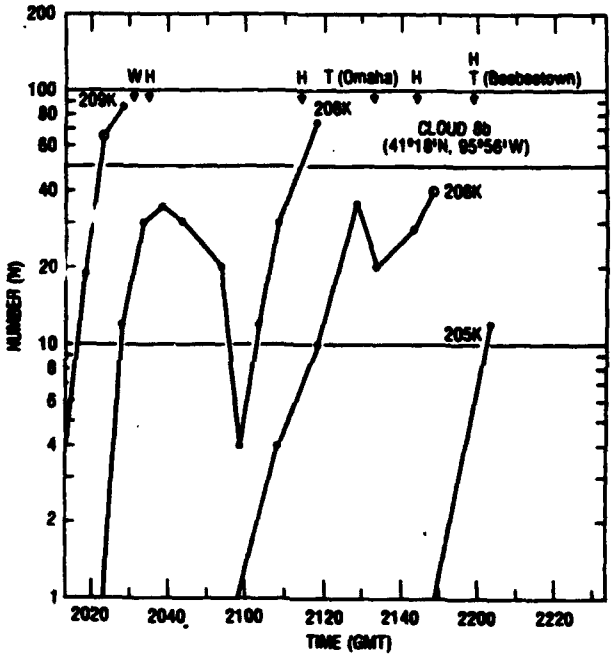

Figure 9. Thunderstorm growth rate diagram where N represents the number of data points in the defined element with blackbody temperature ≥ the labeled threshold temperature. The letter placement indicates the time of occurrence of high winds(W), hail(H) and tornado(T). (From Adler and Fenn, 1979).

1.2.3 Use of Radar Data for Nowcasting

The benefits of Doppler radar to the forecaster are related to its ability to remotely measure air velocities both within storms and in the optically clear boundary-layer

(Wilson and Wilk, 1982). This data can be displayed in a velocity-azimuth display (VAD), a time/height profile of radial wind speeds, to help a forecaster understand current atmospheric events. Three-dimensional fields of air motion can be obtained from using radial velocity data from two or more radars.

The success of Doppler radar in observing and forecasting severe storms comes from the ability to detect strong velocity gradients (Wilson and Wilk, 1982). Cyclonic signatures, gust fronts, downbursts, wind shear, and turbulence can all be either interpreted on the display or detected by WSR-88D system algorithms .

Wind shifts, frequently seen across a frontal boundary or dry line are clearly identifiable on the Doppler velocity display. This allows precise location and close monitoring of movement even in surface data (SAO) sparse regions (Wilson and Wilk, 1982).

Clear air measurements on Doppler radar come from two sources. The first category is from radar returns of insects, seeds, dust, or chaff. The second source is the result of refractive-index gradients (Rinehart, 1991). Radar measurements in clear air allow a forecaster to observe boundary layer convergence lines undetected by other conventional data sources. These lines are observable on the reflectivity display as thin lines of enhanced reflectivity between 0 and 20 dBZ_e (Wilson and Schreiber, 1986). On the velocity display, convergence appears as a line of strong radial gradients in velocity. These lines are important because most thunderstorm nowcasts involve the monitoring of boundary layer convergence zones (Wilson and Mueller, 1993). In a study of over 650 convective storms during an eastern Colorado summer, Wilson and Schreiber (1986)

found near 80% of the storms within radar range initiated close to radar-observed boundary layer convergence lines (Figure 10).

According to Wilson and Schreiber (1986), improvements in nowcasting convective storms are attainable if Doppler radar is used to detect and monitor convergence boundaries, high-resolution satellite images used to monitor cloud growth, and atmospheric soundings used to determine convective potential.

The major limitations of Doppler radar are: 1) a convergence line is not apparent in the Doppler velocity field when the convergence is oriented along a radial (Wilson and Schreiber, 1986); 2) being a fixed, ground-based instrument with limited range, multiple radars are required for adequate coverage of large areas; and 3) echo target features are often obscured by terrain or by intense activity close to the radar source (attenuation).

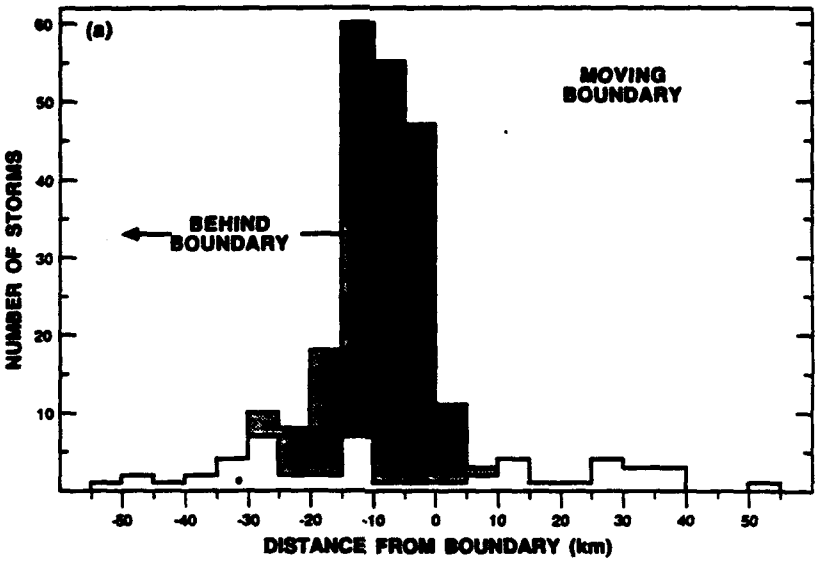

Figure 10. Frequency of storm initiation location relative to moving boundaries. Shows storms are likely to form between 0 and 20 km behind a moving boundary. Shading represents subjectively classified boundary initiated storms. (From Wilson and Schreiber, 1986).

1.2.4 Combined Satellite/Radar Products Used to Study Convective Development

Reynolds and Smith (1979) developed a technique to digitally composite satellite and radar imagery in a common coordinate reference frame. The goal was to demonstrate this composited imagery could increase the understanding of convective development, severe storm development, precipitation mechanisms, and the organization of mesoscale features in relationship to the synoptic scale.

Radar data was acquired in 1-degree elevation PPI scans from 5-cm field radars (WSR-75) associated with the High Plains Cooperative Program (HIPLEX). GOES satellite data was acquired in half-hour intervals for the first case study and in three minute intervals for the second case during a rapid scan period. The satellite data was remapped into a polar stereographic radar projection prior to data integration. GOES visible, infrared, and SWR-75 radar scans were then superimposed. Threshold values were selected to cutoff the lower albedos and higher temperatures in the satellite data and each data source was displayed in a separate color. Therefore, a region with data from all sources appears white, a mix of all three enhancement colors. These regions are considered convectively active and were compared with successive time images to observe changes.

The data from Reynolds and Smith's first case study was compared with a high density rain gauge network to relate satellite signatures to rainfall. Although this topic is a bit of a digression from the study of convective development, the data collected over the network provides information about the relationship between the temporal change of mean albedo, mean and lowest cloud top temperature, and the area encompassed by the

20 dBZ reflectivity contour in a growing thunderstorm complex (Figure 11). The findings from this case include (Reynolds and Smith, 1979):

1) Development of cold cloud tops in the IR data tends to lag echo development.

2) In low wind shear conditions, rainfall occurs underneath the coldest cloud tops.

3) Average area of coldest cloud tops between the half-hour images relates well to the area over which rainfall occurs.

4) Rate of change of cloud top temperature can imply increasing or decreasing rainfall intensities.

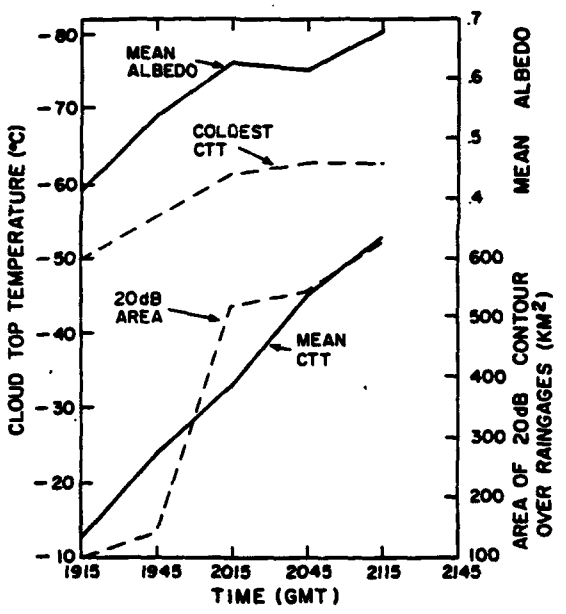

Figure 11. Time rate-of-change of satellite-measured albedo, mean cloud top temperature, and temperature of coldest cloud top, along with area enclosed within the 20 dBZ radar contour for the period of study, 25 May 1976 (Reynolds and Smith, 1979).

The second case study (using rapid scan satellite data) indicated large variations in storm structure can occur between the routine 30-minute satellite scans. This observation emphasizes the importance and need for rapid-scan imagery (Reynolds and Smith, 1979).

Reynolds and Smith concluded that use of this compositing technique could have a dramatic impact on forecast decision making by ultimately providing a more precise definition of satellite parameters which correspond to severe storm events.

A comparison study of satellite infrared data and radar echoes for thunderstorms in the midwest U.S. by Negri and Adler (1981) revealed relationships between these data sources and thunderstorm evolution and intensity. Figure 12 shows how cell evolution was monitored by CTT area changes and radar echo area changes with time. This storm rapidly intensified at approximately 2300 GMT, shown by the expansion of the CTT defined anvil edge and radar echo area and reflectivity increase. The minimum cloud top temperature slightly precedes the maximum radar reflectivity (Figure 12).

In addition to showing a correlation between maximum radar reflectivity and satellite-based estimates of thunderstorm intensity, Negri and Adler (1981) concluded that inferences of thunderstorm updraft intensity can be made from satellite derived quantities such as dT_{BB}/dt and T_{MIN}. High time-resolution data was noted to be essential to accurately define and follow individual storms unambiguously and to accurately measure the rate of change parameters on a time scale appropriate for thunderstorms (Negri and Adler, 1981).

Purdom et al. (1982) studied tornadic thunderstorms by combining NCAR CP-3 Doppler radar reflectivity data converted to constant altitude plan position indicator (CAPPI) scans along with three-minute interval GOES-East VIS and IR data. Since both sources of data provide independent measurements concerning thunderstorms and the

environment, the goal of the study was to use these data sources together to better diagnose severe storms.

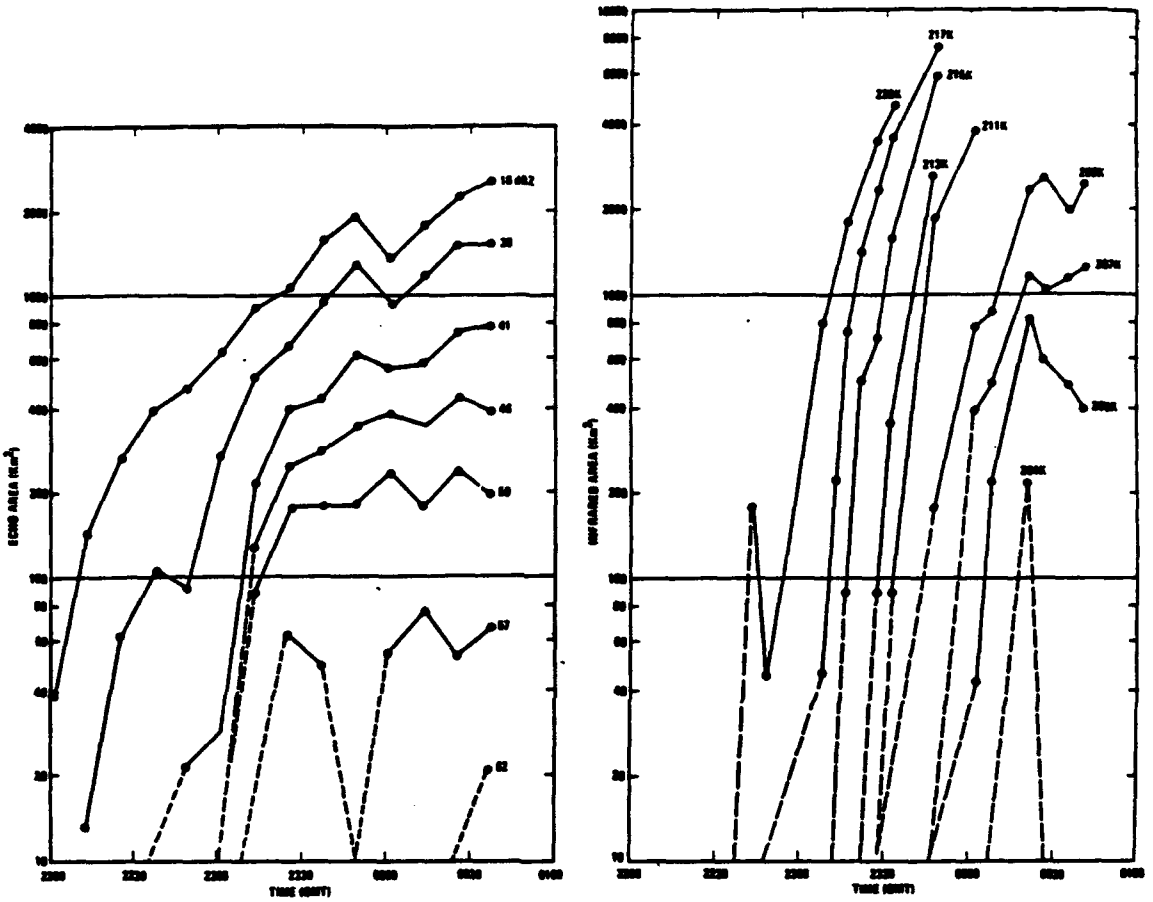

a) b)

Figure 12. a) Echo area (km^2) of selected dBZ thresholds versus time (GMT) and b) infrared area (km^2) of coldest T_{BB} isotherms versus time (GMT) for a western U.S. thunderstorm cell (from Negri and Adler, 1981).

The cases studied by Purdom et al. (1982) were the May 2, 1979 Oklahoma Lahoma and Orienta tornadic thunderstorms. The GOES-East IR data was remapped into a Lambert conformal conic projection and overlaid on selcted CAPPI levels of reflectivity data. Several observations are made concerning convective storm structure and evolution.

The well documented horseshoe-shaped ridge of cold temperatures (Fujita, 1982) is observed in the IR data of the storms. Warmer temperatures are observed inside this ridge, at times masking the temperature information of a developing storm downstream. This cirrus masking effect makes cloud top growth measurements less accurate. The use of high frequency satellite imagery is therefore required to follow the evolution of such a developing storm. When using an integrated satellite/radar product, the CAPPI displays help insure the correct IR anvil area is matched with the correct echo (Purdom et al., 1982).

Also observed was that the coldest cloud top temperatures do not necessarily overlie the low level core of highest radar reflectivity. This is perhaps indicative of a bounded weak echo region and therefore application of this observation could aid in determining the severity of storms.

Combination of the pixel values comprising the separate radar and satellite images while graphically maintaining IR temperature gradient information was accomplished by Green and Parker (1983). The coldest IR brightness temperatures and strongest CAPPI radar reflectivity echoes were compared in image loops which traced the evolution of these features with time. Features on the CAPPI images at all levels were compared with tornado damage locations on the ground.

Green and Parker's integrated product was produced by scaling, parallax-shifting and remapping the satellite data into a Lambert-Conformal projection to match the radar projection. Threshold reflectivity levels were selected on the CAPPI scans (25 and 50 dBZ) and a pixel-by-pixel comparison was made with the IR satellite image. For each

radar pixel meeting the threshold requirements, a constant value (different for each threshold range) is subtracted from the corresponding IR pixel value. The result is a product with three distinct ranges of pixel values in the cloud top area. Modification of the color table produces the combined product image with the two thresholded radar areas displayed in a different color, without sacrificing the GOES cloud top temperature information.

Results from this study once again showed the problem of cirrus masking causing ambiguity in cloud top temperatures of downstream towers (the May 2, 1979 Oklahoma tornadic storm case was used again). The echoes on the low and mid-level CAPPIs were not collocated with the IR cold cloud top centers, indicating a highly sheared environment. The new analysis in this study showed the 1 KM CAPPI's hook echo positions were identical to the tornado damage assessment positions. Wind shear had displaced the upper level echoes so they did not display hook echoes overlaying the tornado damage routes (Green and Parker, 1983).

The major advantage of Green and Parker's satellite/radar composite was determined to be the ability to clearly trace the storm's upper signature even when an upstream storm's cirrus obscures its location on satellite imagery.

1.3 Satellite/Radar Product - Benefits and Problems

Although the benefits of combining satellite and radar data into a single product are numerous, so too are the problems which arise from such a venture. The first challenge comes from trying to combine data from two different sources which provide

independent measurements of thunderstorm growth. Satellite data provides information on cloud top mean vertical growth rates, cloud top temperature and anvil expansion rates. Radar provides reflectivity and velocity information, and volumetric echo properties and their changes in time (Purdom et al., 1982). To combine satellite and radar images in a quantitative way on a pixel-by-pixel basis would involve defining a new variable describing, for example, the resulting value of combining information on reflectivity and cloud top temperature. Being difficult to accomplish this in a meaningful way, data combination efforts have focused instead on methods of graphically displaying the two independent data sources in the same spatial and temporal scales.

Parallax error is always a concern when attempting to combine satellite data with another source. Parallax error is the change in apparent position of a nearby object compared with more remote reference objects when the nearer object is viewed from two different points in space. Parallax is introduced in satellite data when viewing a point on the earth or in the atmosphere from a non-overhead position. The farther the target cumulus cloud is from the satellite subpoint and the higher it develops, the more horizontally displaced (radially away) the target will be viewed when trying to reference it to a ground point (Figure 13). If cloud top temperatures are being investigated, the correction for parallax involves simply shifting the image to its proper reference point above the earth's surface. In doing this, however, data gaps occur in the space above the area on earth behind the target unseen by the satellite sensor.

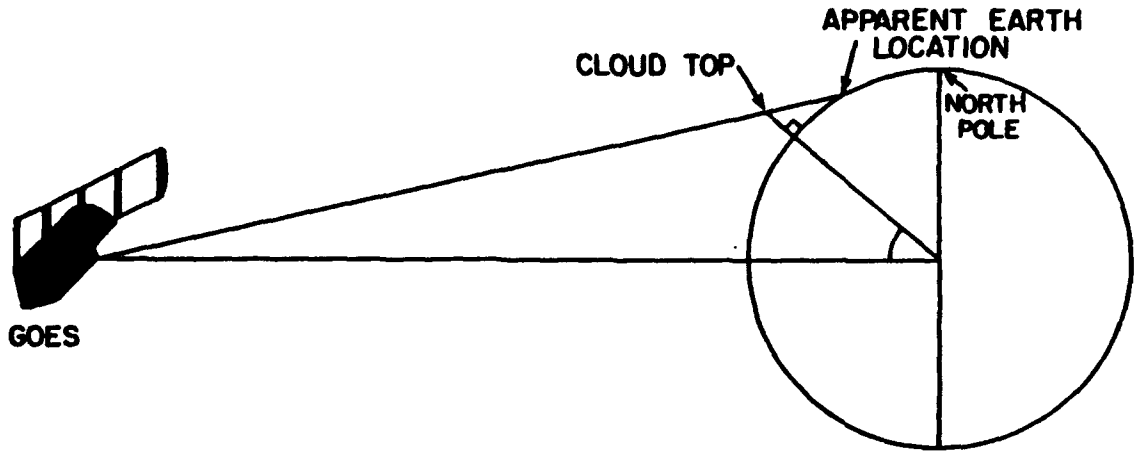

Figure 13. Exaggerated view of apparent displacement of a cloud positioned a finite distance above the earth's surface (Reynolds and Vonder Haar, 1978).

Navigation error on the satellite image can create difficulties when combining it with a radar scan. *Misalignment of the images* by just one pixel can create substantial errors when analyzing the combined data sources.

Without synchronization of radar and satellite data start times, perfect matching of radar data scans to a loop of satellite images is difficult, if not impossible. Simply matching the satellite image time with the radar scan time does not produce a time synchronized product. Since it takes 18.21 minutes for the GOES spin scan radiometer to complete a full disk image, the time it takes for the radiometer to "view" the area of interest must be determined before matching the satellite image to the radar scan. When observing a rapidly evolving mesoscale environment (convective storms, approaching gust front, etc.) significant change can occur in just a few minutes. Combining other data

sources with the satellite image in such instances without considering scan time could lead to large errors.

Different resolutions in the data sources can also pose a problem. Doppler radar can provide (depending on the gate spacing and distance from the radar) pixel resolutions as small as .25 km, whereas the GOES infrared data produces a pixel resolution of approximately 8 km. Therefore subtle, small scale changes in the radar echoes won't be reflected in the lower resolution IR data.

Constant Altitude Plan Position Indicator (CAPPI) scans are more desirable than the use of standard PPI scans. Although the PPI scan is displayed as if it is a flat horizontal surface, it really represents data along a "tilted," or conical surface (Figure 14). Due to the elevation angle of the radar beam, echoes detected at a greater distance from the radar are actually a higher height above the ground than echoes closer to the antenna. The effect is most apparent for small cells moving toward the radar, where the cell will actually "disappear" during low elevation scans when it passes directly overhead.

A major problem to be considered in developing a combined satellite/radar product for operational use is the time consuming nature of processing the data. In order to solve all the previously mentioned problems in the creation of the viable product, a large amount of computer and human time is involved. With the increasing power and speed of computers and increasing automation, however, the time required should eventually be reduced along with a reduction in the amount of necessary human interaction.

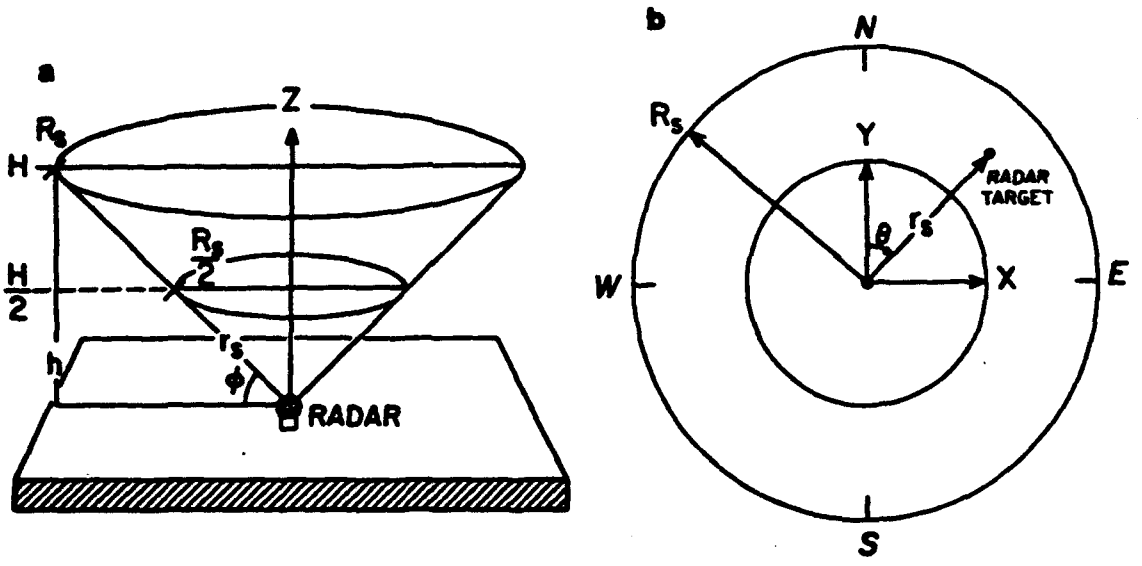

Figure 14. Doppler radar viewing configuration: a) Radar scans about the vertical axis, Z, at a fixed elevation angle, ϕ; b) Resulting PPI scan representation where R_s is the slant range (a) of the edge of the display corresponding to height H above the ground (Brown and Wood, 1987).

The benefits of an integrated satellite/radar product, some of which have already been described in the past research studies, are all useful to an operational forecaster. By combining two different data sources into one product in the same projection, the amount of data assimilation required by the forecaster is greatly reduced. It allows the forecaster to focus his/her attention on the most active areas, rather than spending time attempting to mentally merge the data. This becomes critical for the forecaster when they are simultaneously attempting to issue weather advisories and monitor the convective development.

Since both satellite and radar provide information pertaining to thunderstorm growth, a display combining the two, alerts a forecaster to the most rapidly developing

areas (Reynolds and Smith, 1979). For example, the overlapping regions of coldest cloud tops and highest radar reflectivity would be most closely monitored by the forecaster.

The mesoscale information provided by the radar scans can be used with the much broader areal view of the satellite to tie the larger-scale synoptic features to the smaller scale mesocale features (Reynolds and Smith, 1979). For example, more inferences on development observed on satellite outside of radar range can be made if similar development is seen within the range of the radar.

A composite product may better detect severe weather occurrences if, through research, numerical thresholds indicative of severe weather are determined. The studies by Purdom et al. (1982) and Green and Parker (1983) both addressed the topic of severe weather detection. Green and Parker described the benefits of detecting tornadic activity by using IR satellite data in conjunction with low level radar scans. Purdom et al. (1982) found the product beneficial because the radar scans help the forecaster follow the evolution of cold cloud top temperatures when this data is masked by cirrus from upstream.

The process of convective-scale interaction is fundamental to the evolution and maintenance of deep convection (Purdom and Sinclair, 1988). Satellite, and more recently, radar (Wilson and Carbone, 1984) are used to monitor convective-scale interactions. Used together, Doppler velocity data can detect convergence boundaries even before the development of cumulus cloud fields, while GOES visible imagery can monitor convective development both inside and outside of radar range. Radar, being

limited in range, cannot detect distant outflow boundaries or sea breeze fronts. For example, in Florida the west coast sea breeze frequently propagates across the peninsula during an afternoon. An observant forecaster using satellite imagery could track such a feature and predict its interaction with a cumulus cloud field well before it makes an appearance on the radar display.

Finally, a combined satellite/radar display using IR cloud top temperatures and radar reflectivity data would provide a means to study the relationship between changes in radar echoes along with corresponding changes at the top of the storms. The results from which could make valuable contributions to the study of convective storm evolution. Graphic representation of these changes would be useful to the operational forecaster by displaying the most active, intensifying regions of a storm - both within the storm and at cloud top.

1.4 Research Objectives

Before accurate and precise local forecasting becomes a reality, an improvement in our understanding of convective storm genesis and development is required (Purdom, 1986). One method of attempting to gain this improved understanding is through the intelligent combination of meteorological data sources. Past applications of multi-sensor composite images have enhanced the knowledge of convective development (Reynolds and Smith, 1979). In the operational environment of launch weather forecasting, data assimilation is required to help the forecaster digest the sometimes overwhelming amount of critical data they need to meet stringent space program requirements (Madura et al.,

1992). The benefits of improving in the quality and accuracy of forecasts translates to monetary savings and more dependable protection of resources and human life. The meteorological research community has an active interest in data assimilation as well. NOAA's RAMM Branch at the Cooperative Institute for Research in the Atmosphere have proposed plans to study convective development and evolution using combined 5-minute rapid scan satellite data and Doppler radar data from the 1991 CaPE (Convection and Precipitation/Electrification) experiment (Purdom and Vonder Haar, 1992).

With this in mind, the research objective of this study is to develop a means to correlate and display GOES visible and infrared images with Doppler reflectivity and velocity data in a meaningful, graphic format. From these sources, a combined satellite/radar product display will be selected to investigate several cases of convective storms.

Quantitative measurements will be made using the combined product display to detect possible patterns, trends, or relationships in the satellite/radar data. Such information could be valuable to forecasters attempting to nowcast convective storm evolution.

Chapter 2

DATA AND PRODUCT DEVELOPMENT

2.1 Convection and Precipitation/Electrification (CaPE) Experiment

The greatest advances made in trying to solve the problem of predicting thunderstorm development have been derived from the analysis of data collected during major field experiments (Purdom and Vonder Haar, 1992). The most recent investigation of this type was the CaPE experiment, which took place in east-central Florida from 8 July - 18 August 1991. CaPE was a multi-agency field program sponsored by the National Science Foundation (NSF), Federal Aviation Administration (FAA), National Aeronautics and Space Administration (NASA), National Oceanic and Atmospheric Administration (NOAA), and the United States Air Force (USAF). Of the five stated objectives of the CaPE experiment, theme four pertains most closely to the goal of this thesis: Improving techniques for performing short-period forecasts (nowcasts < 2 hr) of convection initiation, downbursts, and tornadoes (Foote, 1991). East Central Florida was selected as the site of the experiment for a variety of reasons. First of all, the central Florida area is the nation's leader in annual number of thunderstorm days (Court and Griffiths, 1986). This fact, along with the regular appearance of the sea breeze front on the coast, provided assurance for plenty of opportunities to study convection and its initiation in the boundary layer. Secondly, the mesonets and other additional instrumentation could be of use to the Cape Canaveral Forecast Facility and Kennedy

Space Center in support of launch operations. The already existing instrumentation could likewise be helpful to the CaPE experiment. Finally, the close proximity of Air Force and National Weather Service meteorologists made it possible to support a cooperative nowcasting experiment (Foote, 1991).

As an Air Force Launch Weather Officer, I had the opportunity to participate in the nowcasting experiment (entitled: CaPOW). One of the CaPOW objectives was to produce 30-minute nowcasts of the initiation and evolution of convective cells via prediction of the low altitude locations of 40 dBZ reflectivity contours (Foote, 1991). Valuable training and experience was gained from using the CP-4 Doppler radar in conjunction with other data sources (GOES imagery on the Air Force MIDDS, CLASS soundings, PAM mesonet data) in order to produce nowcasts.

2.2 Geostationary Operational Environmental Satellite (GOES)

Geostationary satellites, unlike polar orbiters, provide visible and infrared earth images on a high frequency basis. With updated scans disseminated in near-real-time, at least every 30 minutes, a forecaster is able to observe the motion and rate-of-change of weather systems (Kidder and Vonder Haar, 1992). GOES is maintained at an earth synchronous altitude 35,800 km above the earth's surface. It is spin-stabilized with its spin axis parallel to the earth's axis and orbits in the earth's equatorial plane, remaining stationary at a desired longitude. An attitude control subsystem controls proper earth imaging by maintaining the spin axis alignment and spin rate of approximately 100 rpm. There are normally two GOES in operation (GOES-East at 75°W and GOES-West at

135°W), however presently only one is operational (GOES-Prime located at 98°W in the summer and 108°W in the winter) (Figure 15).

Figure 15. Drawing of GOES-7

The GOES consists of three major subsystems: Space Environment Monitor (SEM); Telemetry, Tracking, and Command (TTC); and the meteorological instrument. The meteorological instrument in GOES-7 is the Visible and Infrared Spin Scan Radiometer (VISSR) Atmospheric Sounder, or VAS. In operational imaging mode, the VISSR scans the earth and gathers data in the reflected visible and thermal infrared portions of the electromagnetic spectrum. In sounding mode, VAS has atmospheric temperature sounding capability, which is used to calculate atmospheric temperature profiles.

The satellite operates with spun and despun portions. The despun portion contains antennas for communications with earth, while the VAS resides in the spun portion, with its instruments sensing the earth only 5% of the time (Kidder and Vonder Haar, 1992). West-to-east scan lines are formed by rotating around the axis of the spinning spacecraft. Radiation from the earth enters the VAS optical reflecting telescope at right angles to its optical axis via the optically flat scan mirror (Clark, 1983). At geostationary altitude, the earth subtends only 17.4°, therefore the scan mirror only needs to scan ± 10° from the sub-satellite point to view the entire hemisphere (Kidder and Vonder Haar, 1992). To complete a full disk (hemispheric) image takes 18.21 minutes (1821 required satellite rotations at a rate of 100 rpm). The VAS starts a new image at 30-minute intervals, using the remaining 10 plus minutes for weather fax transmission or ranging. When in rapid interval scan operations (RISOP) mode, the scan mirror limits the size of the north-south sector viewed providing for up to 12 visible or IR images per hour.

The visible channels are sensitive to the visible spectrum (0.55 to 0.75 μm) which is the sunlight reflected from the earth and clouds. Cloud formations are sensed therefore only during the daylight hours. The resolution of the GOES visible images are 0.9 km at the satellite subpoint. The IR channels sense the emitted radiation in the atmospheric window from the earth and clouds in the 10 to 12.5 μm range. The resolution of the GOES infrared images are 6.9 km at the subpoint.

2.2.1 Use of GOES During CaPE

Most of the archived satellite data during the CaPE experiment was from the GOES-7 satellite. The satellite was being moved during the experiment, so the subpoint varied from 100.4°W longitude on 8 July to 98.1°W longitude on 18 August. The subpoint locations during the case study days of 24, 25, and 26 July 91 were as follows (Williams et al., 1992):

Table 3: GOES-7 Subpoint Locations

Date	Time (UTC)	Latitude	Longitude
24 July 91	1200	00:00:30°S	098:45:03°W
25 July 91	1200	00:00:31°S	098:43:42°W
26 July 91	1200	00:00:32°S	098:42:05°W

High frequency images were available, as the CaPE Operations Director had the authority to select 10 days to put the satellite into rapid scan mode. Data during the rapid scan periods from three of these days were selected for case studies.

2.3 Doppler Radar

Doppler radars provide three basic measurements in the atmosphere:

1) reflectivity: a measure of the intensity of scatterers present in the atmosphere.
2) velocity: using the Doppler frequency shift relationship, the radial component of scatterer motion can be determined.

3) spectrum width: measuring the width of the spectrum of frequencies detected, the turbulence within the sampling volume can be determined (Rinehart, 1991).

Pulse Doppler radars transmit a series of pulses separated in space by a controlled time interval. Some of this transmitted energy is re-radiated back to the radar by scatterers in the atmosphere or on the ground. Doppler radars detect the power of the received signal or the velocity of moving targets. The maximum range of a radar is computed by the time it takes for the emitted pulse to be received back at the radar.

The radar antenna directionally focuses the radar's signal. This is in contrast to an isotropic source, which radiates energy equally in all directions. The gain of the radar antenna is defined as the ratio of the power that is received at a specific point in space (at the point in the beam where maximum power exists, p_1) to the power which would be received at the same point from an isotropic source (p_2). Gain is measured in terms of decibels (dB), the logarithm of a unitless ratio of powers:

$$G = 10 \log\left[\frac{p_1}{p_2}\right]$$

The radar equation states that the power received by the radar due to distributed targets intercepting its beam is proportional to the radar reflectivity factor and inversely proportional to the square of its range. The reflectivity factor is defined as the summation of the diameters of the particle reflectors (raindrops) to the sixth power per unit sample volume:

$$z = \Sigma D^6$$

This definition is valid for Rayleigh scatterers, or for spheres that are small compared to the wavelength of the incident radar beam. The units of the reflectivity factor are: mm^6/m^3, which results in a large range of values with a small change of scatterer diameter. A logarithmic parameter is therefore used instead of the reflectivity factor (z):

$$Z = 10 \log \left[\frac{z}{1\ mm^6/m^3} \right]$$

The logarithmic reflectivity factor value, Z, is given in terms of decibels relative to a reflectivity of 1 mm^6/m^3, or dBZ. For example, values of reflectivity range from -30 dBZ for fog particles, while hail could return values as high as 75 dBZ (Rinehart, 1991).

Correlations can be made between radar reflectivity returns (Z) and rain rate (R). Many experimentally determined Z-R relationships have been documented by researchers, the most commonly used was discovered by Marshall and Palmer:

$$Z = 200\ R^{1.6}$$

This relationship provides a way to translate dBZ values from reflectivity returns into the more comprehensible, quantitative description of rainfall. The strength of a storm viewed by radar is frequently defined in terms of one of six DVIP intensity levels. These levels were defined by the National Weather Service based upon rain rates (Rinehart, 1991):

Table 4: NWS DVIP Intensity Levels

DVIP Level	Rainrate (in/h)	Reflectivity (dBZ)
1	0.1	29.5
2	0.25	35.9
3	0.5	40.7
4	1.25	47.0
5	2.5	51.9
6	4.0	55.1

The problems to be aware of when working with Doppler radar data are both similar to those of conventional radar, like range folding, attenuation, or receiver noise, and unique to Doppler such as velocity aliasing. Range folding occurs when a radar pulse reaches a target at a range greater than the maximum range, determined by the pulse repetition frequency (PRF). The return from this out of range target is not received until the radar transmits the next pulse. The result is a displayed "second trip echo" on the radar plan position indicator (PPI). These echoes not only appear at a closer than true range, but are also characteristically elongated in a radial direction (Figure 16) (Brown and Wood, 1987). Range folding can be corrected by decreasing the PRF until the range of the radar extends to the correct location of the second trip echo, however this hinders the unambiguous Doppler velocity measurements. The maximum detectable Doppler velocity, like the range, is dependent on the PRF of the radar. Since the maximum unambiguous velocity is inversely related to the maximum unambiguous range, an increase in one necessitates a decrease in the other. This is known as the "Doppler dilemma" (Brown and Wood, 1987).

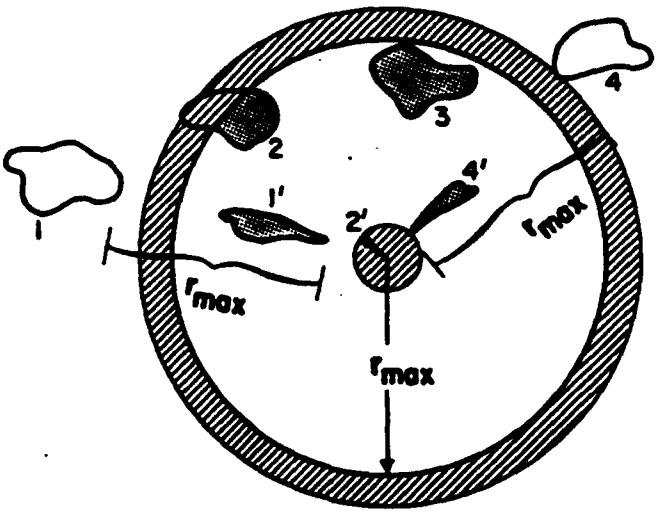

Figure 16. Examples of range folding for a line of four storm cells. The shaded areas represent the locations of measured radar return; those labeled with primed numbers have been range folded into the first trip (Brown and Wood, 1987).

Boundary-layer convergence lines are observable on a radar reflectivity display in the 0-20 dBZ range (see Figure 20a). The signal-to-noise ratio approaches 1 for returns nearing the 0 dBZ level, however, often obscuring important features with receiver noise (shown in the velocity display in Figure 19a). Careful selection of a display threshold can eliminate much of the noise, while preserving the meaningful returns.

Electromagnetic radiation passing through any medium is reduced in power by an amount that depends upon the kind of material present and its density. This reduction in power of the radar beam is called attenuation. Attenuation on radar is almost certain to appear as it detects a thunderstorm or very strong echo. The amount of attenuation depends on the type of radar (wavelength), the strength of the echo, and its horizontal extent. For example, a DVIP level 6 echo on an X-band (2.5-4 cm) radar 10 km in width

will attenuate the beam by 54 dBZ. This will result in a moderate storm behind the thunderstorm going potentially undetected (Rinehart, 1991).

2.3.1 NCAR CP-4 Doppler Radar

Located approximately 10 miles west of Patrick AFB (Figure 17), the NCAR CP-4 radar was one of 6 dedicated radars in the CaPE experiment. Its purpose was to provide, in coordination with the CP-3 radar, sector scans for dual Doppler coverage to support the study of convective initiation, downbursts, tornadoes, and electrification (Foote, 1991). The CP-4 was scheduled to perform regular 360 degree surveillance scans for the purpose of helping in the direction of daily operations. Scans were also sent to the Cape Canaveral Forecast Facility in support of CaPOW, the nowcasting portion of the experiment. To support CaPOW, every 6 minutes (approximately) the CP-4 radar produced PPI surveillance scans at 4 elevation angles. This data, along with other data and products such as PAM station data and CLASS soundings were ingested and displayed on a SUN workstation using NCAR's Zeb software.

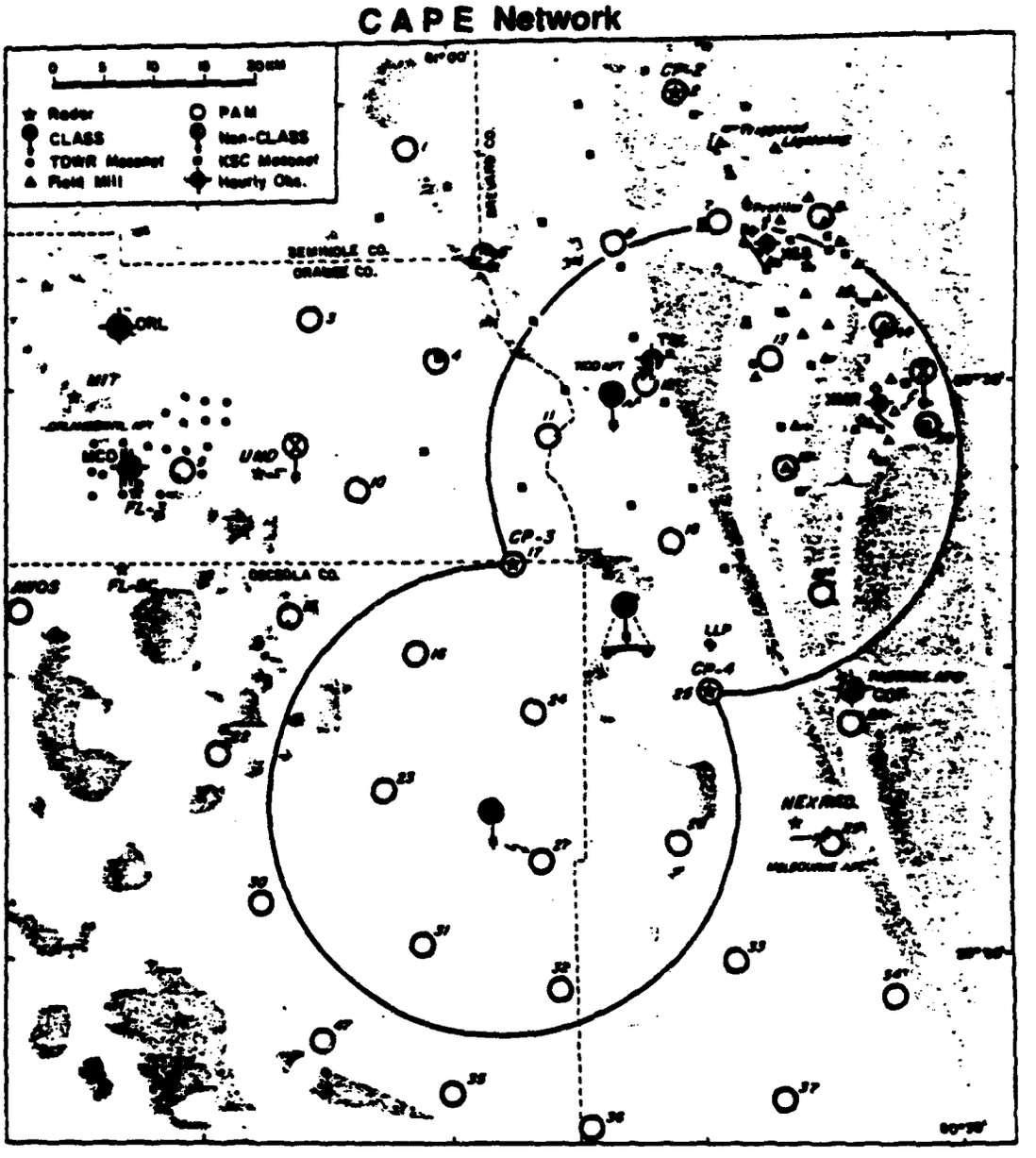

Figure 17. CaPE experimental area and instrumentation network (Foote, 1991).

2.4 Development of Research Platform

Two different software tools were considered for the investigation of convective storm evolution using data from the CaPE experiment. NCAR's Zeb software was used operationally during CaPE and is available for post analysis studies. The Zeb system combines diverse data sets in real-time and in post-processing environments. Zeb does have an ingest module for GOES satellite data, however after installing the CaPE version of Zeb on a Sun SPARC workstation at CSU's computer visualization lab, the capabilities for satellite data analysis were found to be quite limited. Zeb is primarily a useful tool for combining Doppler radar, lightning data, Portable Automated Mesonet (PAM) network data, and CLASS soundings.

With remapping, navigating, and area combination capabilities (just to name a few) on an IBM OS/2 WIDE WORD workstation, the Man computer Interactive Data Access System (McIDAS) provides a much more versatile means for combining radar and satellite data. Not only is it the primary software package used by CIRA's RAMM branch, it is the forecasting and briefing tool used by the forecasters at the Air Force's Cape Canaveral Forecast Facility. Therefore, developing a combined satellite/radar product on this system is advantageous because of: 1) the capabilities of McIDAS; 2) the expertise of experienced scientists in CIRA/RAMM; and 3) the direct applicability to an operational environment.

2.4.1 Data Acquisition

The satellite and radar data used in this project were acquired from the Cooperative Institute for Research in the Atmosphere (CIRA), and the National Center for Atmospheric Research (NCAR/UCAR and NCAR/RDP).

A set of 4 VCR tapes with loops of 1 km resolution GOES-7 visible imagery for each day of the CaPE experiment were prepared by Florida State University. The NCAR Office of Field Project Support (OFPS) provided these tapes for the purpose of browsing for research case studies.

Half-hour visible GOES data in McIDAS image format for the entire experiment was provided by the University Corporation for Atmospheric Research (UCAR) using file transfer protocol (FTP). This data was organized into directories and stored on optical disks. Compressed files of infrared imagery were also obtained from UCAR. However, uncompressing and organizing the files revealed large time gaps in this data set.

The VCR tapes and half hour visible GOES imagery together with the daily meteorological summaries (Williams et al., 1992) were used to select days for case studies. CaPE days experiencing convection, including sea breeze/outflow boundary interactions inciting thunderstorms within CP-4 radar range (within a 65-70 nmi radius of 28.2°N and 80.7°W) were considered. Days with Rapid Scan satellite imagery available were also required in order to match satellite images as closely as possible to the high temporal resolution of the radar scans.

With the satellite data obtained from NCAR being inadequate (no RISOP and missing IR images), all the GOES imagery was instead acquired from CIRA. This involved much processing, as the RAMM branch during CaPE archived the raw satellite images on the VAX as savesets on 8mm exabyte tapes. Visible and infrared data had to be read from the tapes and processed into navigated McIDAS images. The major stages of this multi-step process were:

1) Convert the CIRA AAA-formatted images into raster images using the IRIS image processor.
2) Transfer the raster image files (via FTP) to an optical disk on the McIDAS WIDE WORD workstation.
3) Obtain the navigation for each image from the Space, Science, and Engineering Center (SSEC) McIDAS mainframe in Madison, WI.
4) Attach the navigation parameters to each image area file.

Over 300 visible and infrared images were processed in this manner.

The NCAR CP-4 data surveillance scans from CaPE were obtained from NCAR/RDP (Research Data Program). The data was available in either field binary format or universal format. Universal format was developed in April 1980 in Boulder, Colorado at the Common Doppler Exchange Format Workshop. A common radar data exchange format became necessary as cooperative projects, bringing together independently engineered systems with different data-recording formats, became more routine. In order to facilitate Doppler radar data exchange between participating groups and non-specialist users, Doppler radar universal format was developed (Barnes, 1980).

The CP-4 data was requested in this format for this project in order to process data not only from the CaPE experiment, but also for possible future use with data sets from other cooperative field projects. Unfortunately, the decision to use universal format data for this thesis limited the number of possible case studies. NCAR had not yet converted all the CP-4 scans into this format, and to do so required expensive Cray computer time. Therefore, five days were selected with time intervals corresponding to the dates/times of satellite rapid scan periods. NCAR/RDP sent this data on 8 mm exabyte tapes.

The first major stumbling block in the data processing was encountered when determining the NCAR exabyte tape was produced on a UNIX machine with a high density tape drive. High density tape drives are less common and not as accessible as low density drives. The UNIX-generated tape was an issue, because it created difficulties in transferring the files to a VAX disk. This step was necessary, because the only available high density drive is accessible from the VAX mainframe (the McIDAS PC cannot read 8mm exabyte tapes). This problem was finally resolved after being introduced, by a CIRA programmer, to a Battelle-written VAX utility called MTEXCH. This utility provides the ability to read and write tapes in formats suitable for exchange with non-VAX computers. Using MTEXCH, the record length, record format, character set, carriage control and other attributes from the tape files could be properly copied to a VAX disk. The files containing the CP-4 data were then FTP'd from the VAX disk to PC-McIDAS optical disks. The files were then ready for processing into McIDAS images.

2.4.2 Software Acquisition and Adaptation

By far the most time consuming part of this project was the adaptation of software to convert Doppler radar reflectivity and velocity data from universal format into images displayable on the McIDAS PC. Discovering software already capable of performing this task would have eliminated the hours spent on rewriting, testing and debugging code, using the time instead to concentrate on the more interesting task of data analysis.

The framework for the source code to accomplish the data conversion was obtained from a scientist at NASA's Marshall Space Flight Center in Huntsville, Alabama. The program, titled "UFRECT" (for universal format to rectilinear), converts polar data (universal format data) to Cartesian coordinates and writes a McIDAS image. The MSFC subroutine was quite a few years old, not currently being used and was not guaranteed to still work. The challenge then was to decipher the over 500 lines of mostly uncommented FORTRAN and McIDAS code to determine if it could be rewritten into a version capable of running on the PC. Since it ran on a McIDAS mainframe as opposed to a PC, JCL statements handled input specifications such as record length, blocksize, and format. A new method of inputting the data had to first be written.

Not only did new input code have to be incorporated, but since the PC uses an alternate byte ordering scheme from the byte ordering of the host (data generating) computer, big-endian to little-endian bit conversion had to be accomplished for every byte in each file. Initially this was accomplished by a brute force method of processing each byte in the data file one by one. Efficiency was tremendously increased when the source code was changed to perform the same task on the data one block at a time. Such

improvements in software code efficiency saved enough time to enable over 650 radar scans to be processed for case studies.

The final notable change to the UFRECT program was to add code to extract velocity data and create McIDAS velocity image areas. Although MSFC's program was intended to include this option (velocity data was listed as a selection in the command line instructions) the code required to extract and manipulate it was never written.

2.4.3 Testing and Debugging

Each record of universal format radar data contains a header block, followed by the data itself. The format specifies the content of every word in the header block, each word containing information describing the data, or how the data is organized in the record (Appendix E). The header information, printed to a file (Appendix F), was used to debug the UFRECT program. Nonsensical values returned to this file indicate a problem in reading the universal format data. After assurance that the CP-4 data was properly read and an image created, testing for data quality was accomplished by comparing the produced radar images to the 1 km resolution GOES visible data.

The first significant problem encountered with display of the data was due to McIDAS image areas being unable to store and display negative values. Only numbers ranging from 0-255 can represent pixels which comprise a McIDAS image. This obviously poses a problem when trying to display negative dBZ values, indicative of very small water droplet targets, or clear air returns. The Doppler velocity display also uses negative values to indicate radial motion toward the radar. The fix for this problem turned out to be relatively simple. A color table bias of 100 was added to every pixel

value in the conversion program when processing the images. Therefore, negative data values are represented and displayed by pixel values less than 100.

Another quality control problem was the display of bad data. Second trip echoes were prevalent in the scans. Although these displaced echoes could not be removed from the display, their characteristic signature (Figure 18a) and comparison with the visible satellite imagery (Figure 18b) made identification possible. The bad data in the velocity field was due to receiver noise. To correct this problem, a function was built into the UFRECT conversion program to filter out the bad velocity data by comparing it to the reflectivity data. Velocity data pixels corresponding to reflectivity pixels below a calculated threshold were considered noise and set to the value 255 (i.e. not displayed by the color table). In order to not eliminate clear air returns, this function was written to vary the threshold to stay at the receiver's limit of detectability. This limit varies with range squared (r^2), so the threshold increases using the same relationship with increasing range. The result is a displayed scan preserving only the valid velocity measurements (Figures 19a,b,c).

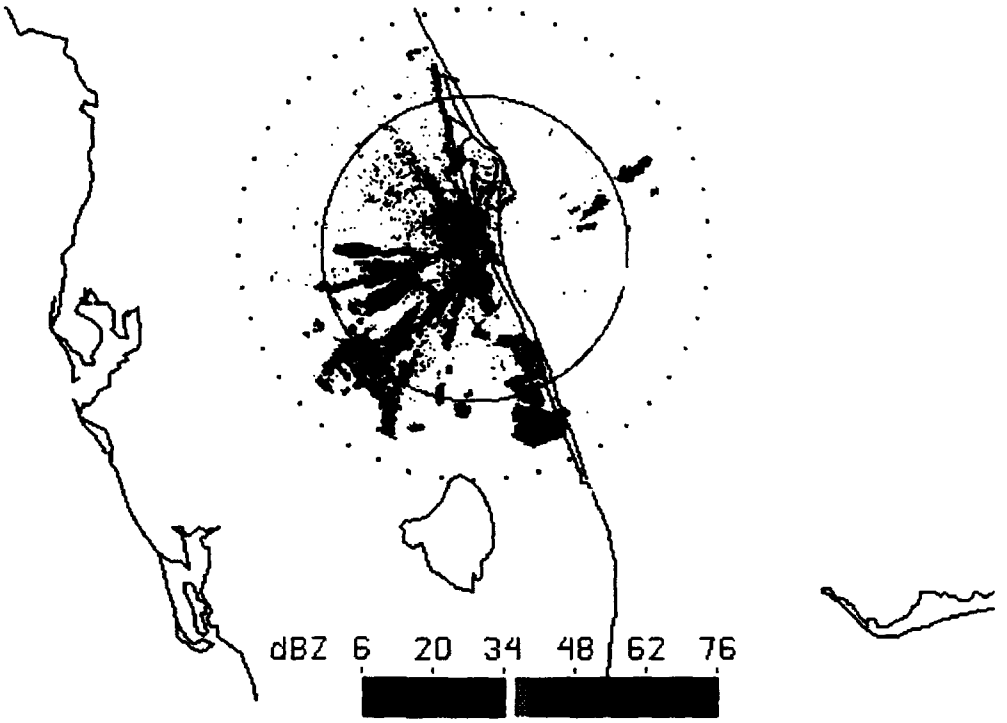

Figure 18a. Example of second trip echoes from a CP-4 radar scan - 24 July 91/1904Z. Compare the appearance of these echoes with those in Figure 16.

Figure 18b. GOES visible image - 24 July 91/1901Z. The convection just outside of radar range east of Tampa is responsible for the range folding problems in Figure 18a.

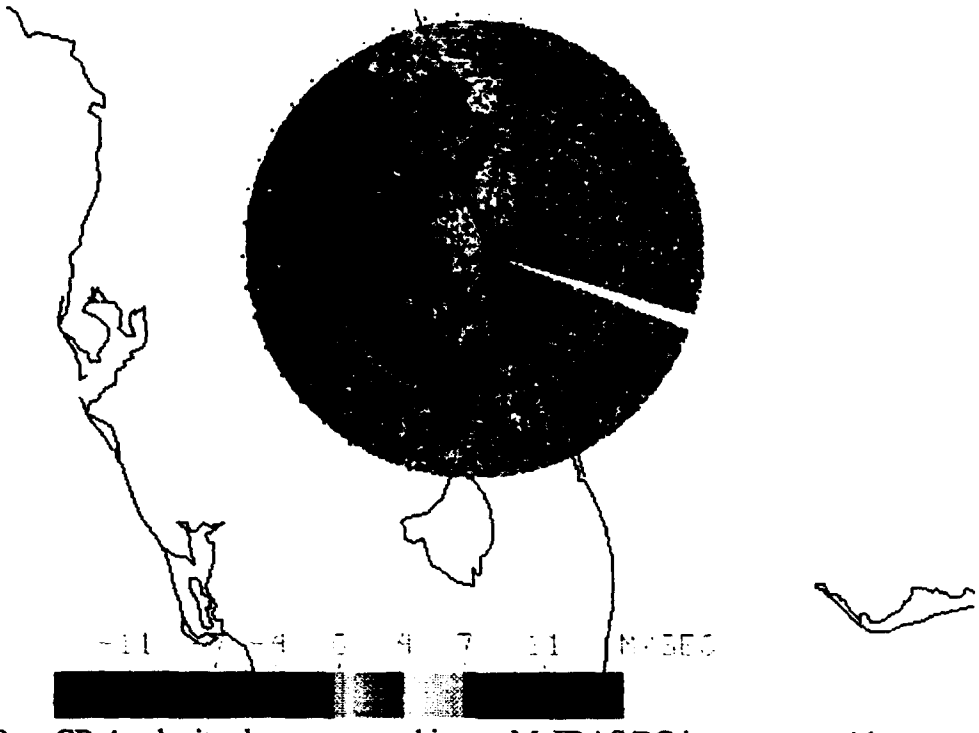

Figure 19a. CP-4 velocity data processed into a McIDAS/PC image area without noise filtering the data - 26 July 91/1928Z.

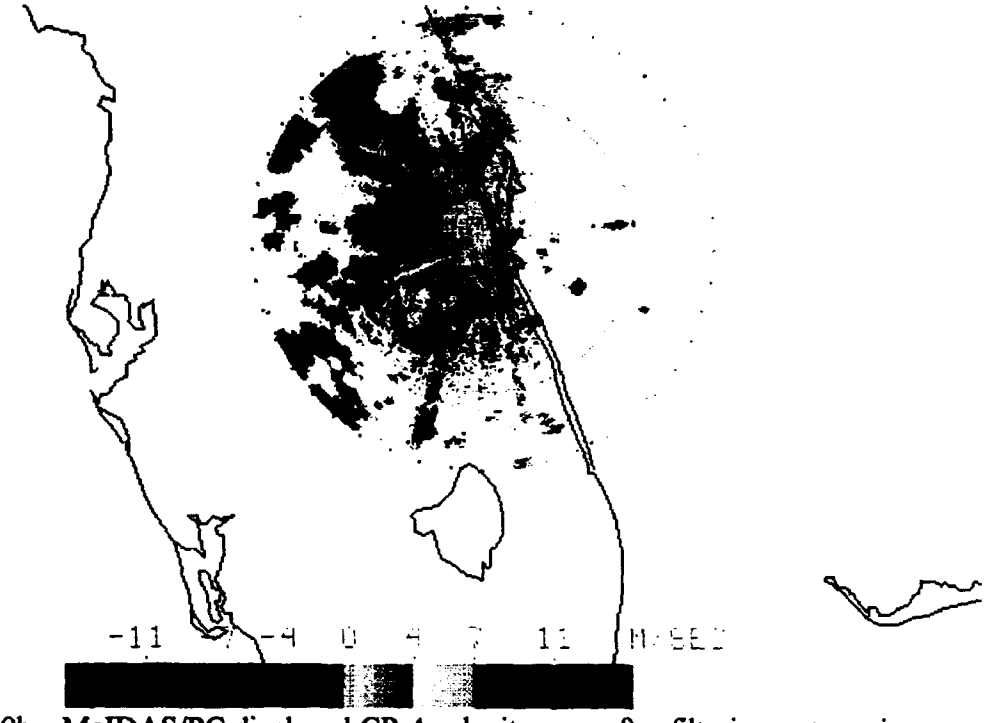

Figure 19b. McIDAS/PC displayed CP-4 velocity scan after filtering out receiver noise - 26 July 91/1928Z. Note the NE-SW oriented line of thunderstorms moving toward the radar at up to 16 m/s (maximum velocities are aliased).

Figure 19c. GOES visible image - 26 July 91/1926Z.

2.5 Product Development

2.5.1 Combining the Satellite and Radar Images

Preparing the satellite and radar images for display in a combined product on the McIDAS PC involved a few prepatory steps. The satellite images had to be remapped into the radar projection and enhancements developed for the radar scans. The radar enhancements for reflectivity and velocity were modeled after those from the University of North Dakota C-band Doppler weather radar (Rinehart, 1991) and the NEXRAD WSR-88D (USAF Doc. 1990) (Figures 20a,b,c).

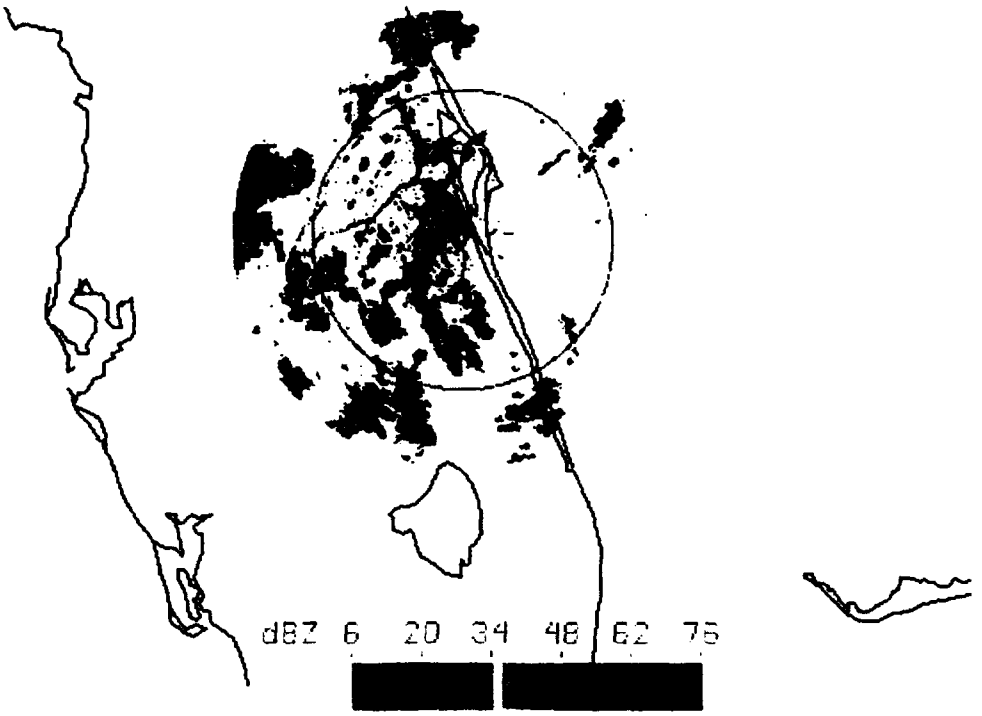

Figure 20a. CP-4 Doppler radar reflectivity scan with McIDAS/PC color table - 25 July 91/2019Z. The range ring radius is 75 km (46.6 mi).

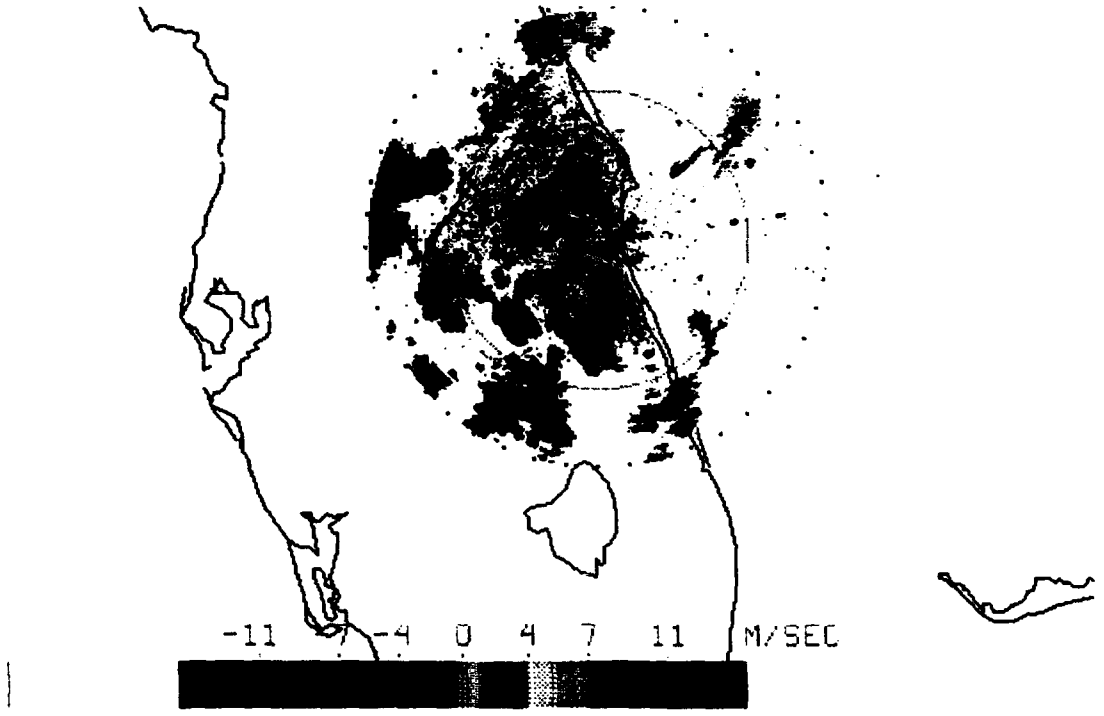

Figure 20b. CP-4 Doppler radar velocity data with McIDAS/PC co[illegible]able - 25 July 91/2019Z. Negative values represent movement toward the radar, positive values indicate movement away. The outer range ring radius is 116 km (72.1 mi).

Figure 20c. GOES visible image - 25 July 91/2016Z. Using the information from the corresponding velocity scan in Figure 20b: cells A and B have a component of motion from south to north; the NE cells in the cloud streets C are moving slowly away from the radar at 3-6 m/s while velocities of up to 10 m/s are detected in a well-defined line to the SW.

By remapping the satellite images into the radar on the McIDAS PC, the coarser resolution satellite image is converted into 1 km size pixels by multiplying the data points by simply dividing up the original pixels. Of course this does not improve the image resolution, but it allows a pixel-by-pixel comparison with the radar image in which every pixel represents the same amount of earth area.

Since satellite image times and radar scan times were not synchronized during the CaPE experiment, radar scan times had to be matched to the available satellite images. During the RISOP periods, it takes GOES 2 minutes and 27 seconds to scan to 28.2°N latitude, 80.7°W longitude - the location of the CP-4 radar during CaPE. Normal scan

mode requires 3 minutes and 28 seconds to reach the same point. To achieve as close to a synchronized product as possible, every satellite image used in the case studies was matched with a radar scan within 3 minutes of the image time plus the appropriate scan time.

To combine the images into a single display, the selected CP-4 scans (at the desired elevation angle) and satellite images were loaded into opposite McIDAS image frames. By using the McIDAS PC dual channel enhancement capability, the system can toggle the radar pseudo-coloring table in and out of the video refresh path, combining the current (satellite) and opposite (radar) images pixel by pixel (Figures 21a,b). The combined data sources can then be looped through the sequential image times. By this method, there is no loss of gradient information from either source. Another advantage is the ability to quickly toggle on and off the CP-4 data. For an operational forecaster, this allows for closer inspection of details in each source separately, if needed.

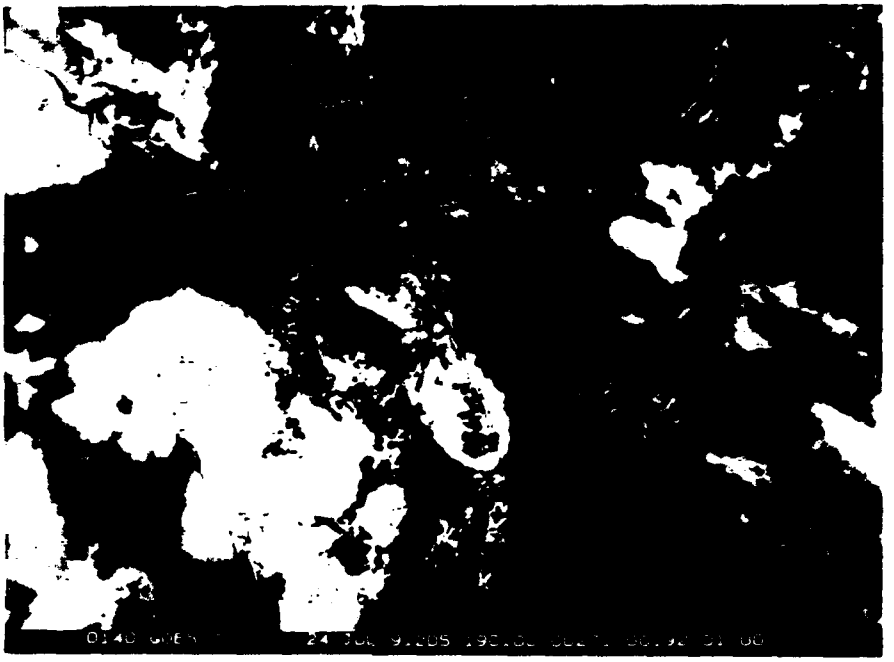

Figure 21a. Combined satellite and radar display using the GOES visible image from Figure 18b and the CP-4 reflectivity scan at 0.3 degrees elevation from Figure 18a. The source of the second trip echoes can easily be determined.

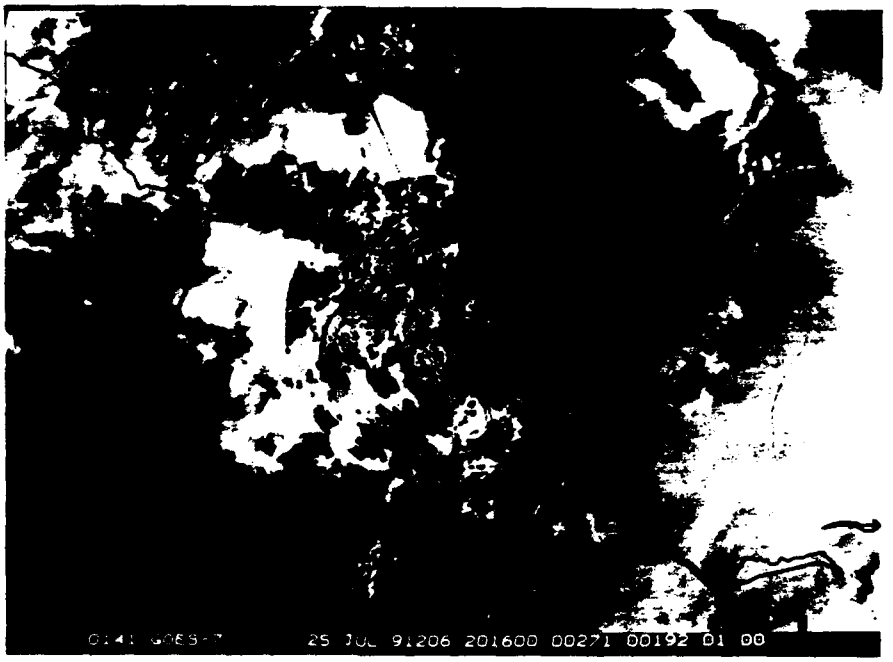

Figure 21b. Combined satellite and radar display using the GOES visible image from Figure 20c and the CP-4 velocity display at 0.3 degrees elevation from Figure 20b.

Figures 22a,b show the error in the combined display due to parallax. The cloud tops viewed in this image are radially displaced away from the satellite subpoint (shown in Figure 13) in the direction indicated by the yellow dotted line (Figure 22a). Since rapidly growing thunderstorm cells are being studied, the error changes on each successive image, making correction difficult. The images in the following case studies were not adjusted to correct for parallax.

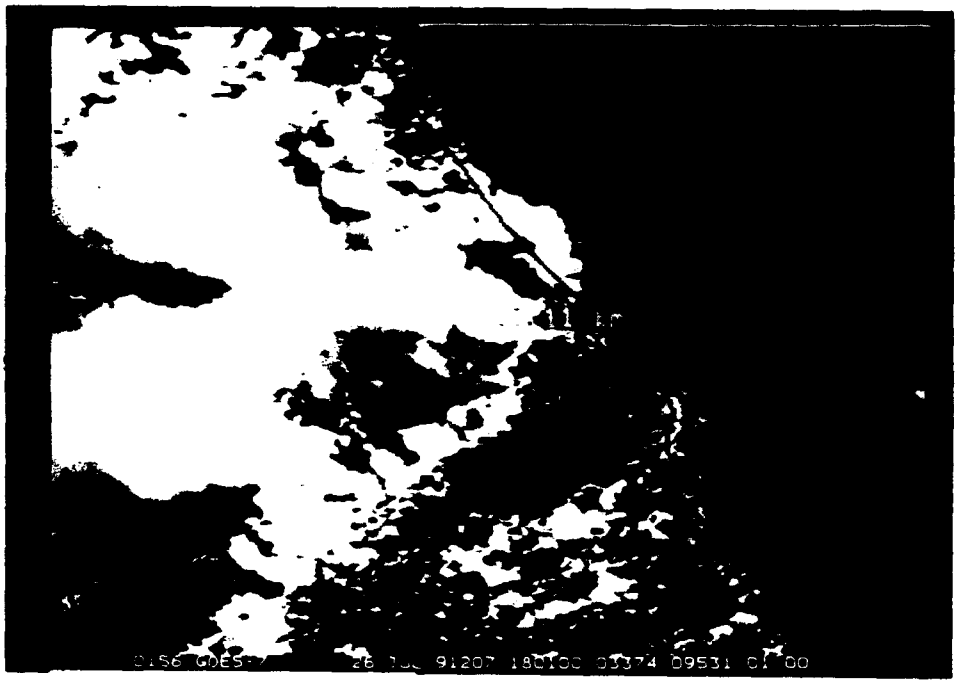

Figure 22a. McIDAS/PC calculation of cloud height on a GOES visible image from the cloud edge and shadow (13.11 km).

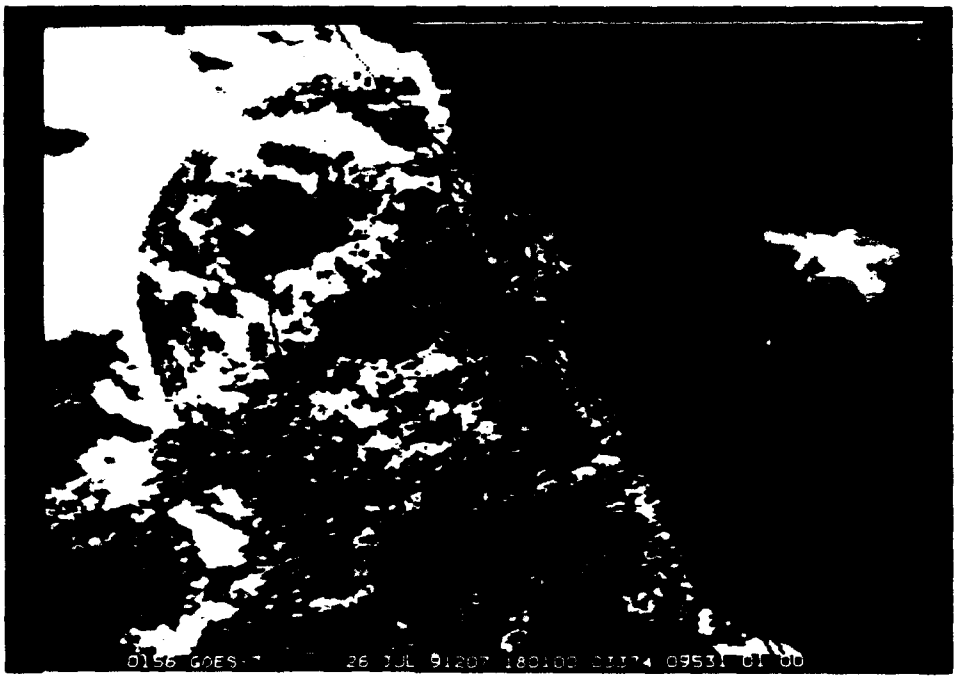

Figure 22b. Combined satellite/radar display shows the increasing offset of cloud tops from radar echoes with increasing storm height. Parallax error estimates range from 5 km to 11 km in this image .

2.5.2 Combined GOES/IR Radiances and CP-4 Reflectivity Data Product

Of the four types of processed data from CaPE, infrared cloud top temperatures and radar reflectivity returns were selected for combination to investigate convective storm evolution. Both measurements provide information on thunderstorm growth, and storm intensity. In NCAR field experiments, thunderstorms are defined by radar reflectivity measurements. For nowcasting studies, a precipitating cloud is considered to be a thunderstorm if its corresponding radar echo is > 30 dBZ (Wilson and Mueller, 1993). DVIP thunderstorm intensity level thresholds are also based upon reflectivity (see Table 4). Cloud top temperature is an indicator of intensity of convection. Colder

temperatures imply higher thunderstorm heights, which have long been related to thunderstorm severity (Adler and Fenn, 1979).

Enhancements on the case study images were created or adjusted to highlight threshold values. Reynolds and Smith (1979) used -30°C to define cloud top temperature in their composite, while Adler and Fenn (1979) considered -47°C the threshold defining cloud top. Selected radar values also varied considerably based upon the type of study from 20 dBZ (Reynolds and Smith, 1979) to 25 and 50 dBZ levels (Green and Parker, 1983) to 30 or 40 dBZ values (Wilson and Mueller, 1993). Obviously each value was selected to be case/experiment specific. What is important is not the selected threshold number, but how that cloud top region or echo changes in area, relates to an observed event on the ground, or how changes in the cell area as defined by the two data sources compare to each other.

In order to compare the time rate-of-change in area of a storm's cloud top to the rate-of-change in area of its radar reflectivity return, a procedure was devised to extract this data from the McIDAS PC images. Isolating cells to study was not an easy task. The case studies all feature rapid development, rapidly moving storms and frequent interactions with outflow boundaries and the sea breeze front. A McIDAS image statistics routine was used to encircle the enhanced cloud top and associated radar echo (Figures 23a,b), returning a histogram with a count of pixels at or above selected threshold levels (Tables 5 and 6). In difficult cases, visible satellite imagery helped to define the extent of a storm cell and help outline the associated reflectivity echo. Due to

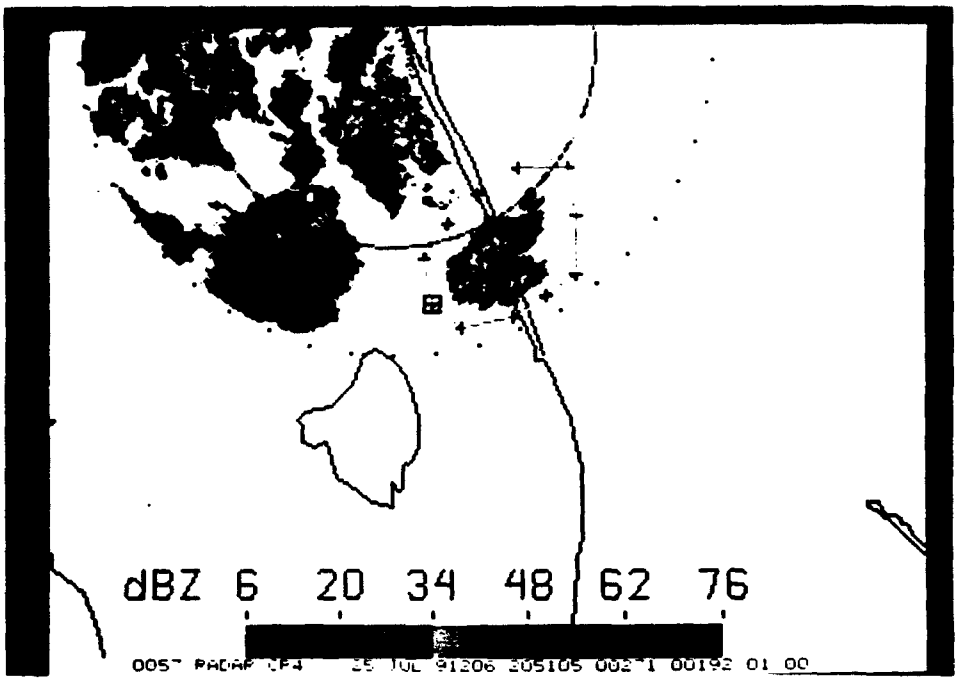

Figure 23a. Circled CP-4 reflectivity cell on the McIDAS/PC (25 July 91/2051Z). Statistics from this selected area are returned in tabular form (Table 5).

Figure 23b. Circled GOES/IR enhanced cloud top temperatures corresponding to the CP-4 echo in Figure 23a. Statistics on brightness count values within this area are shown in Table 6.

Table 5. McIDAS area (km^2) statistics output with histogram. The number of pixels in "brightness count" ranges within the circled area (Figure 23a) are displayed. In this example, the range values represent reflectivity returns (dBZ + 100) greater than or equal to 25 dBZ.

Area	Unit	Pixels	Minimum	Maximum	Mean	StD	Mode	Median	Lo-Tail	Hi-Tail
224	BRIT	489	125	162	136	8	125	135	125	155

Bin	0% 25% 50% 75% 100%	Pixels	%	Range	Gray
0	|********	101	20	125-128	15
1	|*****	66	13	129-131	30
2	|******	84	17	132-135	45
3	|*****	72	14	136-138	60
4	|******	81	16	139-142	75
5	|**	34	6	143-145	90
6	|**	26	5	146-149	105
7	|	10	2	150-152	120
8	|	7	1	153-156	135
9	|	3	.61	157-159	150
10	|	5	1	160-163	165
11	|	0	0	164-166	180

ASTAT: Done

Table 6. Same as Table 5, except the range of pixel values represent brightness counts greater than or equal to 201 encircled in Figure 23b.

Area	Unit	Pixels	Minimum	Maximum	Mean	StD	Mode	Median	Lo-Tail	Hi-Tail
1024	BRIT	1783	201	210	205	2	206	205	202	202

Bin	0% 25% 50% 75% 100%	Pixels	%	Range	Gray
0	|****	223	12	201-202	28
1	|**********	469	26	203-204	56
2	|***************	679	38	205-206	84
3	|******	296	16	207-208	112
4	|**	116	6	209-210	140
5	|	0	0	211-212	168

ASTAT: Done

parallax, complex convective interactions, and perhaps wind shear with height, the radar echo did not always neatly underlie the infrared cloud top.

The statistics extraction procedure was continued on each cell until: it dissipated below the threshold values, moved out of the radar range, or satellite rapid-scan coverage for the day ended. Analyzing the data involved plotting the change in the coldest cloud top area and highest reflectivity returns versus time and the rate-of-change of these values (Figures 24a,b). In all cases, the cloud top temperature area greatly exceeds the radar echo area. A cross section of a supercell thunderstorm (Figure 25) shows the large area coverage of the anvil compared to that of the rain/precipitation shaft. The ratio of these areas depends on the strength of the storm, the stage of its development, and the temperature selected to define the cloud top. To better compare the changes of satellite and radar data, a scaling factor was used to increase the radar area values. The factor used is indicated in the legend of each chart (Figures 24a,b).

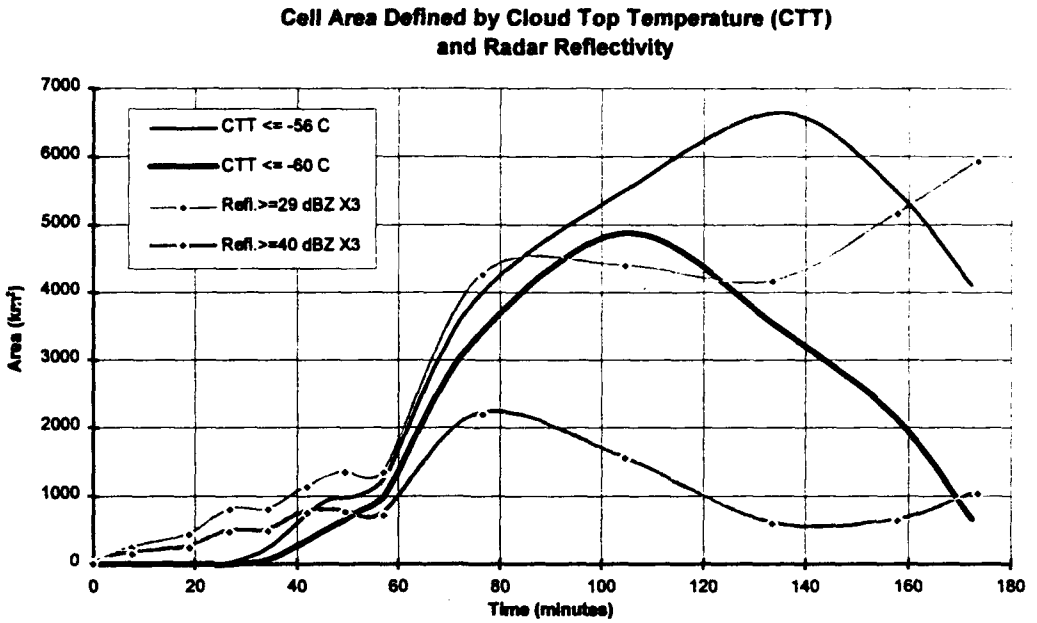

Figure 24a. Plot of a thunderstorm cell area based on thresholded values of satellite derived cloud top temperature and radar reflectivity versus time. The reflectivity values are multiplied by a factor of 3.

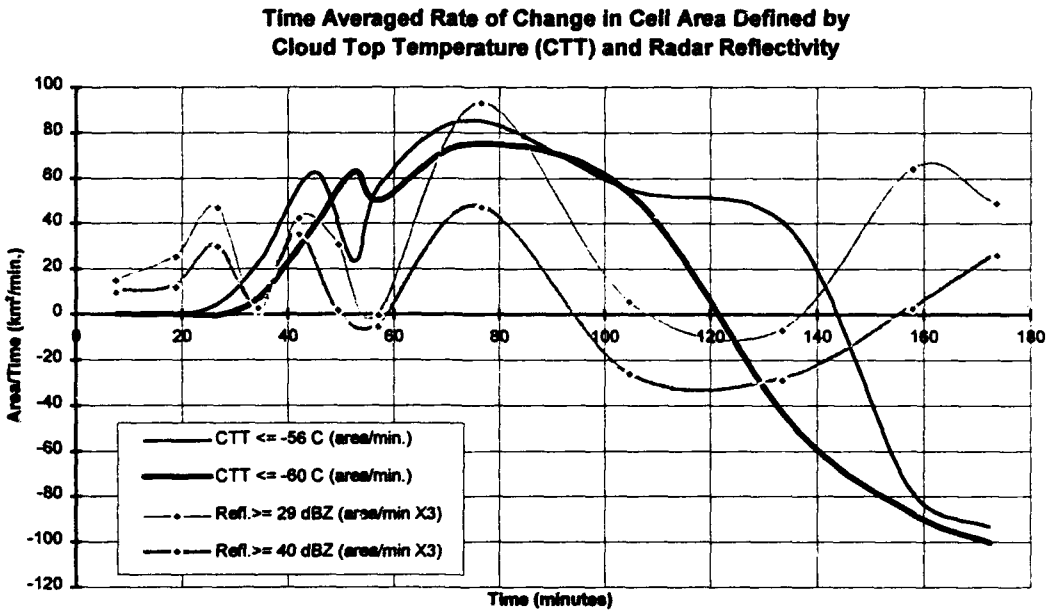

Figure 24b. Plot of the time averaged rate of change of the data in Figure 24a versus time. Points above the x-axis represent area increases, while data below represents decreasing areas. The reflectivity values are multiplied by a factor of 3.

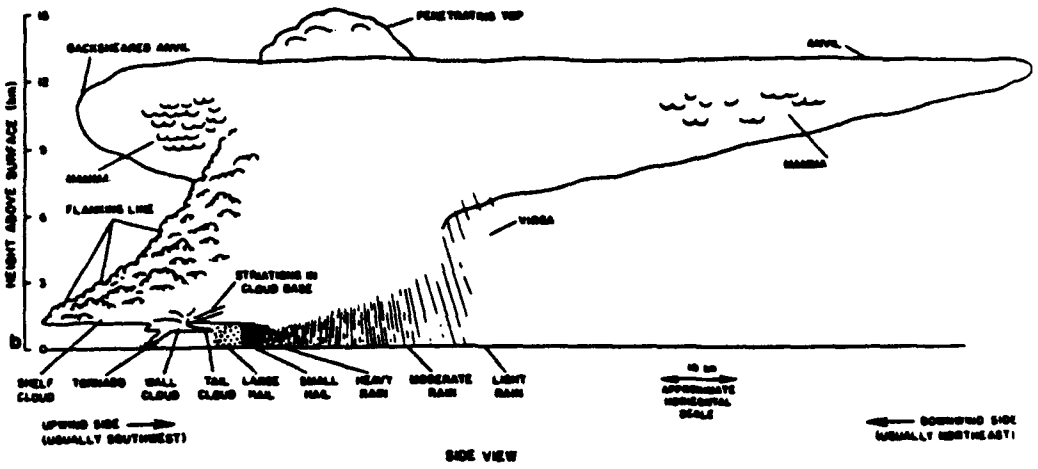

Figure 25. Cross section of a supercell thunderstorm (from Bluestein and Parks, 1983).

Unfortunately, there are many possible sources of error in this procedure. First of all, due to the elevation angle of the PPI scan, an echo from a cell moving toward the radar represents precipitation from lower in the storm. This effect is minimized by using the lowest available elevation scan of 0.3°.

Additional reflectivity pixels could be erroneously included during the statistics gathering process due to the appearance of second trip echoes, or a nearby cell. Or data could be missed due to attenuation of the radar signal, especially when the storm is located near the maximum range of the radar.

Parallax and slight navigation errors, however should not greatly impact the results. This is because the process of encircling the cloud top or echo with the cursor does not require the images to be perfectly aligned. Knowledge of the maximum amount of parallax error for the region of study provides enough information to adequately match a cells cloud top temperature with its radar echo. Parallax is therefore subjectively compensated for during data analysis.

Chapter 3

CASE STUDIES

The three days chosen for study from the CaPE data set were July 24, 25, and 26th. These consecutive days were selected because of the amount of convection and convective interaction present within the range of the CP-4 radar surveillance scans during GOES RISOP coverage. Rapid scan imagery was considered critical in this study of convective storm evolution because of the great amount of change which can take place in a 30 minute period. Trying to isolate and track a single cell is difficult due to the many interactions and rapid development common in Florida thunderstorms. In one half hour (normal time interval between GOES scans), a cell can go through many intensifying and weakening cycles, be absorbed by another cell, or disappear completely.

From the three study days, a total of nine cells were analyzed using the combined satellite/radar display on a McIDAS PC. To help describe the convective potential for each day, a brief discussion of the surface and upper air conditions is given. Data used in the discussions come from the McIDAS satellite/radar loops, soundings, and analyzed upper air maps and meteorological summaries from NCAR/OFPS.

Also accompanying each case day are visible satellite images identifying the studied cells by number at three times during development. Photographs of the McIDAS IR satellite/radar composite show the sequence of images from which the cloud top

temperature and reflectivity data were extracted. Plots of this data provide insight into the relationship of the two information sources during the evolution of the cell.

3.1 Case Study #1: July 24, 1991 (1731-2201 UTC)

Early analysis on the 24th revealed upper-level and surface features indicating an unstable environment and therefore a high probability for afternoon convection. An upper level low in south Florida observed at 200 and 500mb produced southeasterly winds of 20-30 kts across the central region of the state (Figures 26a-c). On the surface, a pressure trough extended from the Carolinas southwestward into the Florida panhandle (Figure 26b). To the south of the CaPE area, an east-west ridge axis from an Atlantic high protruded across the southern peninsula. As a result of these features, west to southwesterly winds in the lower 2.5 km were observed (Figure 26c). Cold temperature at 500 mb (-8.2°C) with low level moisture, the indices from the CCAFS late morning sounding reveal an unstable atmosphere (CAPE of > 4000 J/kg).

Convection on the east coast was initially hindered as cirrus clouds in the southeast flow moved across the Cape, delaying rapid surface heating. In addition, visible imagery shows the region just north of Cape Canaveral to be drier than central and southern Florida (Figure 27a). Just south of the Cape, however convection began along the sea breeze front early in the afternoon near Vero Beach (Cell #1, Figure 27a). This cell grew both to the north and south along the sea-breeze boundary as it slowly traveled westward, eventually producing an outflow boundary at 2001Z (Figure 27b). This

outflow contributed to the intensification of a cell in Osceola county (Cell #2, Figure 27b).

The storm in the southwest sector of CP-4 radar range grew steadily from its moderate cumulus stage (Cell #3, Figure 27a), producing 1-inch hail and damaging winds in Frostproof, FL (Polk county) in the time period from 1915-1945Z. The most intense convection of the day in central Florida was due to outflow from early morning thunderstorms on the west coast near Tampa. This boundary traveled eastward across the peninsula during the afternoon. In addition to intensifying cell #3, the west coast outflow developed severe storms over Orlando. Wind gusts of 58 mph were produced at the International Airport at 2045Z. Hail up to 1 1/4 inch in diameter was reported during this time. This storm was not studied since it occurred after the satellite RISOP period.

Cell #1 (Vero beach) data analysis: During the first hour (1731Z-1831Z) steady growth was observed, followed by a more rapid increase in CTT area during the second hour (Figure 29a). An even more rapid decrease in intensity occurred at 2000Z as the cell dissipated after producing a westward moving outflow boundary. Figure 29b shows a maximum decrease in the rate-of-change in 40 dBZ cell area just prior to rapid increases in growth rates in both cloud top temperature (CTT) and radar reflectivity (RR) areas. The two coincident, highest peaks in CTT(-58°C) and RR(40 dBZ) (Figure 29b) indicate both CTT and RR detect maximum thunderstorm growth rate.

Cell #2 (Osceola Co.) data analysis: Began as an isolated cell (Figure 27b) growing rapidly with the help of an outflow boundary from cell #1 (Figures 28f-i). The CTT and RR areas increased rapidly from this point for about 30 minutes, fluctuated a bit during a 40-minute period of more moderate growth before entering a steady dissipating phase (Figure 30a). Like cell #1, the time rate-of-change of this cell was defined similarly by CTT and RR with the same number of maximum and minimum points in both data sources. The reflectivity area changes however precede those in the CTT by approximately 5 minutes (Figure 30b).

Cell #3 (Frostproof, Polk Co.) data analysis: A steady increase in CTT area for approximately 60 minutes preceded a gradual weakening of the storm first observed in RR(40dBZ) at 40 minutes, then CTT(-64 C) at 60 minutes (Figure 31a). During the hour of development, the maximum peaks of RR area rate increases preceded those in CTT by approximately 10-12 minutes (Figure 31b). During the period of decreasing -64 C CTT area, the secondary thresholds maintain this apparent relationship with CTT area changes lagging RR changes by approximately 5 minutes. The CTT maximum rate of change decrease also slightly lags that of RR (Figure 31b). Observation of this cell was cut short due to the radar echo moving out of range as well as the cloud top being obscured by neighboring convection. The CTT contamination being due to expanding cirrus anvil from the hail producing cell to the N-NE over Orlando and advecting cirrus cloud from cell #2 to the southeast (Figures 27c,28j).

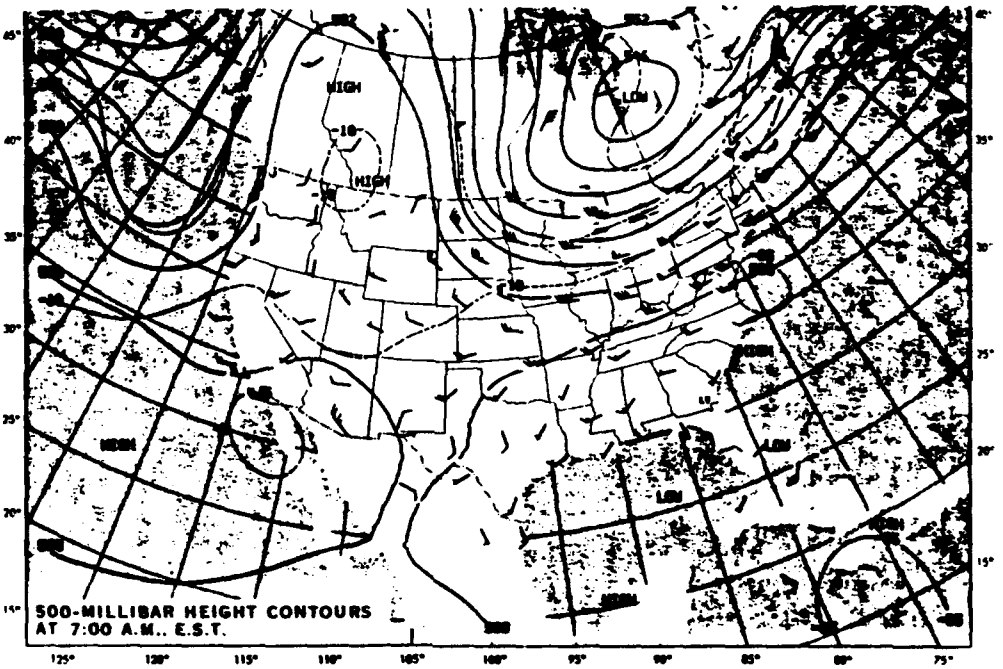

Figure 26a. 500mb height contours - 24 July 91/12Z (from Climate Analysis Center, Daily Weather Maps).

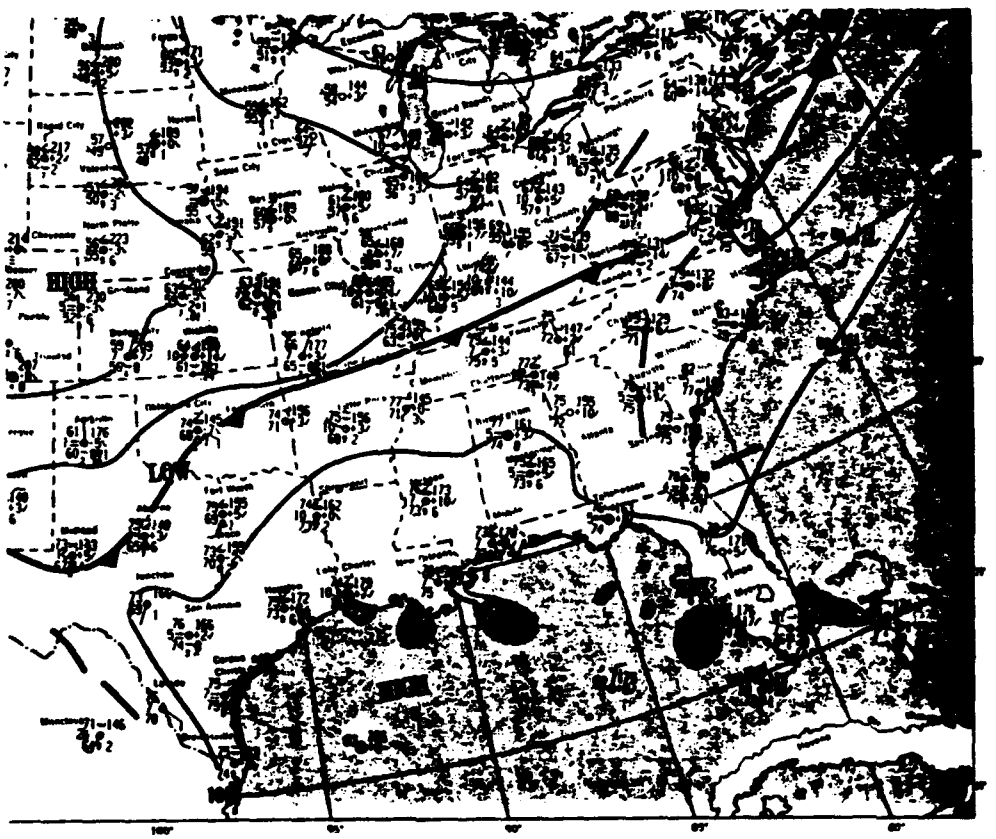

Figure 26b. Surface pressure analysis and station plots - 24 July 91/12Z (from Climate (Analysis Center, Daily Weather Maps).

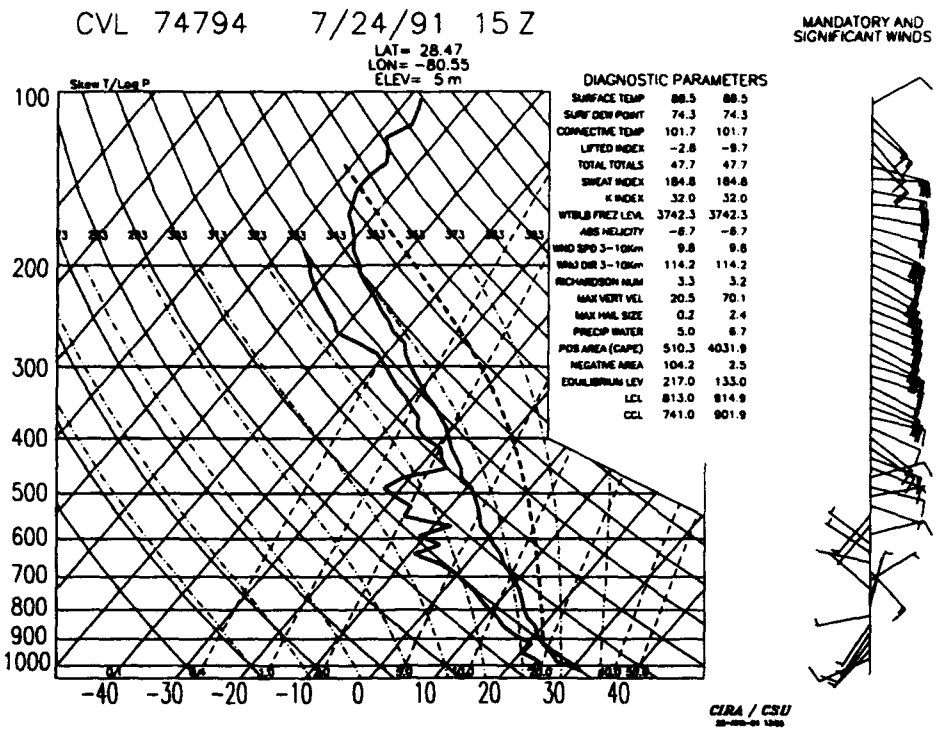

Figure 26c. Cape Canaveral AFS Skew-T - from 24 July 91/1501Z rawinsonde.

Figure 27a. GOES visible satellite image - 24 July 91/1831Z.

Figure 27b. GOES visible satellite image - 24 July 91/2001Z.

Figure 27c. GOES visible satellite image - 24 July 91/2051Z.

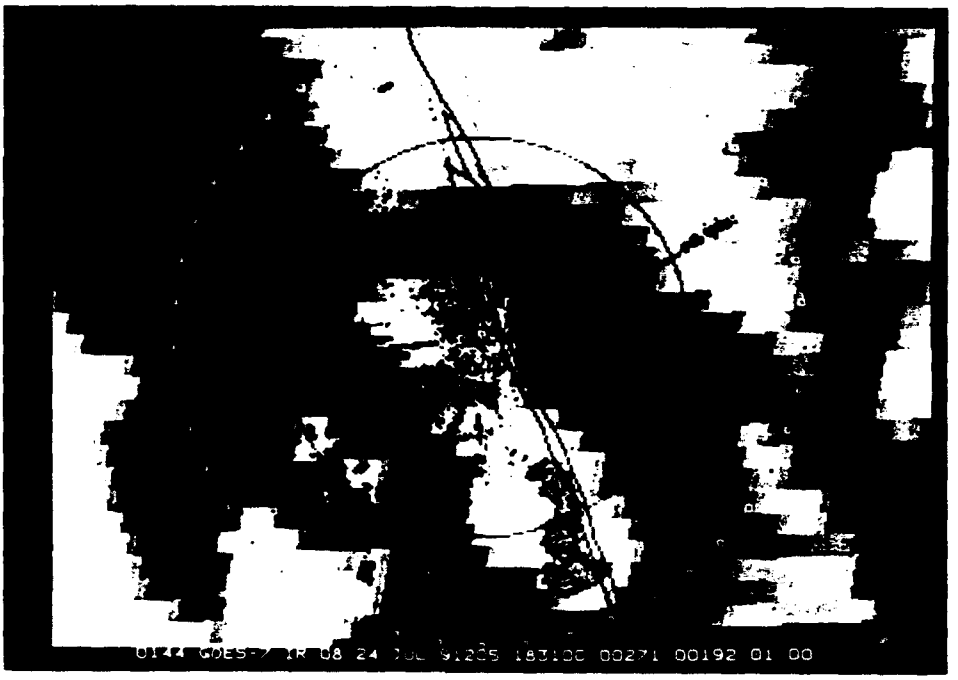

Figure 28a. Combined GOES/IR image and CP-4 Doppler radar reflectivity scan displays - 24 July 91/sequence loop from 1831Z-2131Z. Although more images are available and were used in the study, only 10 images are included for this time period.

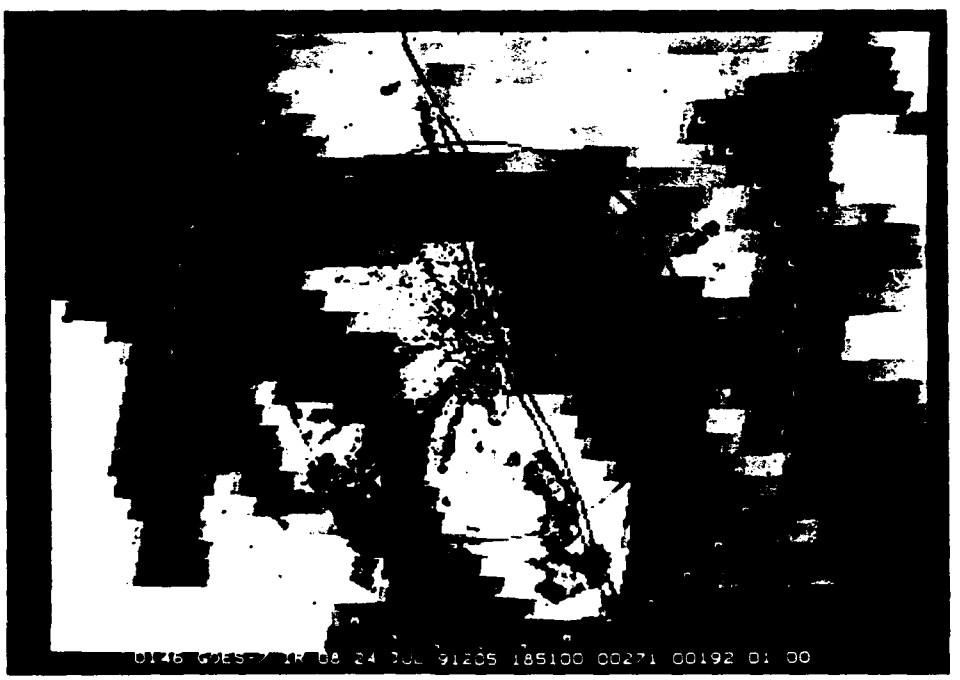

Figure 28b. Combined GOES/IR image and CP-4 Doppler radar reflectivity scan display - 24 July/1851Z.

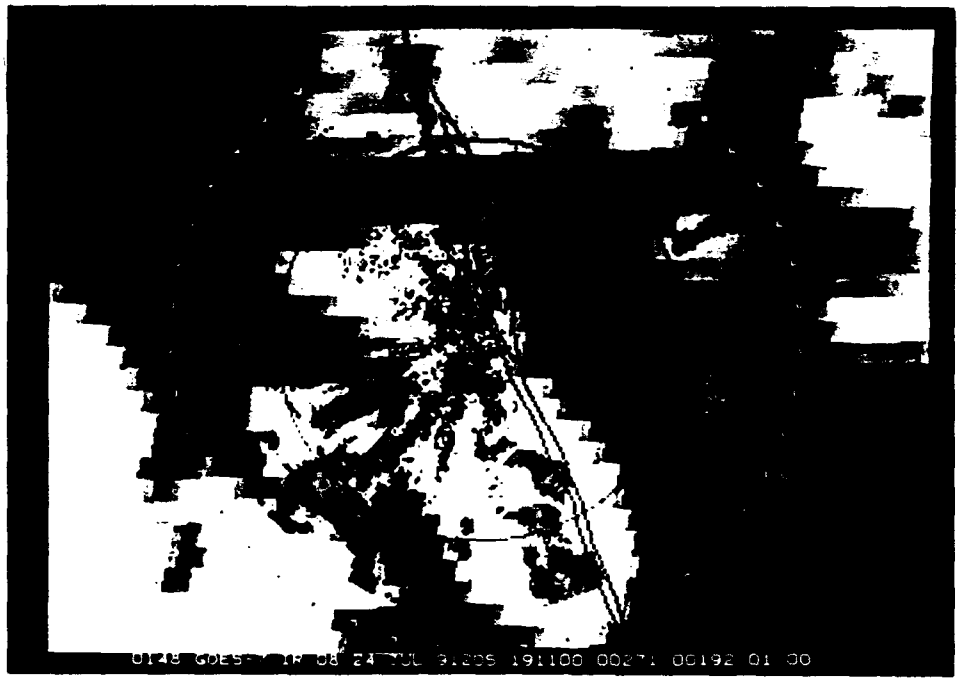

Figure 28c. Combined GOES/IR image and CP-4 Doppler radar reflectivity scan display - 24 July/1911Z.

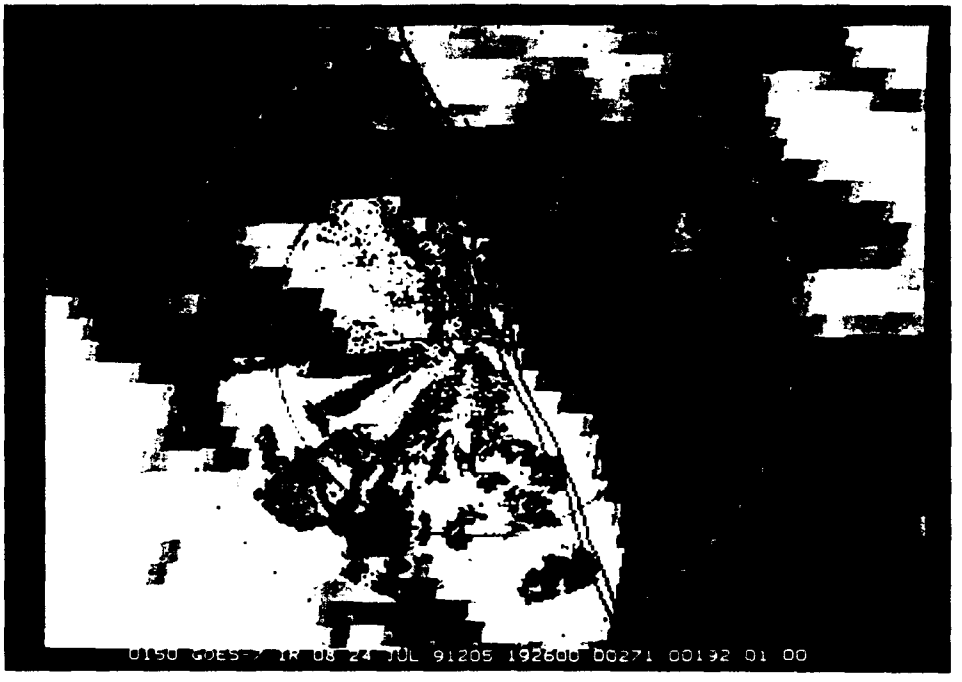

Figure 28d. Combined GOES/IR image and CP-4 Doppler radar reflectivity scan display - 24 July/1926Z.

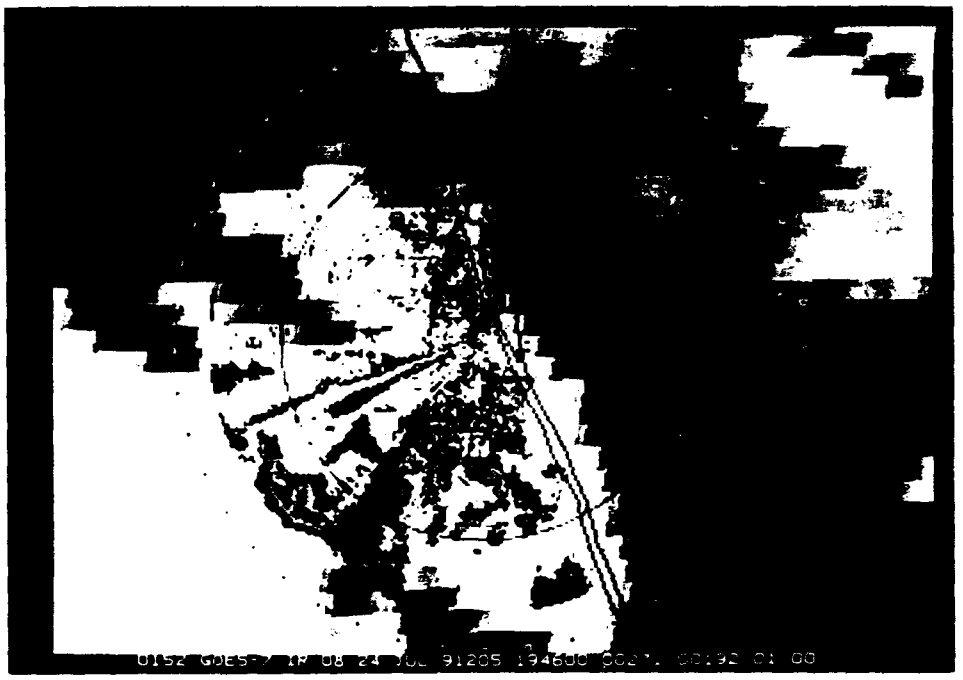

Figure 28e. Combined GOES/IR image and CP-4 Doppler radar reflectivity scan display - 24 July/1946Z.

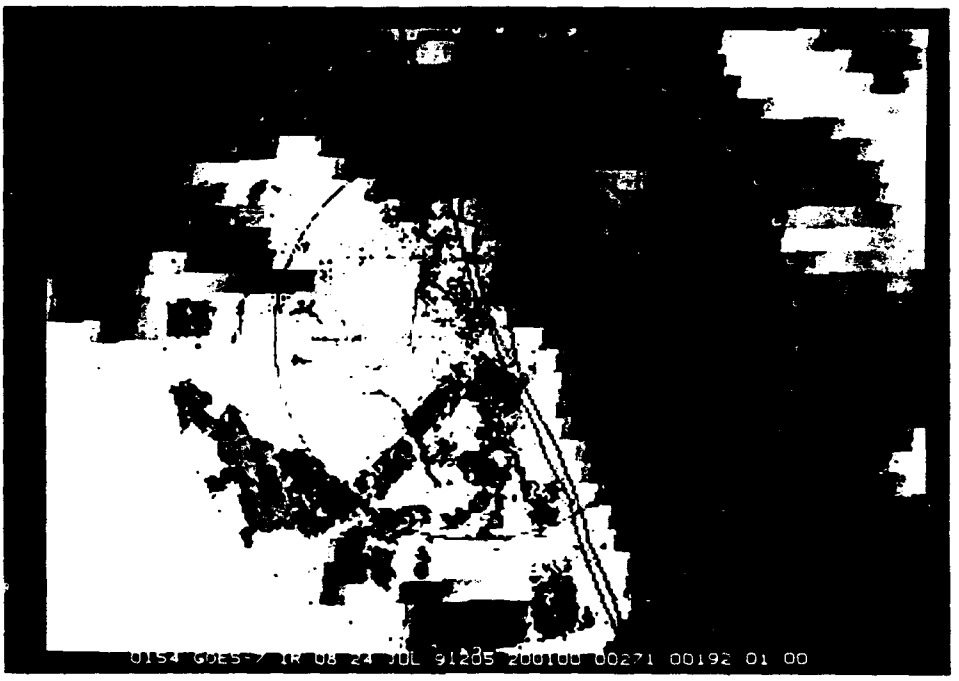

Figure 28f. Combined GOES/IR image and CP-4 Doppler radar reflectivity scan display - 24 July/2001Z

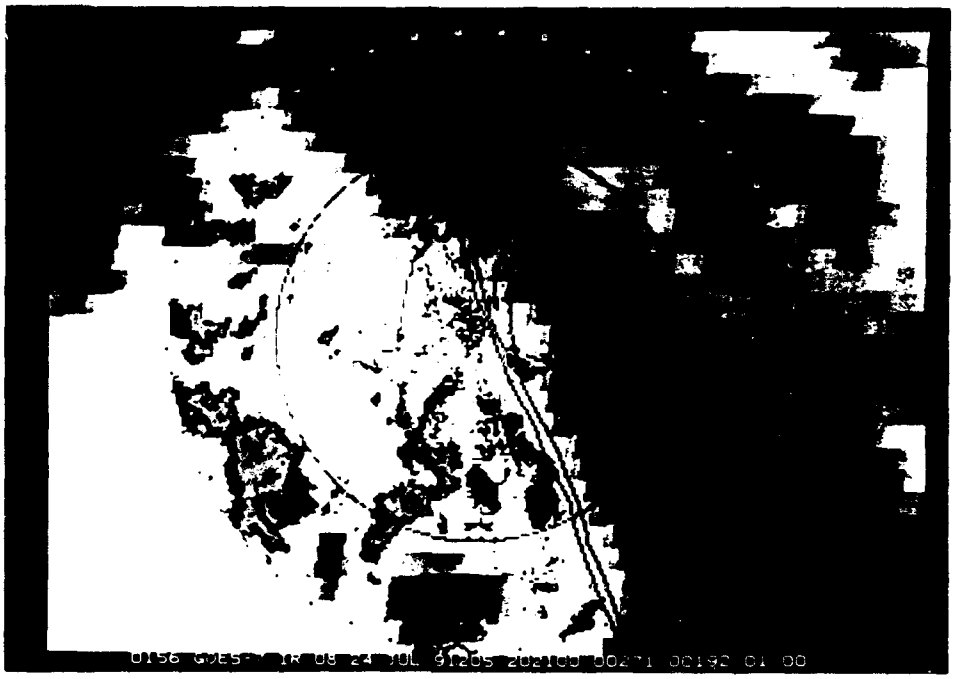

Figure 28g. Combined GOES/IR image and CP-4 Doppler radar reflectivity scan display - 24 July/2021Z.

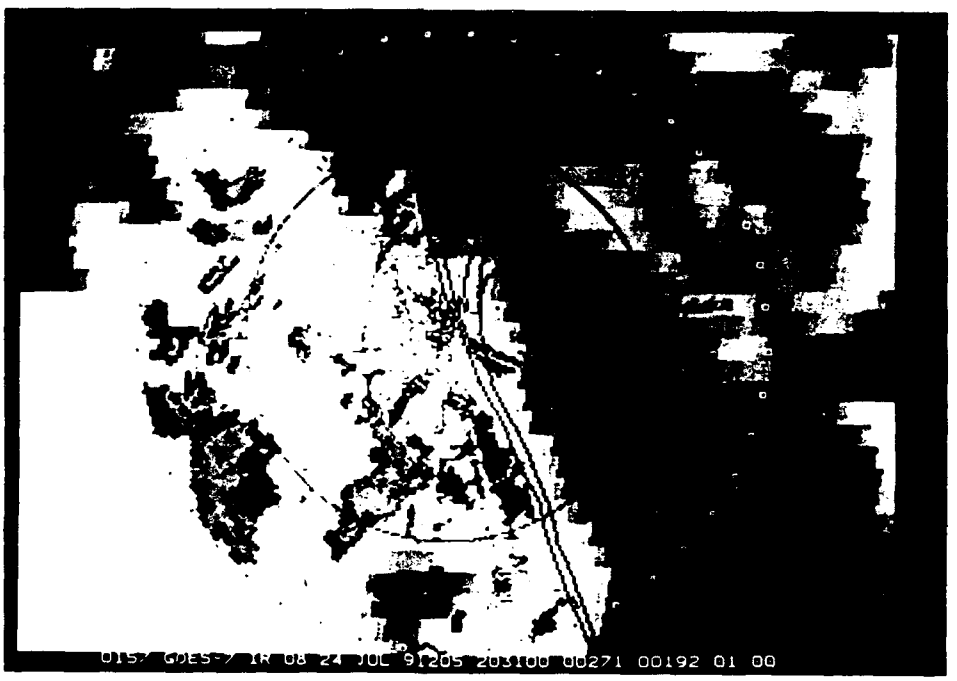

Figure 28h. Combined GOES/IR image and CP-4 Doppler radar reflectivity scan display - 24 July/2031Z.

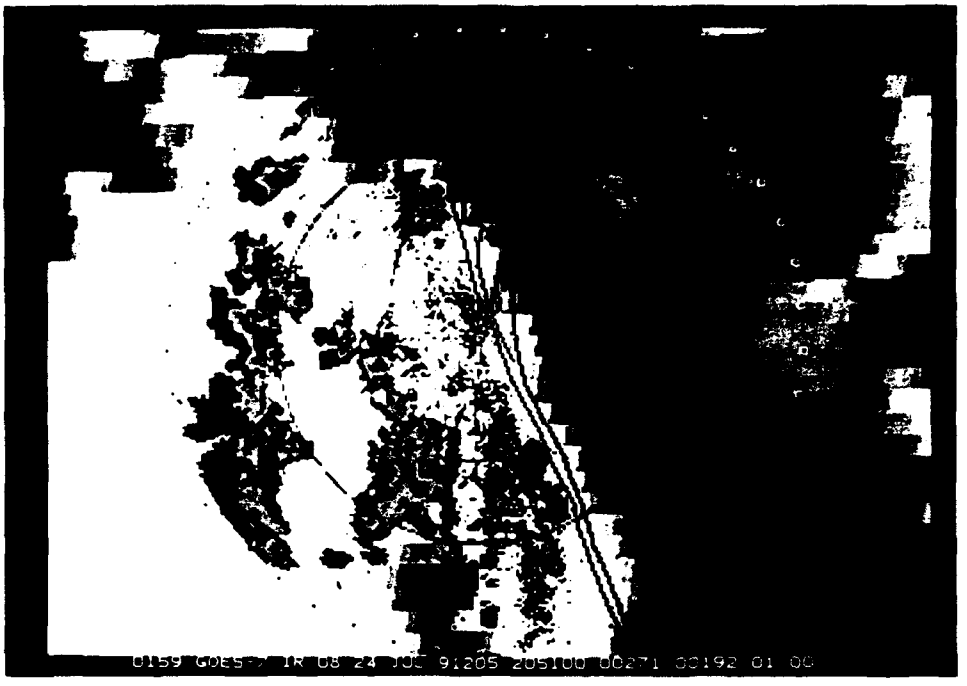

Figure 28i. Combined GOES/IR image and CP-4 Doppler radar reflectivity scan display - 24 July/2051Z.

Figure 28j. Combined GOES/IR image and CP-4 Doppler radar reflectivity scan display - 24 July/2131Z.

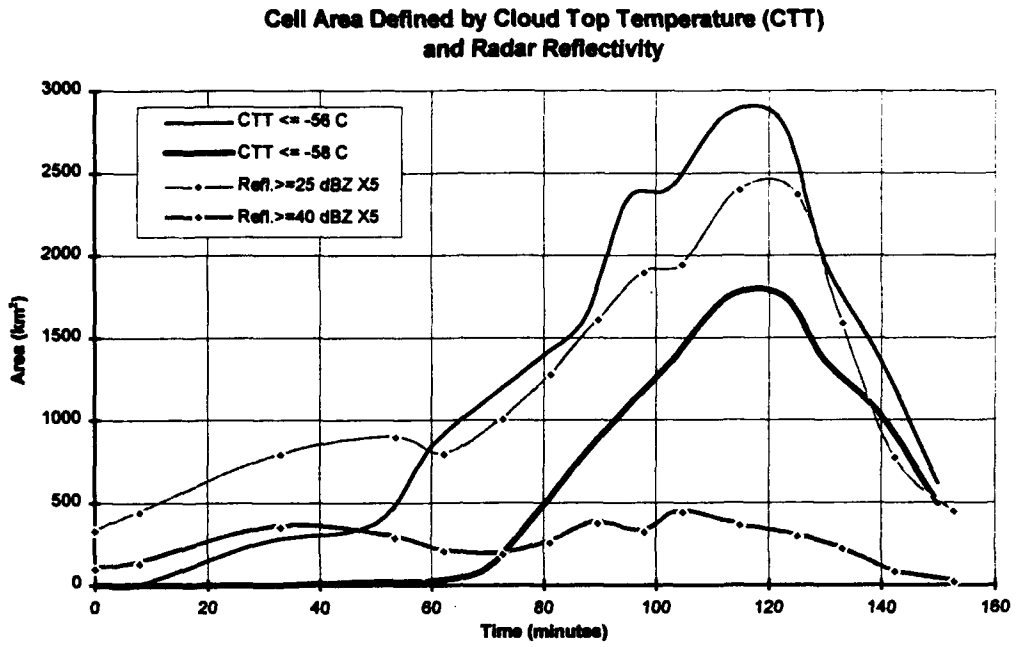

Figure 29a. Area of Cell #1 (Vero Beach) based on satellite derived cloud top temperature and radar reflectivity thresholded values versus time. The reflectivity values are multiplied by a factor of 5. The date/time at the origin is 24 July 91/1746Z.

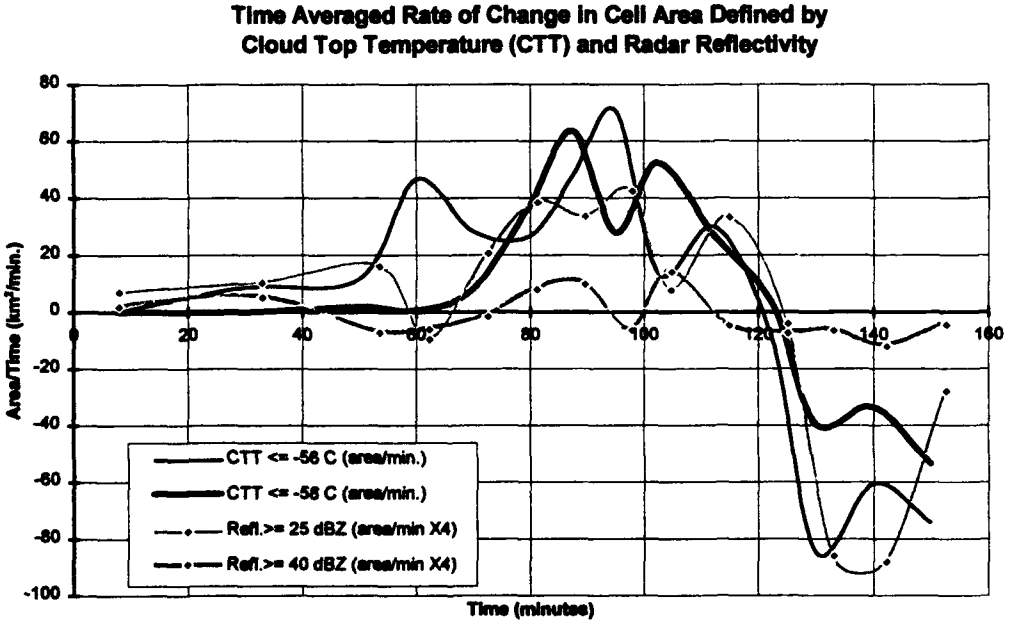

Figure 29b. Time averaged rate of change of the data in Figure 29a. The reflectivity values are multiplied by a factor of 5. The date/time at the origin is 24 July 91/1746Z.

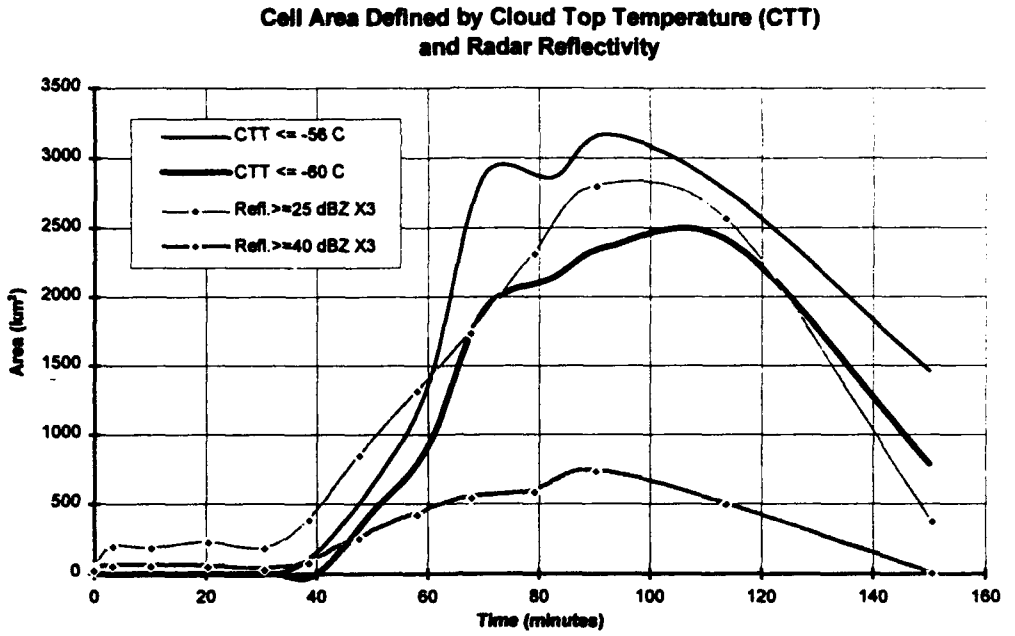

Figure 30a. Area of Cell #2 (Osceola Co.) based on satellite derived cloud top temperature and radar reflectivity thresholded values versus time. The reflectivity values are multiplied by a factor of 3. The date/time at the origin is 24 July 91/1916Z.

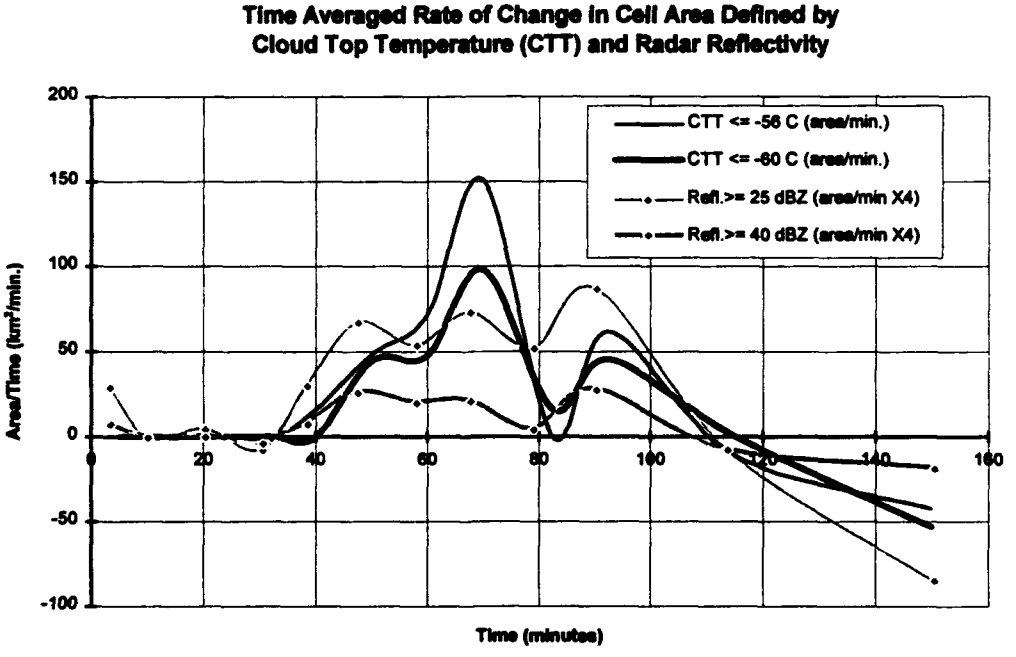

Figure 30b. Time averaged rate of change of the data in Figure 30a. The reflectivity values are multiplied by a factor of 3. The date/time at the origin is 24 July 91/1916Z.

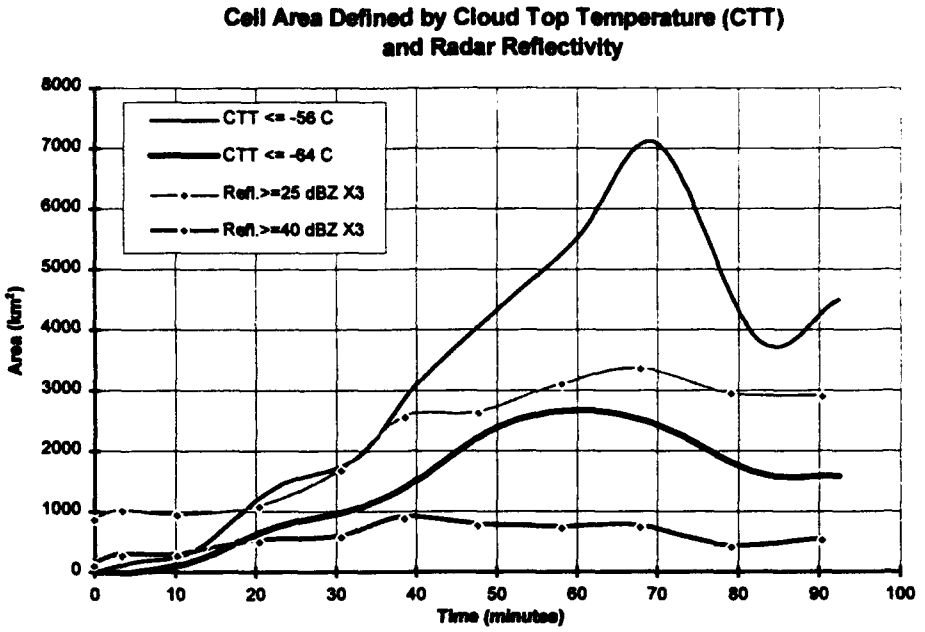

Figure 31a. Area of Cell #3 (Polk Co.) based on satellite derived cloud top temperature and radar reflectivity thresholded values versus time. The reflectivity values are multiplied by a factor of 3. The date/time at the origin is 24 July 91/1916Z.

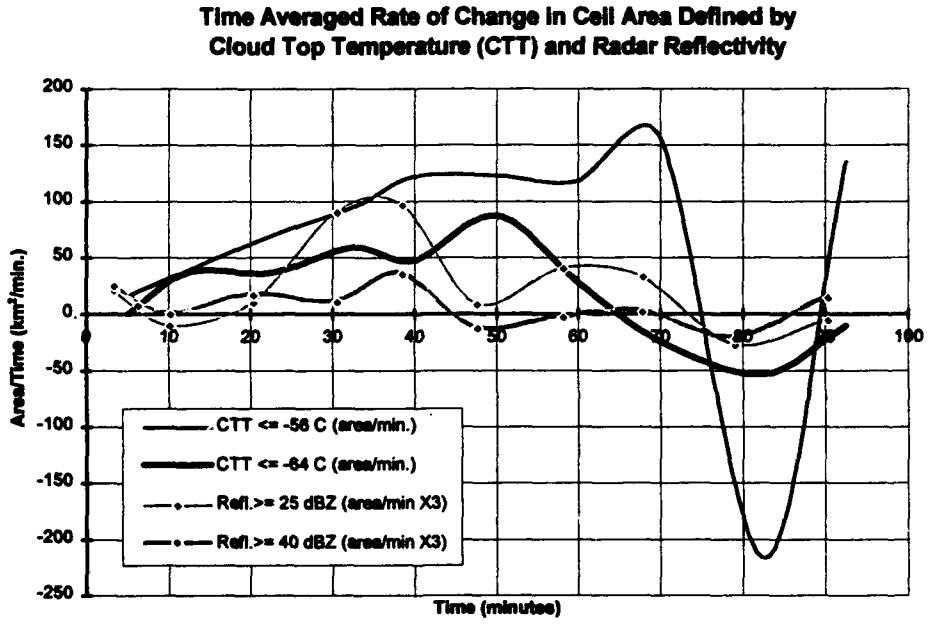

Figure 31b. Time averaged rate of change of the data in Figure 31a. The reflectivity values are multiplied by a factor of 3. The date/time at the origin is 24 July 91/1916Z.

3.2 Case Study #2: July 25, 1991 (1646-2316 UTC)

The primary synoptic upper level features in the southeast U.S. on July 25 were: a 200 mb high in the Atlantic off the Carolina coast, and a trough over Florida. The trough is evident at 500 mb by the cyclonic turning in the wind field over the Florida peninsula (Figure 32a). Southerly flow along the coast increased the mid-level moisture especially in the 700-500 mb level. The 1740Z Cape sounding (Figure 32c) shows this increase along with a 5-10 kt increase in the southwesterly winds up to 15 Kft from the prior day. Moderate-to-strong convection was expected from the sounding analyzed stability parameters, LI: -5.7 and CAPE of > 2000 J/kg. At the surface, the frontal boundary went stationary to the north of Virginia and west of Tennessee while the surface high pressure over the Atlantic built in slightly (Figure 32b). With the ridge axis remaining to the south of the Cape area, boundary layer winds were southwesterly. Wind flow from this direction over Florida tends to inhibit the inland penetration of the east coast sea breeze front. This typically leads to the development of a line of cumulus clouds and eventually an intense frontal zone parallel to and slightly inland from the coast (Wakimoto and Atkins, 1993).

Debris cloud from nocturnal thunderstorms originating off the Florida coasts prevented early heating and therefore shut down early development. While only weak convection developed over the Cape in the early afternoon, the more significant development began in the central portions of the state. Thunderstorms formed along a line from Daytona Beach through Tampa and from Melbourne southwestward. The storm just entering radar range approximately 72 miles west-northwest of Melbourne

(Figure 34a) produced winds which uprooted trees and downed power lines in southern Marion county. A wind gust of 58 kts was reported in Geneva, due to a cell developing in the cloud streets just west of cell #3 (Figures 33b,34e).

Cell #1 and #2 (Fort Pierce) data analysis: Remaining isolated for most of its lifetime, this cell was the easiest to analyze. For this reason, radar reflectivity data was collected from this cell at two different elevation angles: 0.3 degrees (cell #1) and 3.0 degrees (cell #2). The altitude difference of the echo at a range of 55 miles between the two antenna elevation angles is significant. Returns from the cell at 0.3 degrees are 1,540 ft above the ground, while an elevation angle of 3.0 degrees returns data at an altitude of 15,400 ft. A comparison of figures 35a and 36a shows the radar reflectivity area at the selected thresholds to be greater for the 3.0 degree elevation scan, or higher up in the storm. Achieving maximum area at the higher elevation scan lags the 0.3 degree scan's peak by approximately 5 minutes.

The development over Fort Pierce began on the east coast sea-breeze front and quickly intensified after 2000Z due to outflow from the dissipating cell to its northeast (Figures 34b,34c). At both elevation angles, the rate of change of the RR area reaches its maximum decrease rate just prior to the point of maximum increase in CTT area (Figures 35b,36b). The second peak in RR rate at 90-100 minutes is due to the cell merging with a cell to its north at 2131Z (Figures 33c,34g-j). At this point in time, the CTT information between the two cells merged, becoming indistinguishable. Although the RR area reached a maximum, the rate of change of CTT area continued to decrease

steadily. Radar data from the 3.0 degree elevation scan stops at 130 minutes due to sectors of no data on the radar scan starting at 2231Z (Figure 34i).

Cell #3 (Indian River/north KSC) data analysis: With weak penetration of the sea breeze in the strong southwest flow regime, cell #3 grew slowly within a group of northeast-southwest oriented cloud streets close to the coast (Figure 33a). A gust front from the storm due west of the CP-4 location intersected with this cell, beginning its intensification phase. The increase in area after 55 minutes (Figure 37a) is due to the cell expanding to include the developing storms in the neighboring cloud streets (Figures 33a-b,34d-g). The rate of change of area observed in CTT and RR increased concurrently during the period from 55 to 75 minutes (Figure 37b). After 120 minutes, the rate of change of radar echo area became positive while the rate-of-change in CTT area decreased steadily. This pattern, seen also in the evolution of cell #1, is perhaps due to convective precipitation becoming stratiform during the mature stage of the thunderstorm (Figure 34h-j). The cloud top typically descends during this phase (Figure 38).

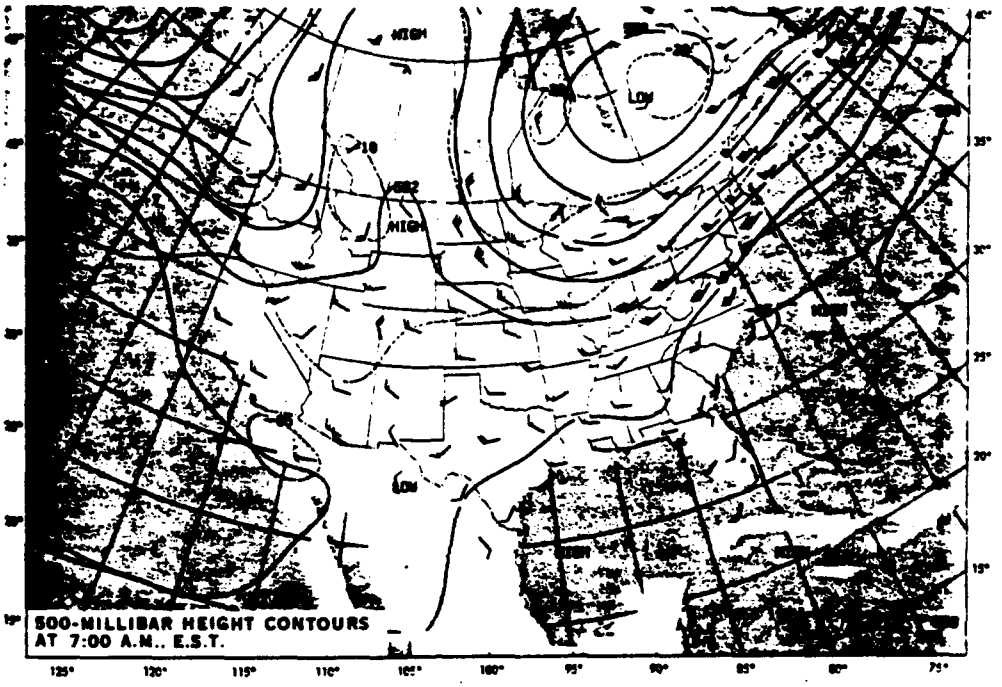

Figure 32a. 500mb height contours - 25 July 91/12Z (from Climate Analysis Center, Daily Weather Maps).

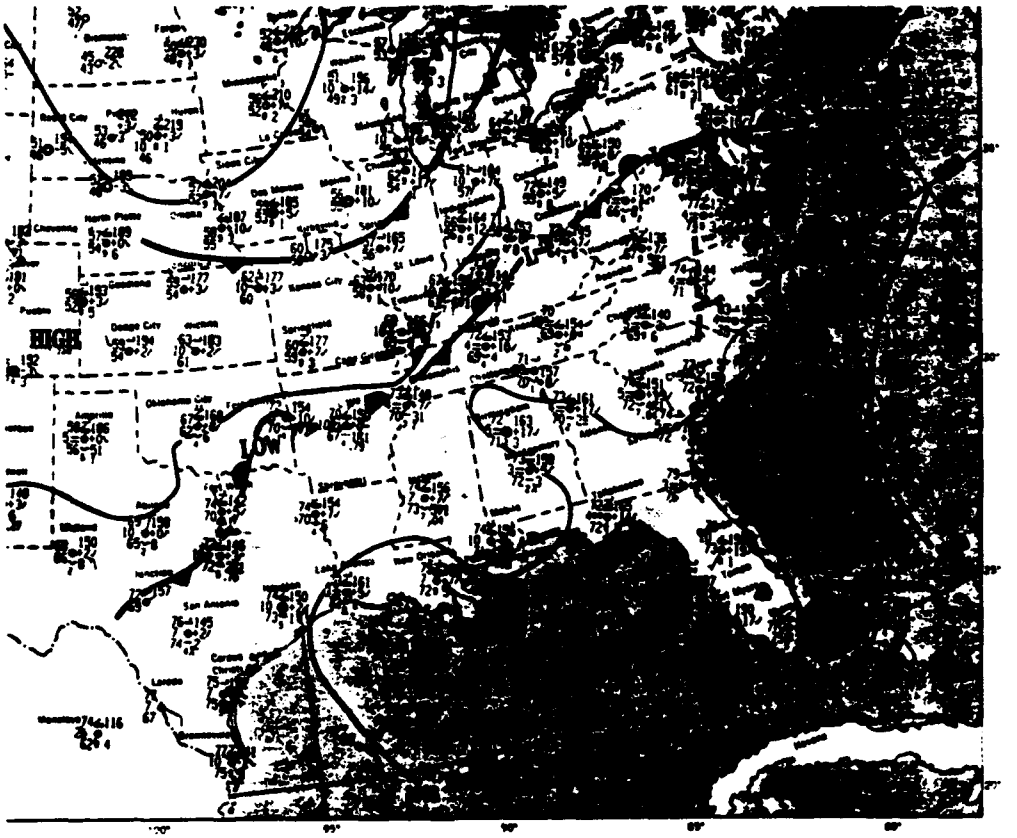

Figure 32b. Surface pressure analysis and station plots - 25 July 91/12Z (from Climate analysis Center, Daily Weather Maps).

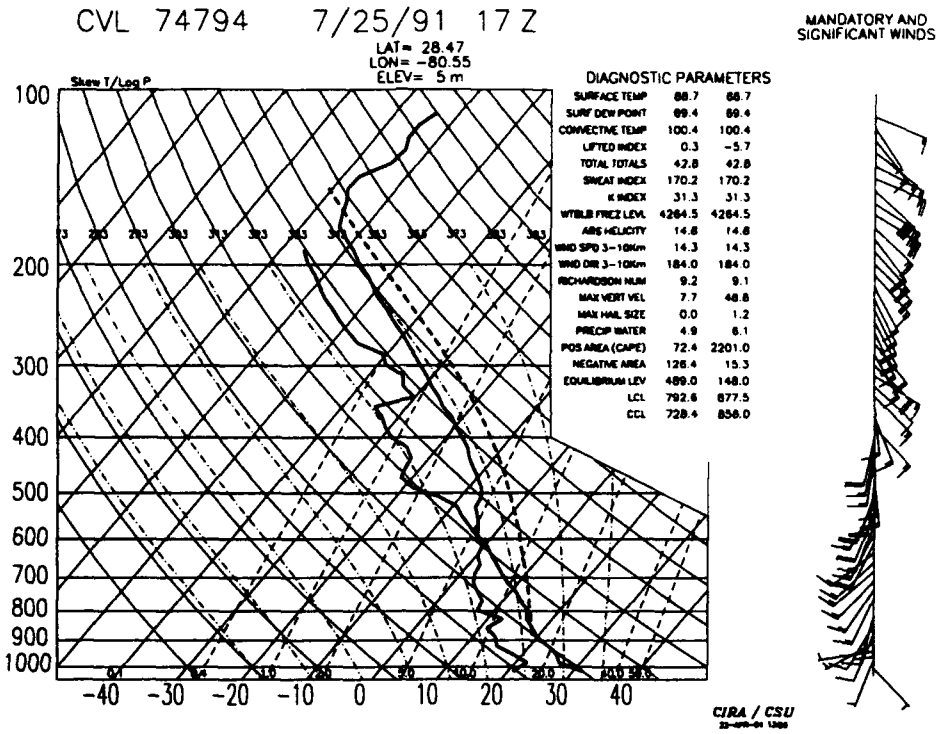

Figure 32c. Cape Canaveral AFS Skew-T - from 25 July 91/1740Z rawinsonde.

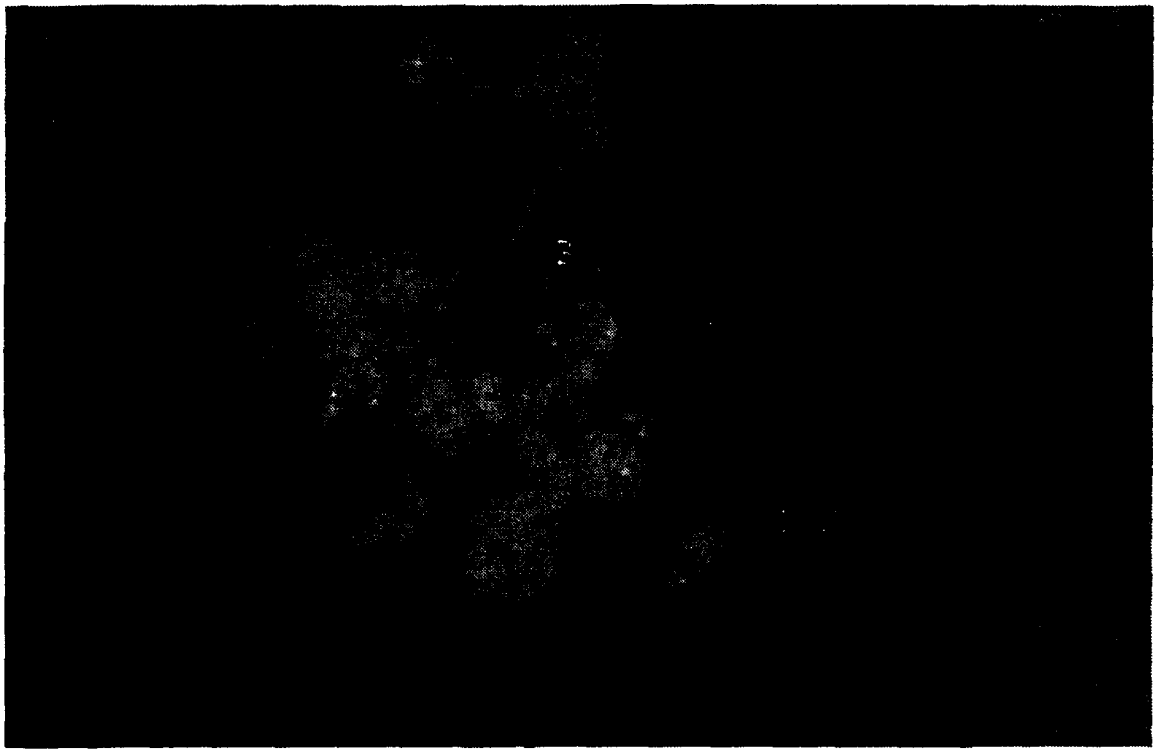

Figure 33a. GOES visible satellite image - 25 July 91/2016Z.

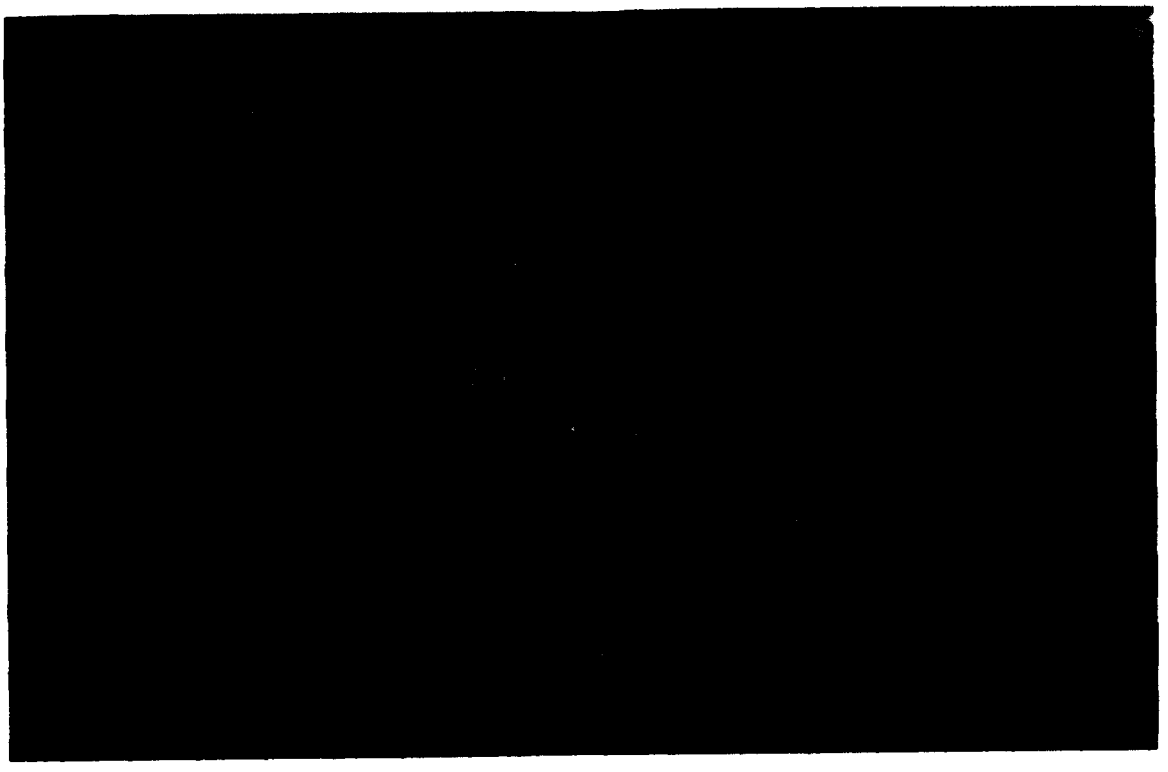

Figure 33b. GOES visible satellite image - 25 July 91/2056Z.

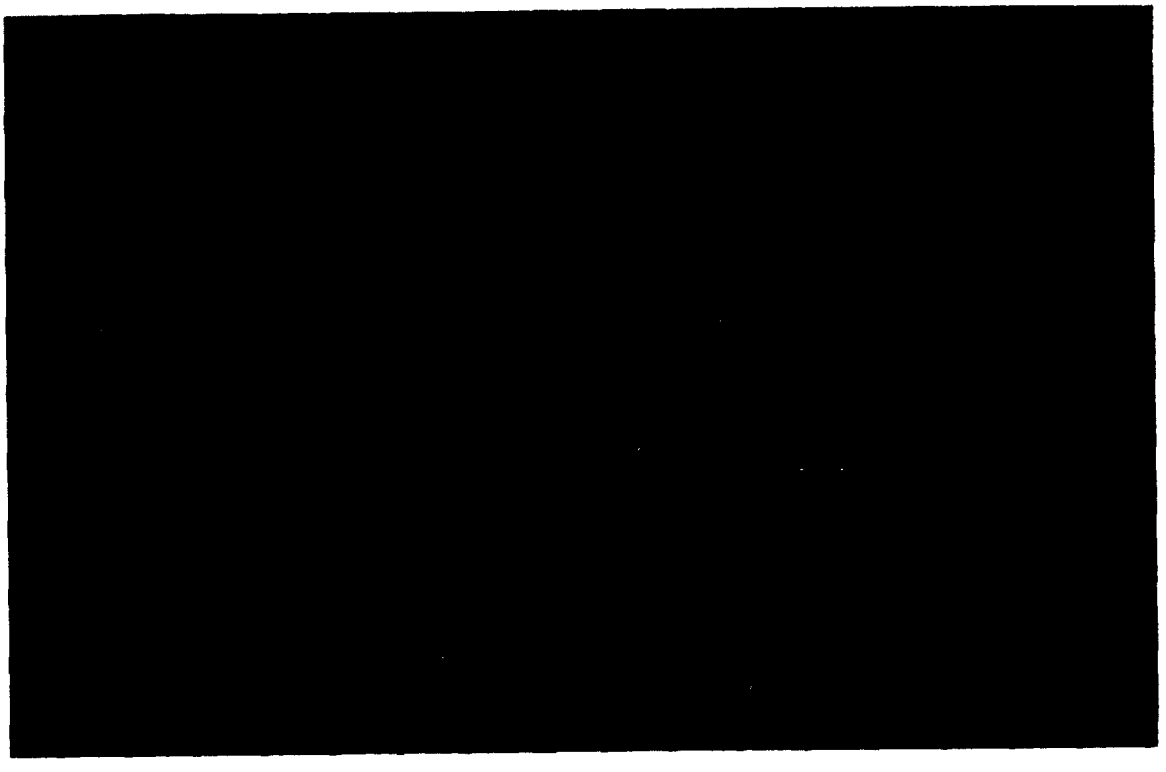

Figure 33c. GOES visible satellite image - 25 July 91/2131Z.

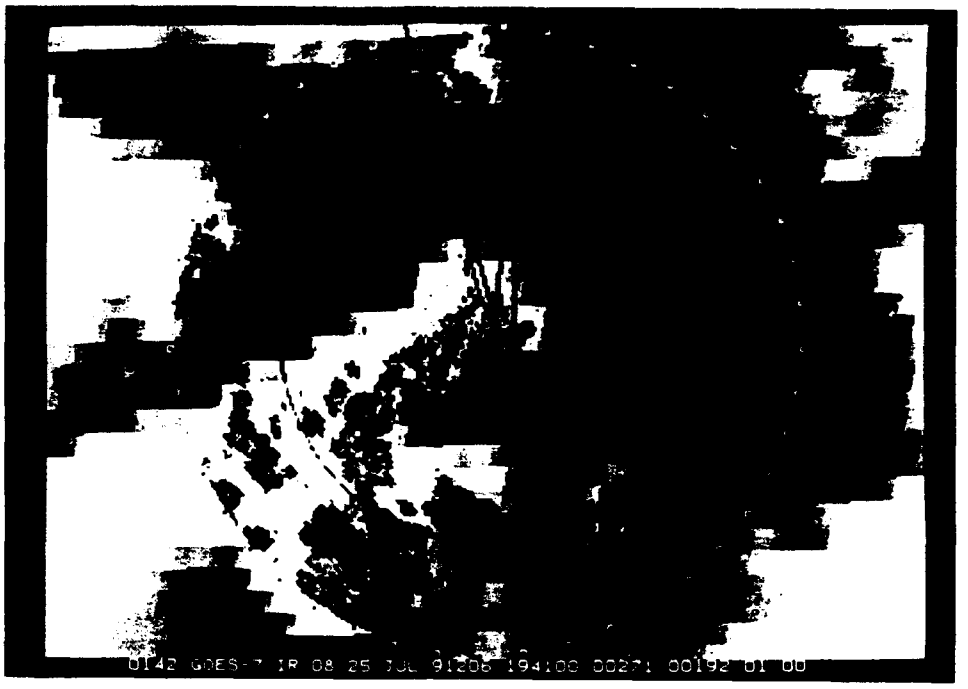

Figure 34a. Combined GOES/IR image and CP-4 Doppler radar reflectivity scan displays - 25 July 91/sequence loop from 1941Z-2246Z. Although more images are available and were used in the study, only 10 images are included for this time period.

Figure 34b. Combined GOES/IR image and CP-4 Doppler radar reflectivity scan display - 25 July/2001Z.

Figure 34c. Combined GOES/IR image and CP-4 Doppler radar reflectivity scan display - 25 July/2016Z.

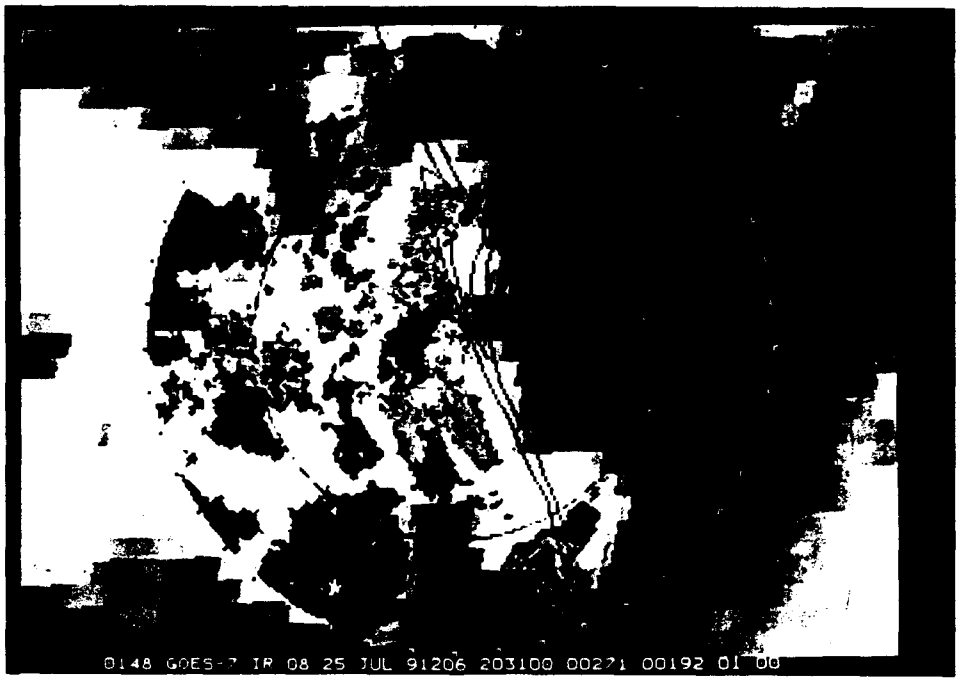

Figure 34d. Combined GOES/IR image and CP-4 Doppler radar reflectivity scan display - 25 July/2031Z.

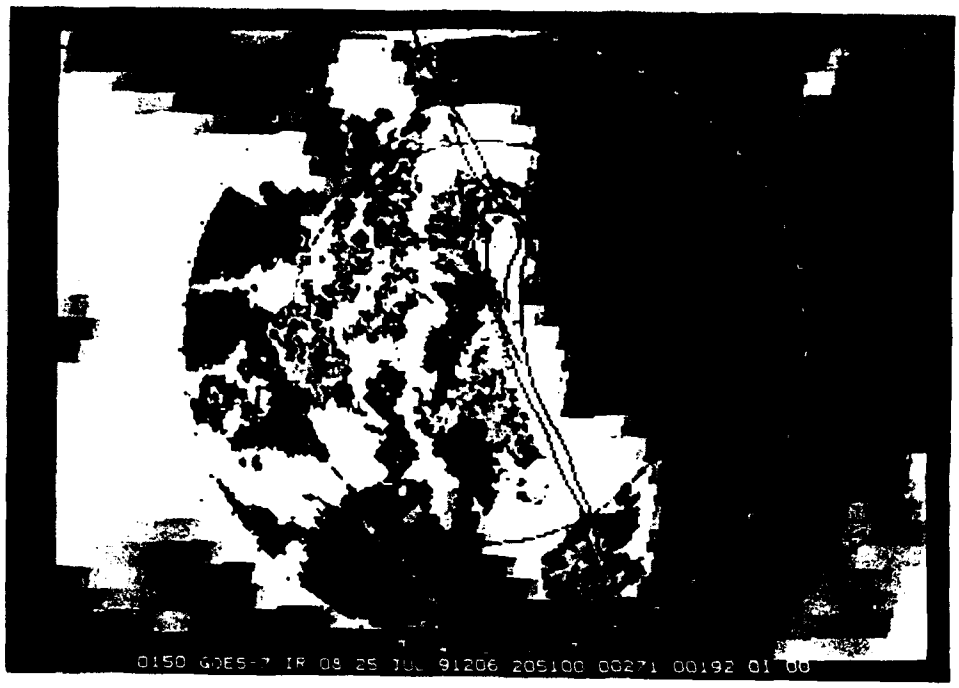

Figure 34e. Combined GOES/IR image and CP-4 Doppler radar reflectivity scan display - 25 July/2051Z.

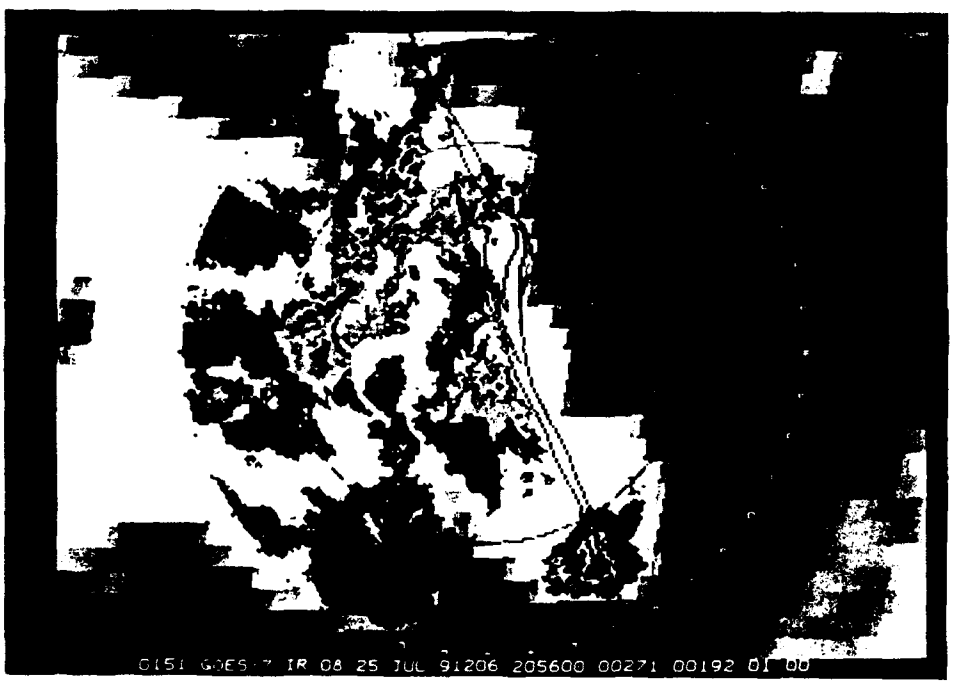

Figure 34f. Combined GOES/IR image and CP-4 Doppler radar reflectivity scan display - 25 July/2056Z.

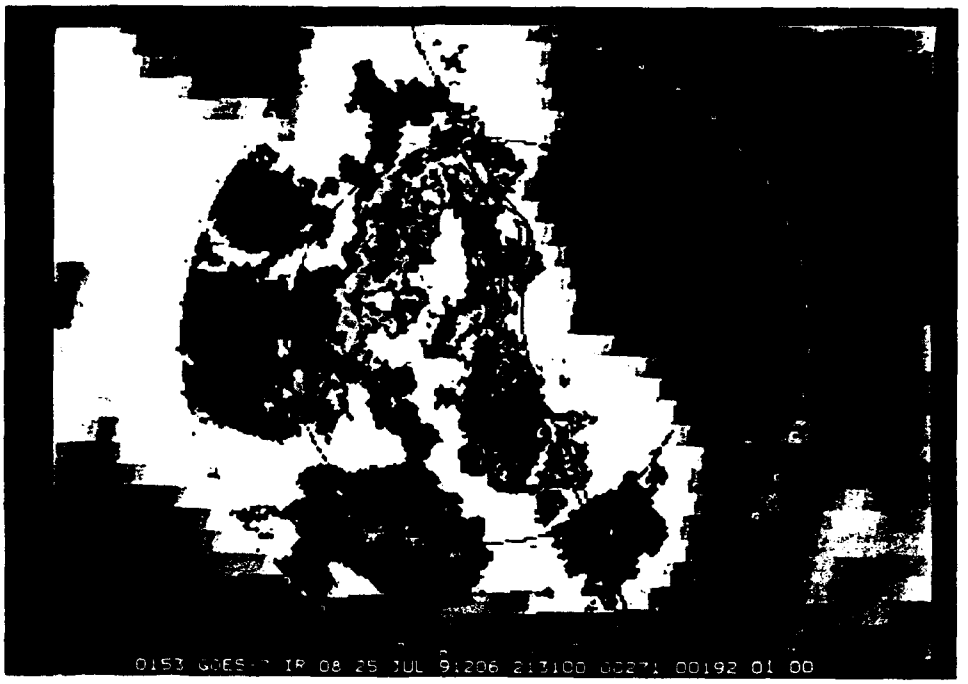

Figure 34g. Combined GOES/IR image and CP-4 Doppler radar reflectivity scan display - 25 July/2131Z.

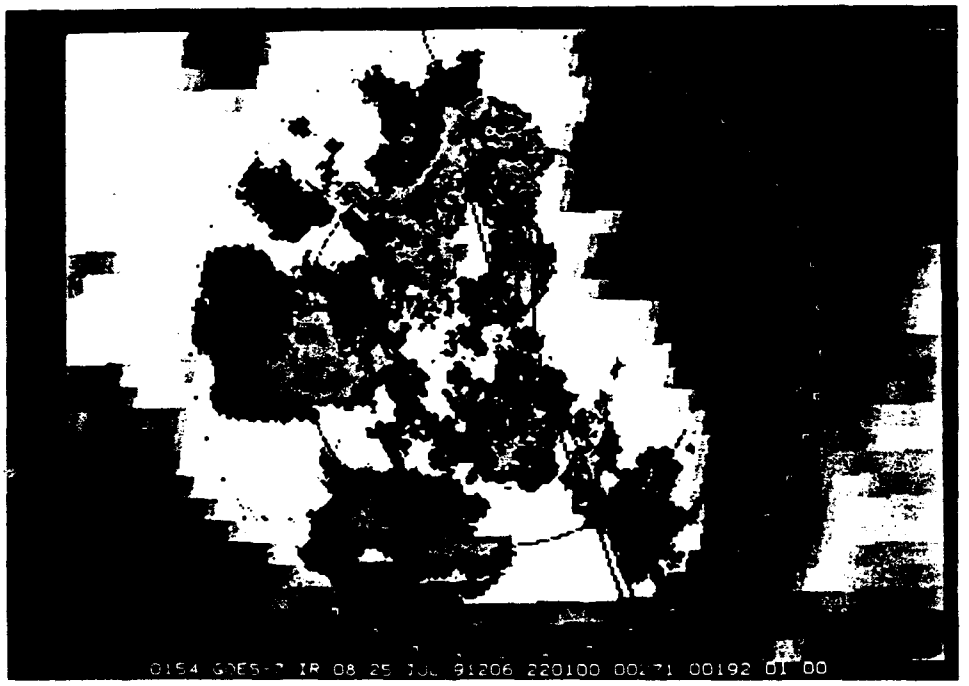

Figure 34h. Combined GOES/IR image and CP-4 Doppler radar reflectivity scan display - 25 July/2201Z.

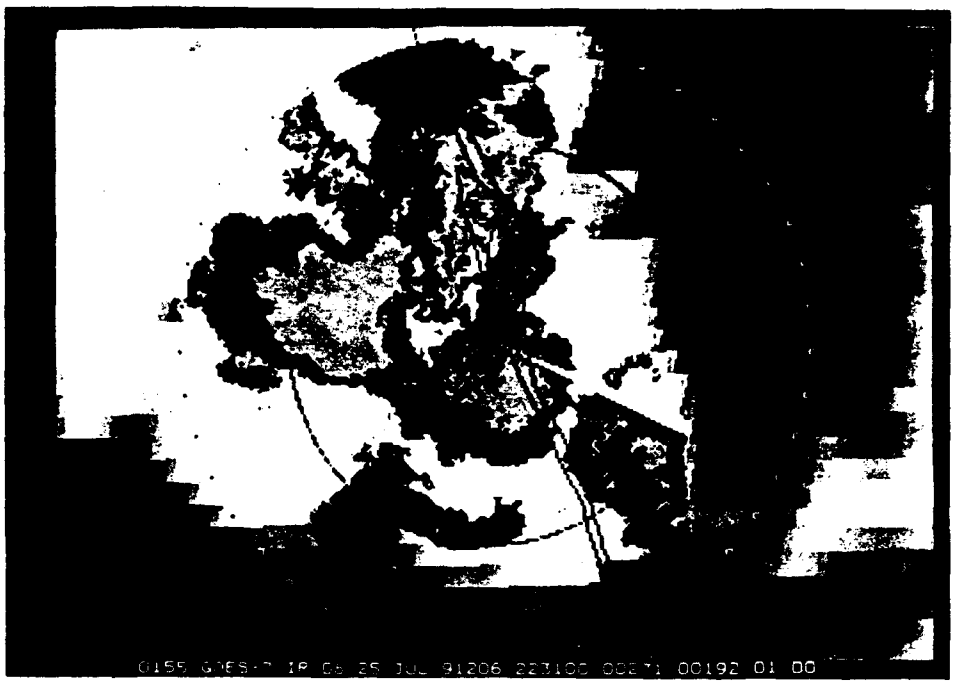

Figure 34i. Combined GOES/IR image and CP-4 Doppler radar reflectivity scan display - 25 July/2231Z.

Figure 34j. Combined GOES/IR image and CP-4 Doppler radar reflectivity scan display - 25 July/2246Z.

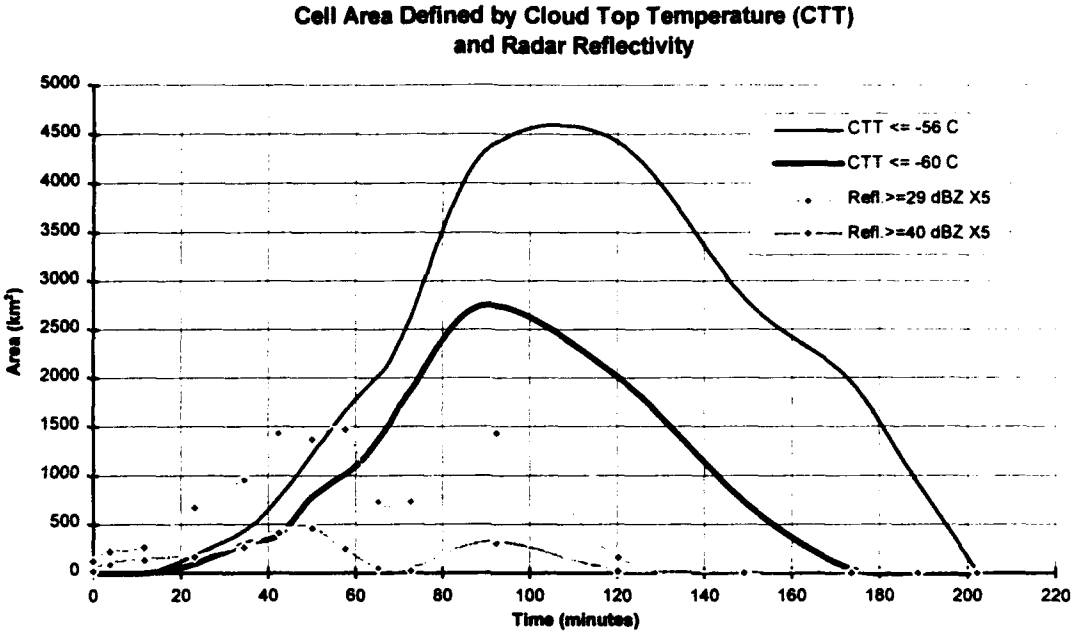

Figure 35a. Area of Cell #1 (Fort Pierce) based on satellite derived cloud top temperature and radar reflectivity thresholded values versus time. The reflectivity values are multiplied by a factor of 5. The date/time at the origin is 25 July 91/1946Z.

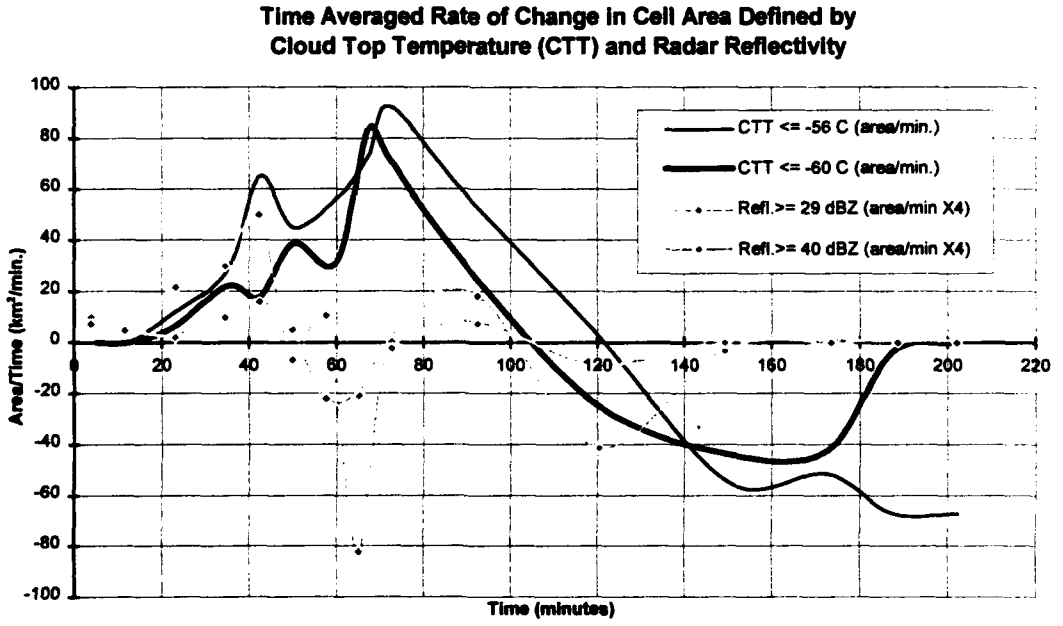

Figure 35b. Time averaged rate of change of the data in Figure 35a. The reflectivity values are multiplied by a factor of 4. The date/time at the origin is 25 July 91/1946Z.

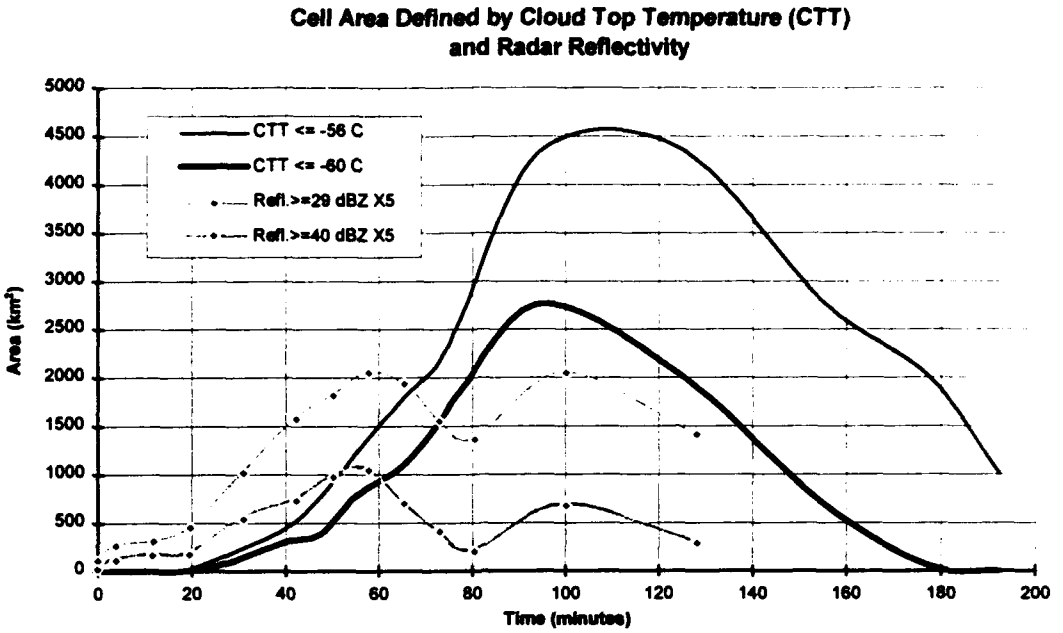

Figure 36a. Area of Cell #2 (same cell as #1, except using 3.0 degree elevation scan) based on satellite derived cloud top temperature and radar reflectivity thresholded values versus time. The reflectivity values are multiplied by a factor of 5. The date/time at the origin is 25 July 91/1941Z.

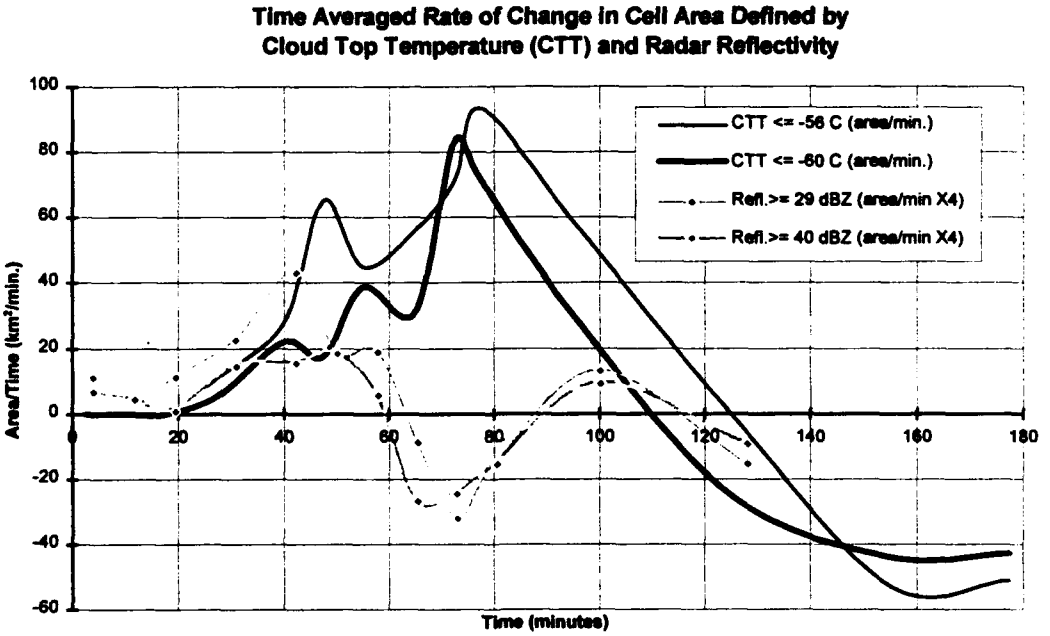

Figure 36b. Time averaged rate of change of the data in Figure 36a. The reflectivity values are multiplied by a factor of 4. The date/time at the origin is 25 July 91/1941Z.

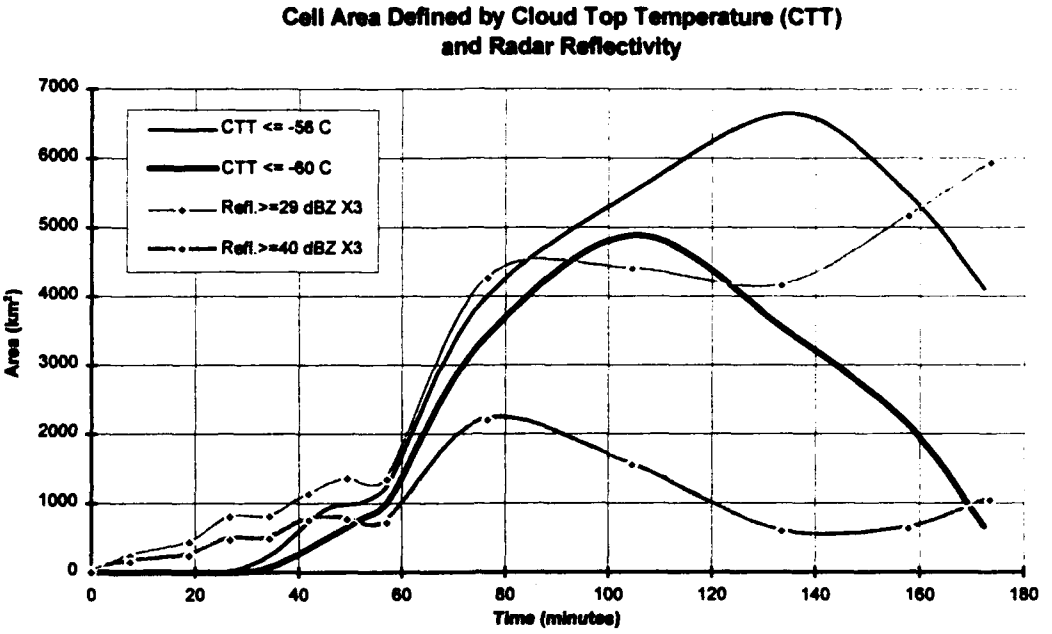

Figure 37a. Area of Cell #3 (Indian R./N. KSC) based on satellite derived cloud top temperature and radar reflectivity thresholded values versus time. The reflectivity values are multiplied by a factor of 3. The date/time at the origin is 25 July 91/2001Z.

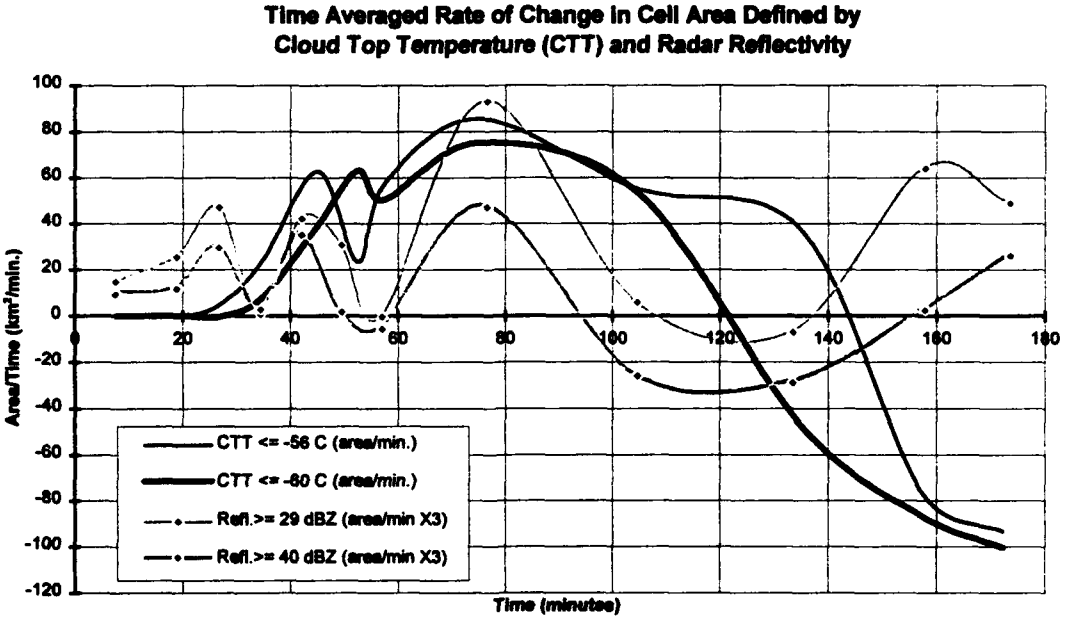

Figure 37b. Time averaged rate of change of the data in Figure 37a. The reflectivity values are multiplied by a factor of 3. The date/time at the origin is 25 July 91/2001Z.

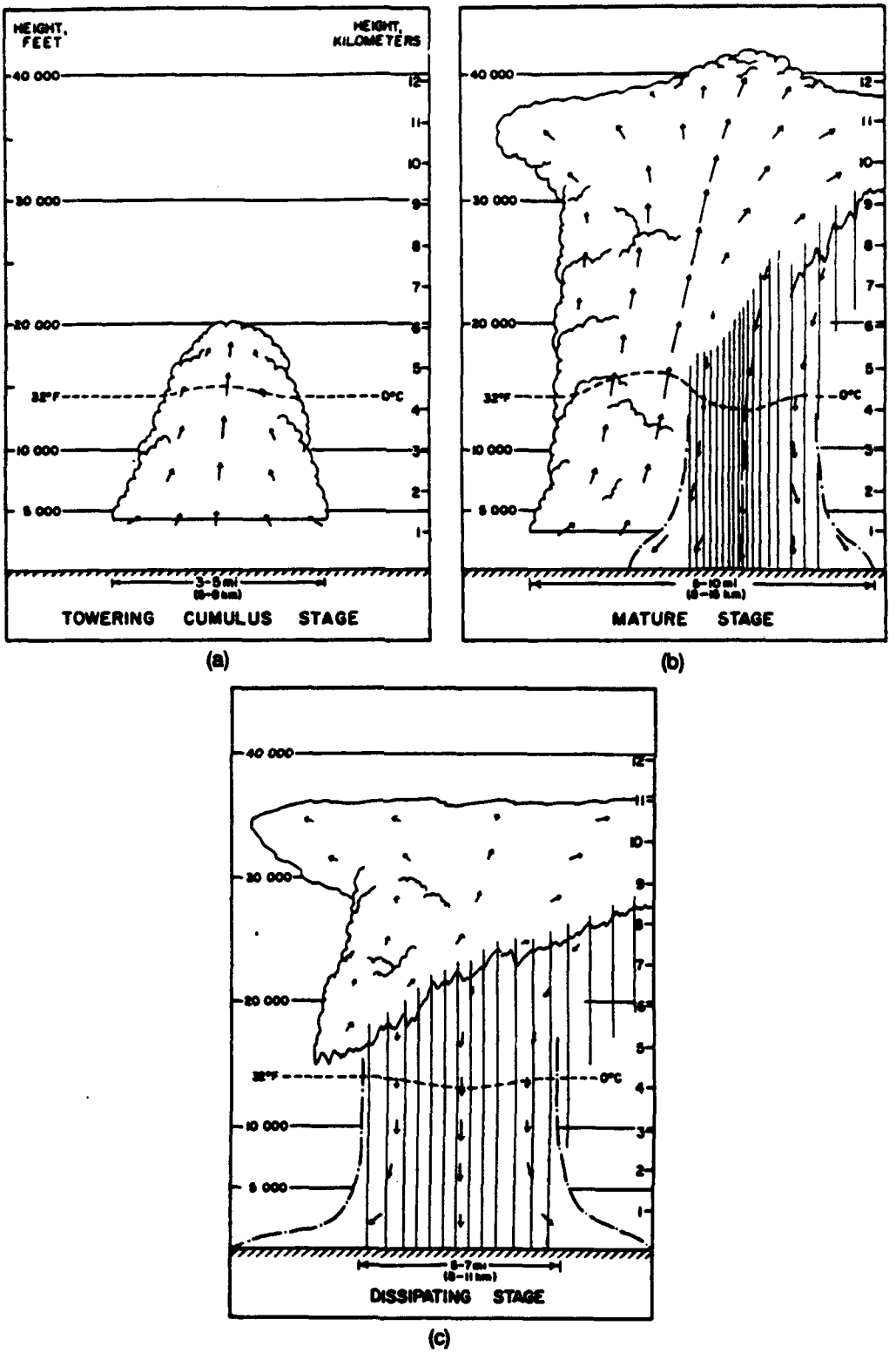

Figure 38. The Byers-Braham model of the three stages in the life of a thunderstorm: a) towering cumulus stage, b) mature stage, c) dissipating stage. In stage c) note the decreasing altitude of the cloud top and the stratification of precipitation (from Bluestein, 1993).

3.3 Case Study #3: July 26, 1991 (1731-2101 UTC)

Southwesterly steering flow and a weak upper trough persist. The 500 mb trough is once again evident by the cyclonic turning of the winds along the Alabama-Georgia border and southward on through central Florida (Figure 39a). The surface front in the mid-Atlantic states pushed slowly southward to just north of Alabama-Mississippi. The surface high built into south Florida with the ridge axis remaining to the south of Cape Canaveral through Fort Myers (Figure 39b). The 1531Z Cape sounding shows unstable conditions with southwesterly steering flow at 10-15 kts and a large amount of moisture (Figure 39c).

Nocturnal convection once again occurred off the Florida coast. The first thunderstorms during the day formed in the west coast sea breeze near Tampa Bay and in the north-central portions of the state. After 18Z, a broken line of convection developed from Mosquito Lagoon (north of KSC) southwestward to a point southeast of Tampa (Figures 40a, 41c). The cells in this synoptically driven line were moving to the northeast while the line continued to advance southeast. The cells developed or intensified as they intersected with the east coast sea breeze front creating some intense thunderstorms (Figures 40b-c, 41g-l). A thunderstorm wind gust of 58 mph from cell #4 (Figure 40a) was reported at the KSC shuttle landing facility early in the afternoon. The line of convection continued moving south throughout the afternoon initiating strong convection and leaving behind an area of stratiform precipitation. At 2200Z, the Vero Beach airport sustained damage to three parked planes due to thunderstorm winds.

Cell #1 (S. Osceola Co.) data analysis: Observation of this cell began at 1931Z after it completely entered the southwest limit of radar range (Figures 40b, 41i). The 85 minutes of available data only followed this cell through part of its intensification phase (Figure 42a). The initial RR peak in this figure leads the start of the CTT (-69°C) increase by 10 minutes. Approximately 15 minutes separates the dip in the middle of both plots. The two maximum peaks in the RR time rate of change in cell area plots at 43 and 55 minutes precede similar peaks in CTT by approximately 15-18 minutes (Figure 42b).

Cell #2 (St. Cloud) data analysis: Began as a small cell at 1731Z approximately 40 miles NW of Melbourne near St. Cloud. By 1841Z it became a line with >48 dBZ returns at its northeast end (Figures 40a, 41d) and its growth in RR area leveled off (Figure 43a). The CTT area meanwhile was increasing rapidly until shortly after 1900Z (or 95 minutes). The decrease in the rate-of-change of the CTT area from +25 km^2/min. to -135 km^2/min. in a 10-minute period (Figure 43b) is possibly due to analysis error. This type of rapid drop in CTT area is uncharacteristic unless the storm cell is dissipating. The second rapid drop in Figure 39b indicates the true dissipation of the storm cell. At this time, outflow from this cell raced to the east and collided with cell #3 (Figures 41i-l) and the cell #2 dissipated (Figures 40b-c). Ignoring the exaggerated drop in CTT area, previously observed patterns are seen in Figure 43b. Increasing rates of change in CTT area are preceded by a moderate increase in radar reflectivity area during the first 50 minutes. Also, the two points of maximum rate of change in area based on CTT (-55°C) at 85 and 115 minutes lag those based on RR (at 80 and 102 minutes). Finally, the maximum

negative rate of change of RR (40 dBZ) occurs 5-10 minutes before the corresponding CTT negative change rate of -120 km^2/minute (Figure 43b).

Cell #3 (Titusville) data analysis: After two hours this cell finally began to grow appreciably in area both in CTT and RR (Figure 40a). Located downstream of cell #2, its growth at the 120 minute point is a result of the St. Cloud cell's outflow (Figures 40b-c,41i-l) and collision with south-east moving cell #4 (Figures 40a-c,41e-i). A peak in rate of change in RR area at 98 minutes in Figure 44b precedes the start of the increasing CTT change in area rates. No other correlations can truly be made between the CTT and reflectivity data after this point. Perhaps this is due to the complex interactions occurring during this period. Observation of this cell was terminated at 2031Z because of its interaction with a cell directly over the "blind spot" of the radar (Figures 40c, 41m).

Cell #4 (Mosquito Lagoon) data analysis: Initiating on the sea breeze, this cell began rapid growth at the start of the data set (Figures 40a, 41a-d). After this initial 50 minute growth, the CTT area defined by -55°C remained generally constant at 1100 km^2 (Figure 45a) until the southern portion of the cell was "overtaken" by cell #3. The northern portion of the cell #4 simultaneously experienced growth in reflectivity area (Figures 41f-h) followed closely by an increase in CTT area. The net effect of this interaction is shown graphically in Figure 45b between the 95 and 115 time period, or from 1856Z to 1916Z (Figures 41e-h). By 1946Z this cell had almost completely dissipated on radar.

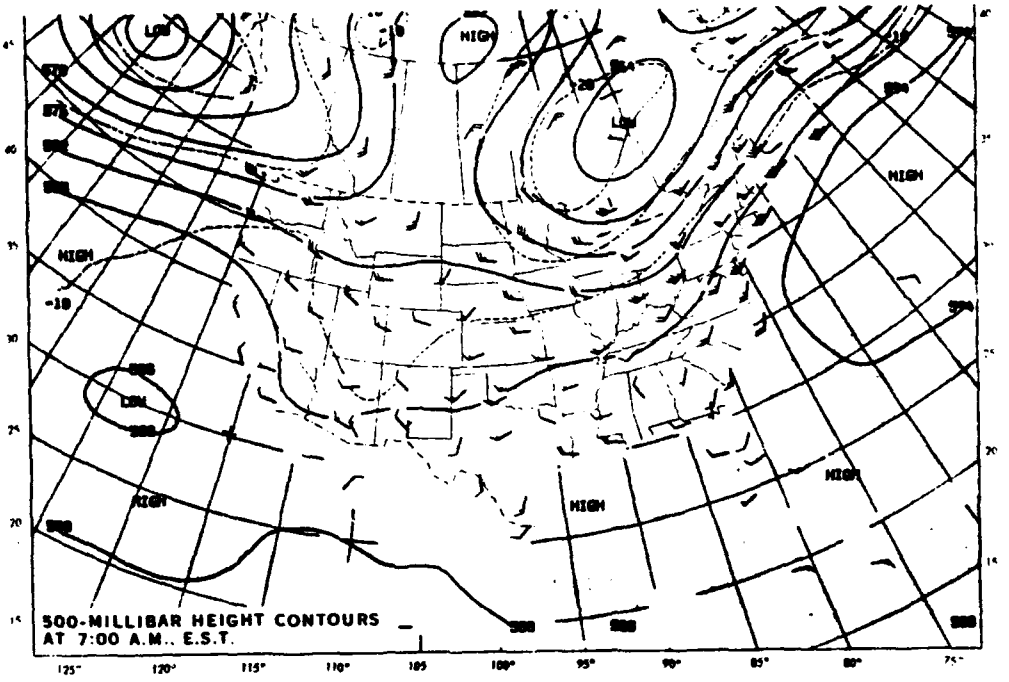

Figure 39a. 500mb height contours - 26 July 91/12Z (from Climate Analysis Center, Daily Weather Maps).

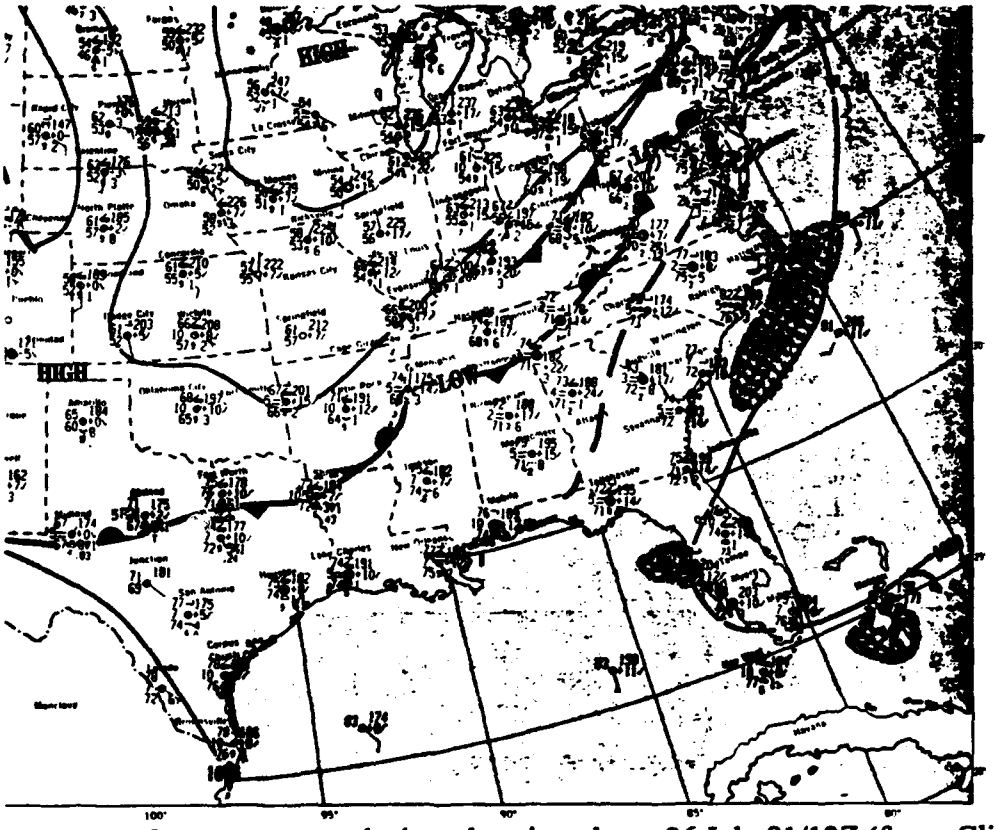

Figure 39b. Surface pressure analysis and station plots - 26 July 91/12Z (from Climate Analysis Center, Daily Weather Maps).

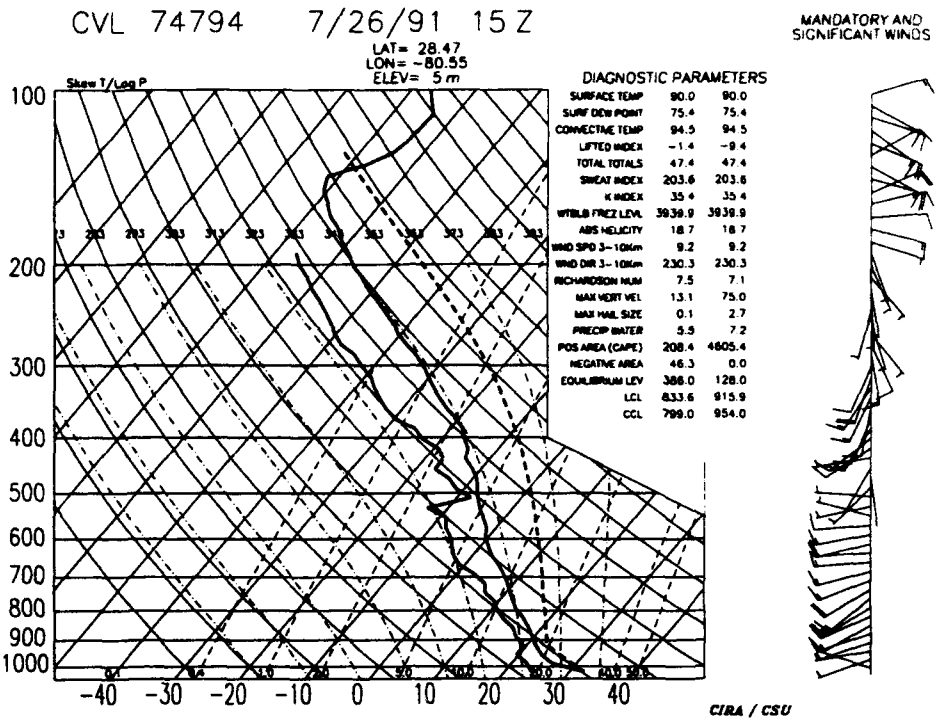

Figure 39c. Cape Canaveral AFS Skew-T - from 26 July 91/1531Z rawinsonde.

Figure 40a. GOES visible satellite image - 26 July 91/1841Z.

Figure 40b. GOES visible satellite image - 26 July 91/1941Z.

Figure 40c. GOES visible satellite image - 26 July 91/2041Z.

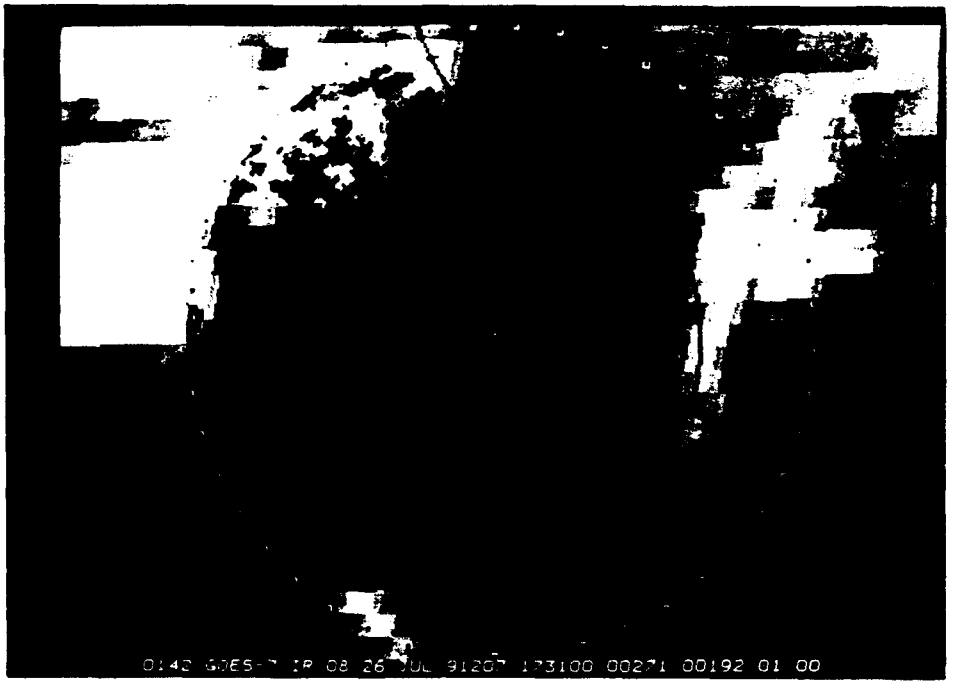

Figure 41a. Combined GOES/IR image and CP-4 Doppler radar reflectivity scan displays - 26 July 91/sequence loop from 1731Z-2101Z. Although more images are available and were used in the study, only 14 images are included for this time period.

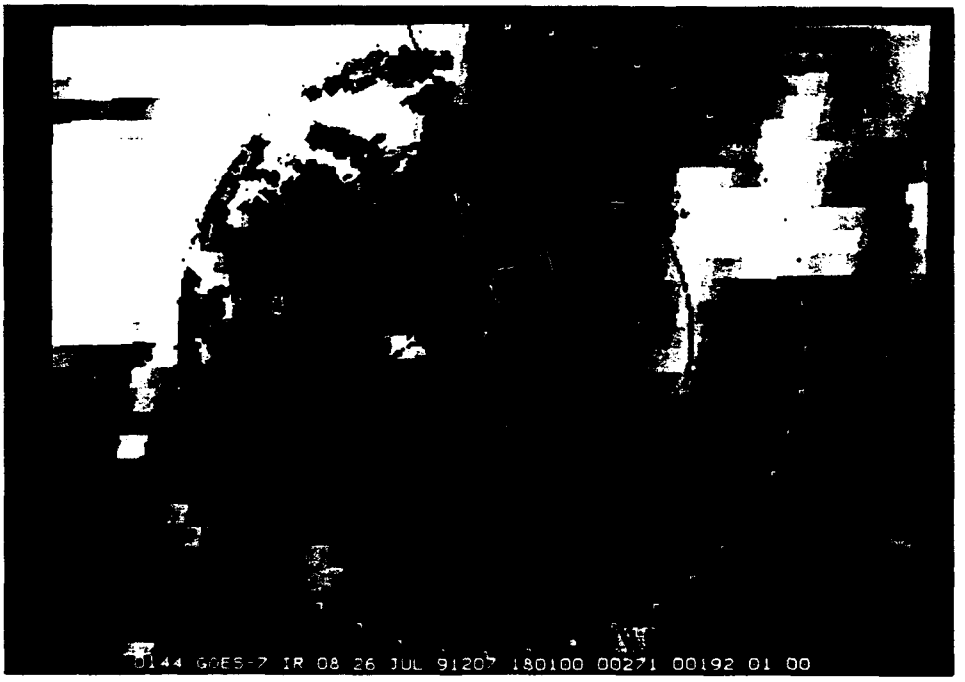

Figure 41b. Combined GOES/IR image and CP-4 Doppler radar reflectivity scan display - 26 July/1801Z.

Figure 41c. Combined GOES/IR image and CP-4 Doppler radar reflectivity scan display - 26 July/1831Z.

Figure 41d. Combined GOES/IR image and CP-4 Doppler radar reflectivity scan display - 26 July/1841Z.

Figure 41e. Combined GOES/IR image and CP-4 Doppler radar reflectivity scan display - 26 July/1856Z.

Figure 41f. Combined GOES/IR image and CP-4 Doppler radar reflectivity scan display - 26 July/1901Z.

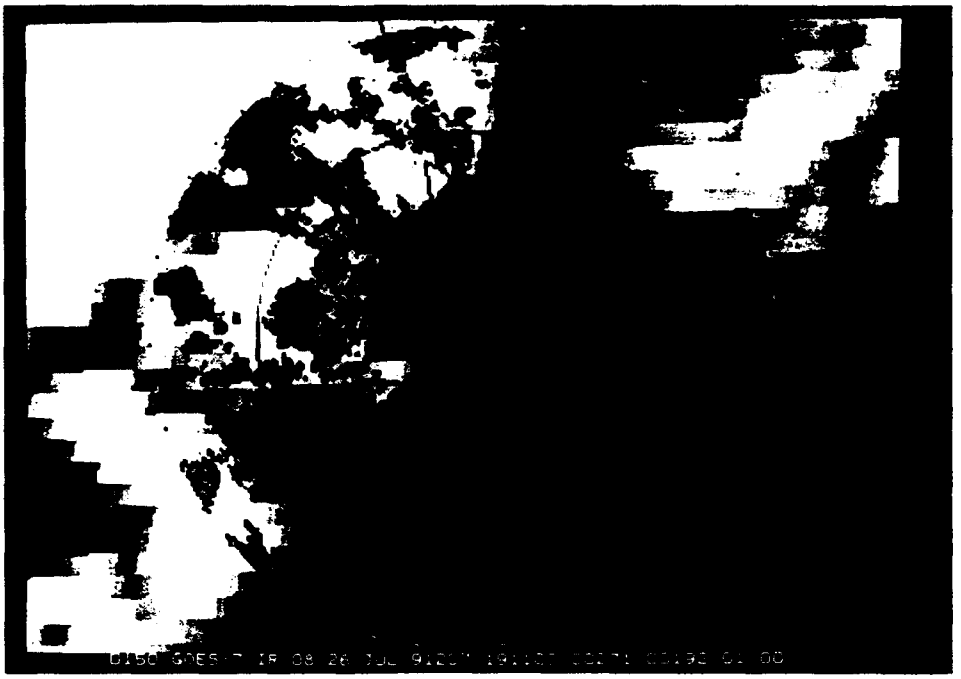

Figure 41g. Combined GOES/IR image and CP-4 Doppler radar reflectivity scan display - 26 July/1911Z.

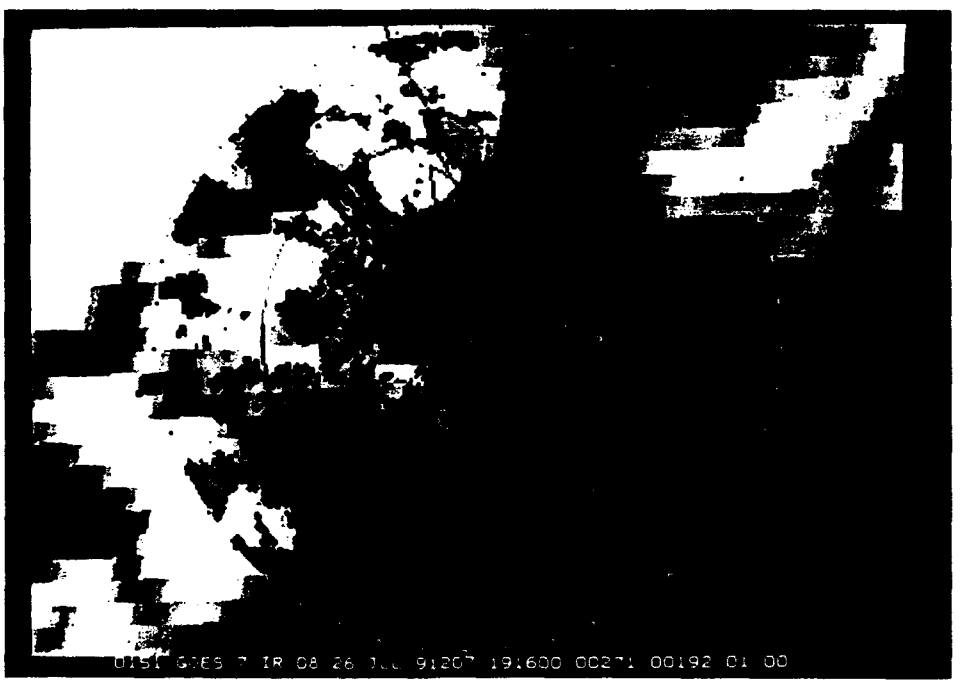

Figure 41h. Combined GOES/IR image and CP-4 Doppler radar reflectivity scan display - 26 July/1916Z.

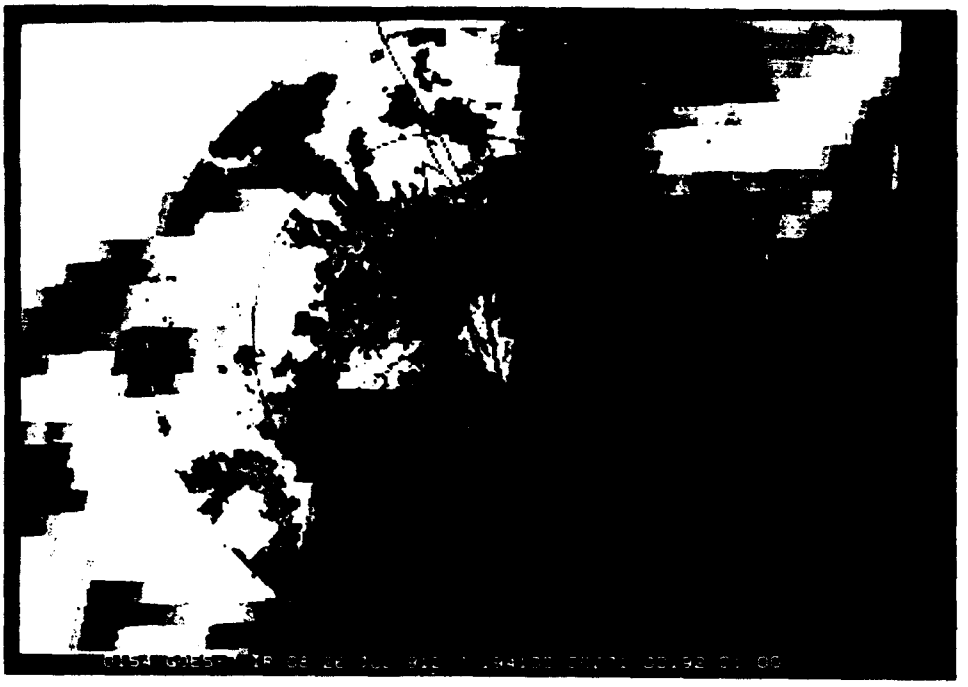

Figure 41i. Combined GOES/IR image and CP-4 Doppler radar reflectivity scan display - 26 July/1941Z.

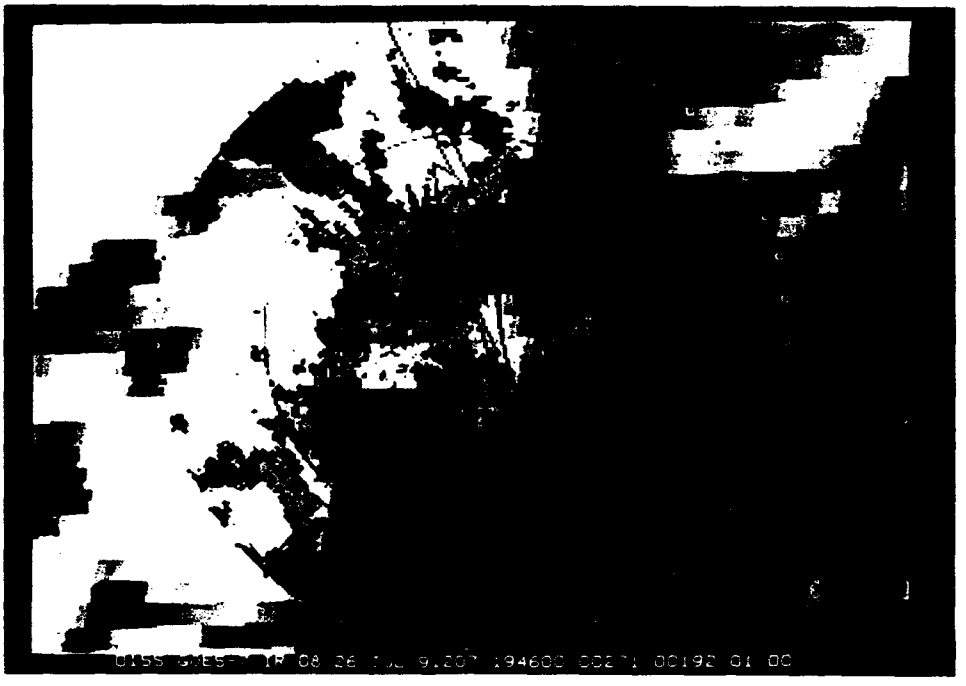

Figure 41j. Combined GOES/IR image and CP-4 Doppler radar reflectivity scan display - 26 July/1946Z.

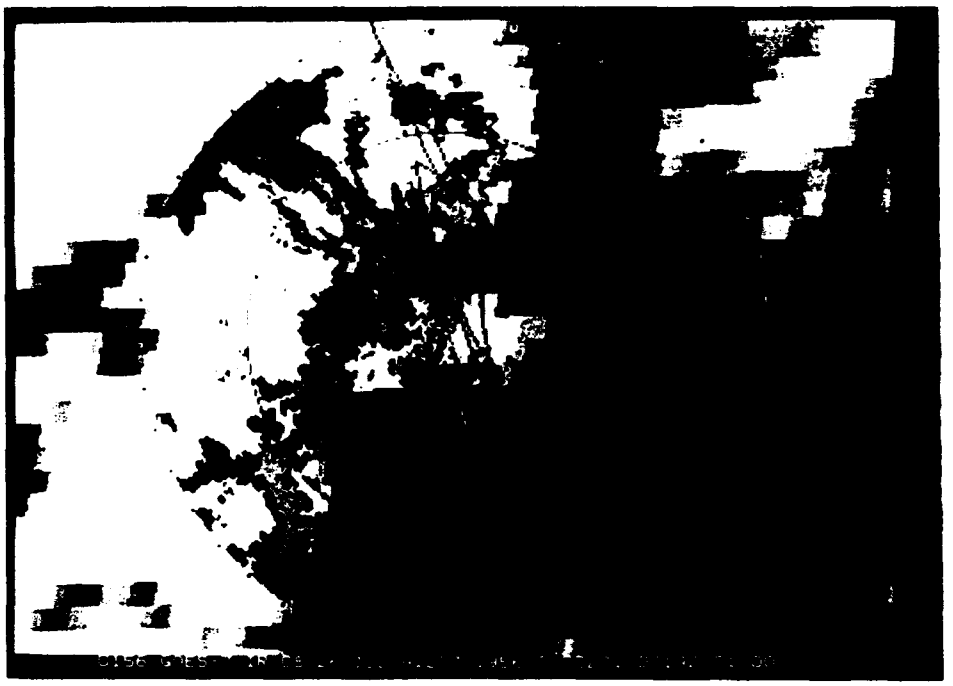

Figure 41k. Combined GOES/IR image and CP-4 Doppler radar reflectivity scan display - 26 July/1956Z.

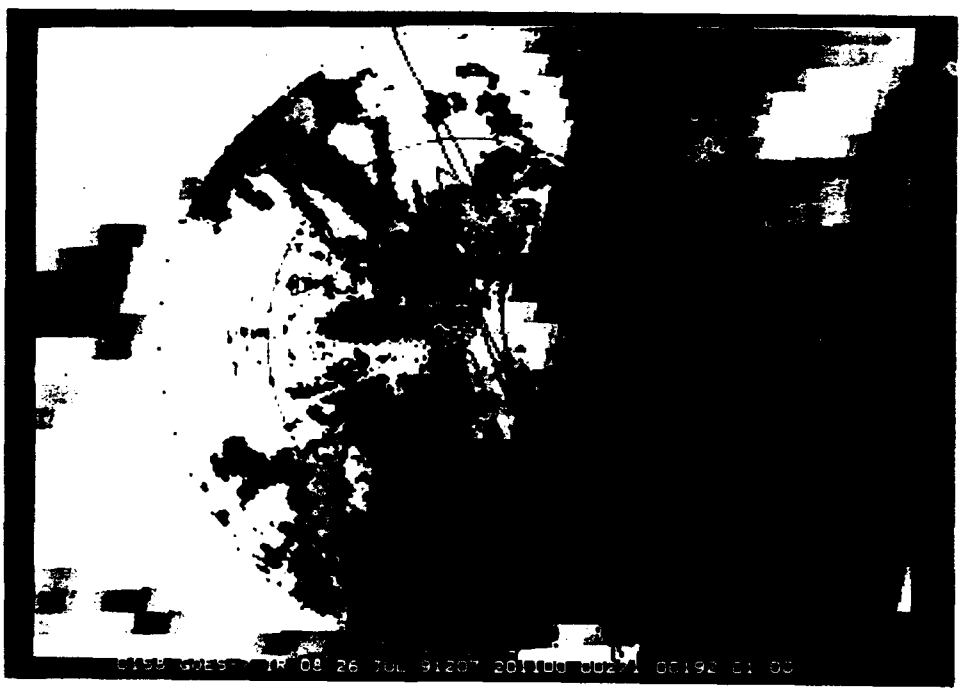

Figure 41l. Combined GOES/IR image and CP-4 Doppler radar reflectivity scan display - 26 July/2011Z.

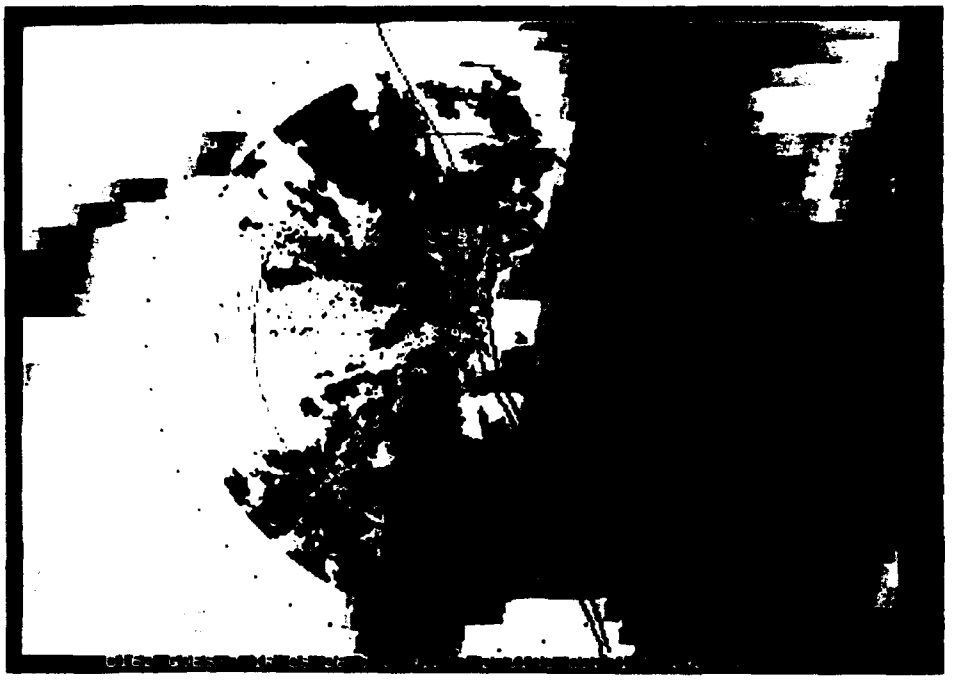

Figure 41m. Combined GOES/IR image and CP-4 Doppler radar reflectivity scan display - 26 July/2031Z.

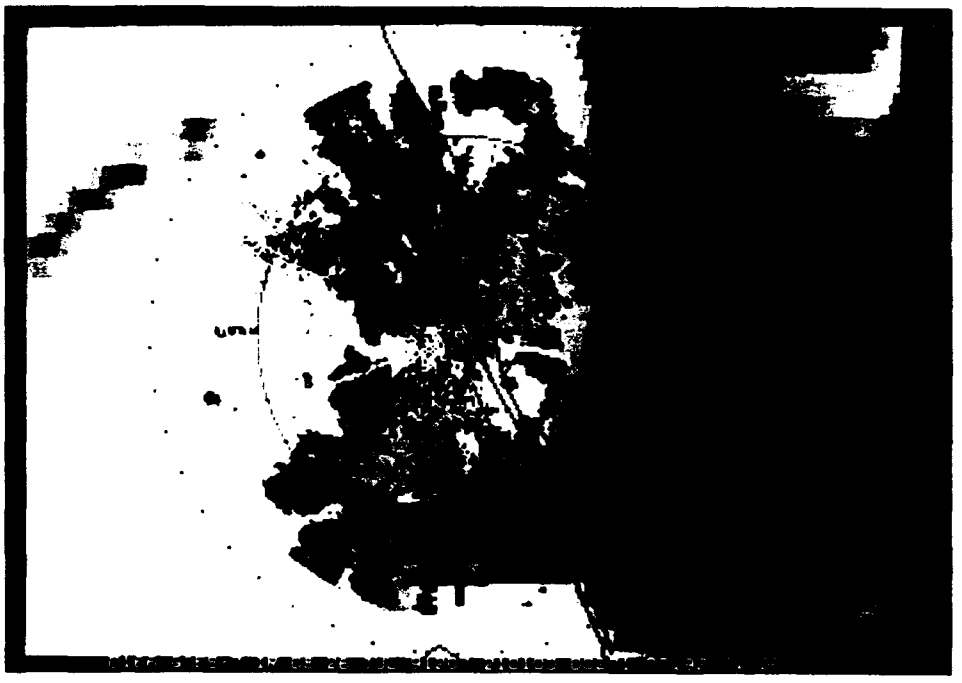

Figure 41n. Combined GOES/IR image and CP-4 Doppler radar reflectivity scan display - 26 July/2101Z.

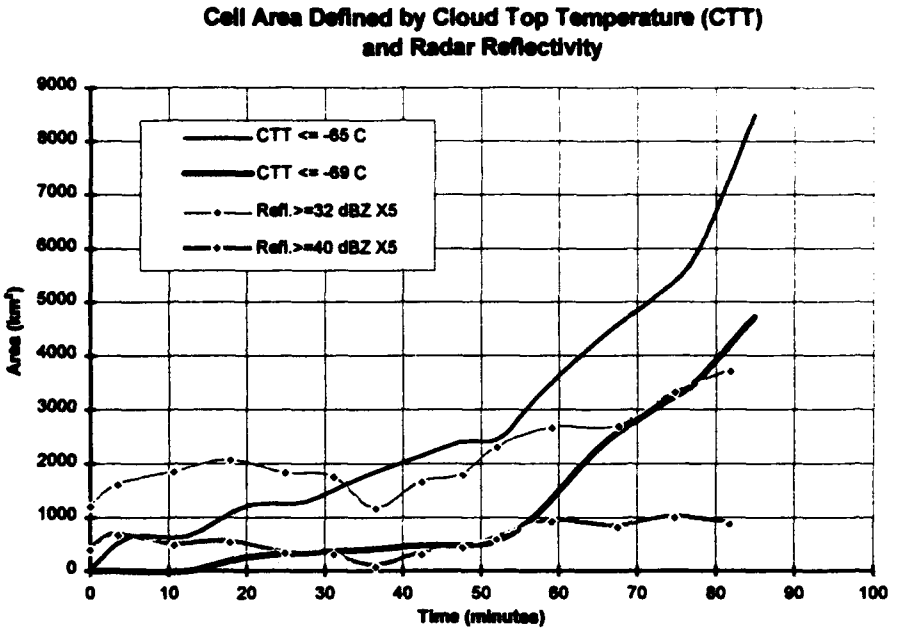

Figure 42a. Area of Cell #1 (S. Osceola Co.) based on satellite derived cloud top temperature and radar reflectivity thresholded values versus time. The reflectivity values are multiplied by a factor of 5. The date/time at the origin is 26 July 91/1931Z.

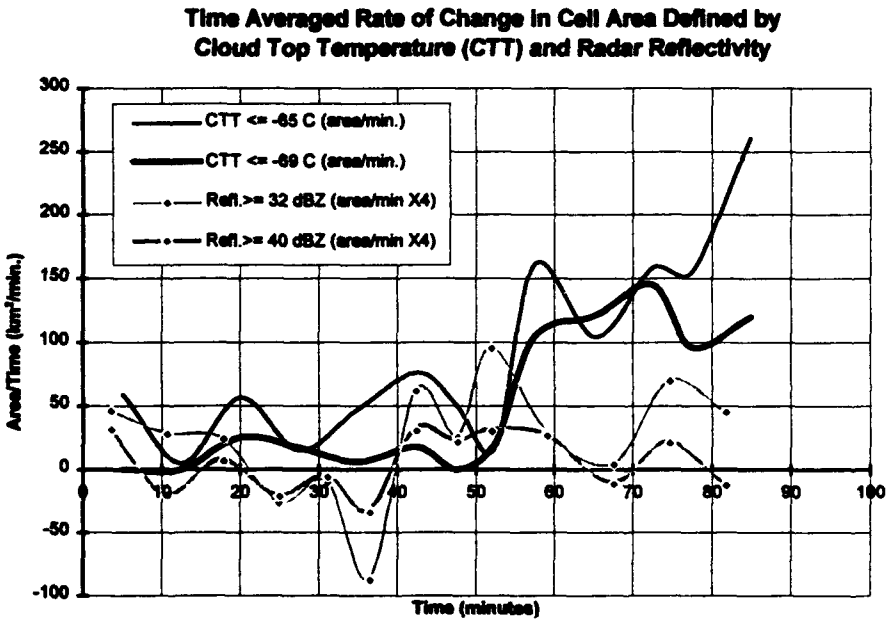

Figure 42b. Time averaged rate of change of the data in Figure 42a. The reflectivity values are multiplied by a factor of 4. The date/time at the origin is 26 July 91/1931Z.

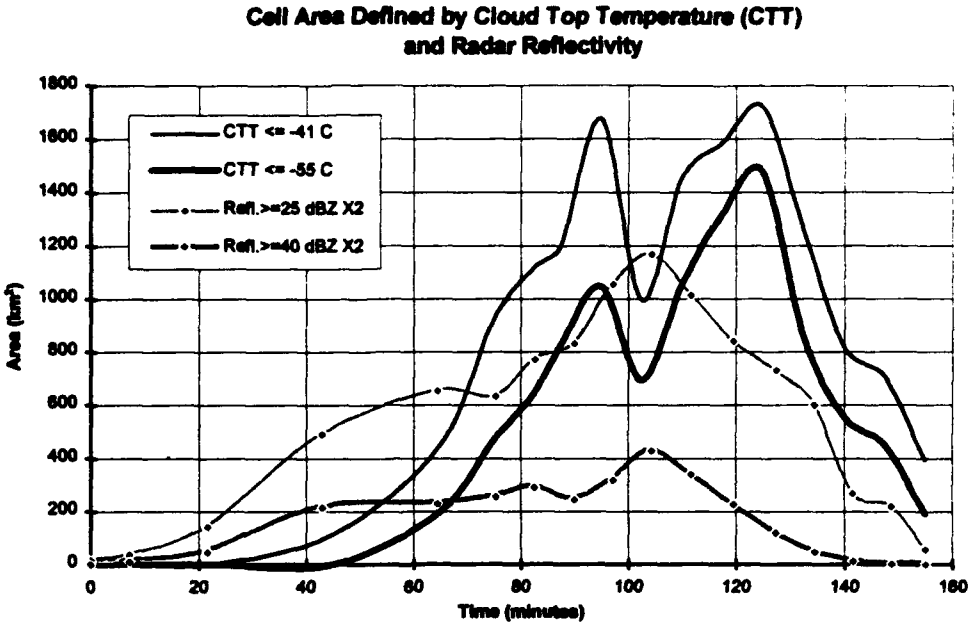

Figure 43a. Area of Cell #2 (St. Cloud) based on satellite derived cloud top temperature and radar reflectivity thresholded values versus time. The reflectivity values are multiplied by a factor of 2. The date/time at the origin is 26 July 91/1731Z.

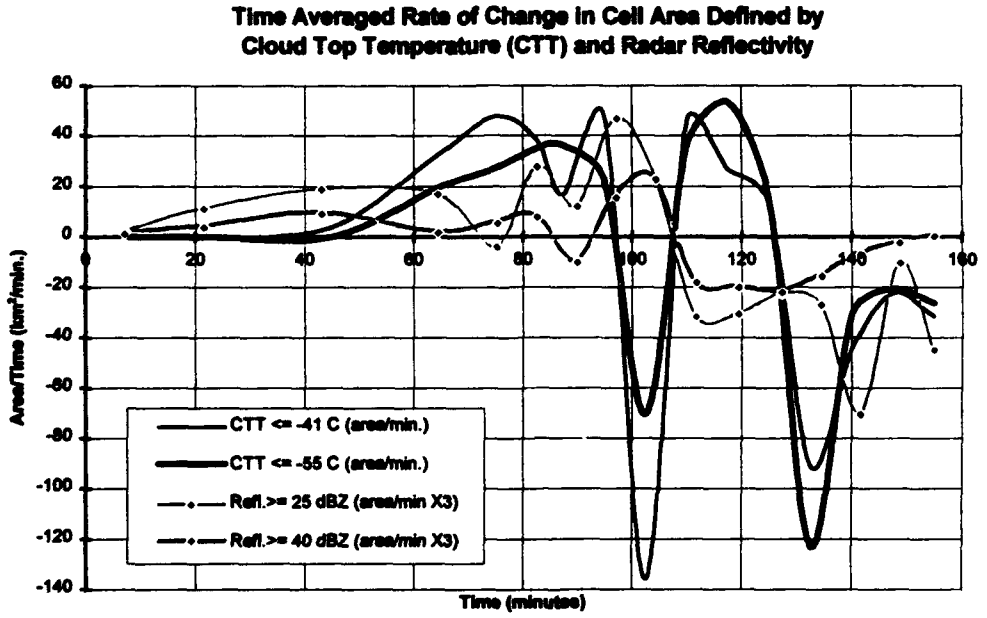

Figure 43b. Time averaged rate of change of the data in Figure 43a. The reflectivity values are multiplied by a factor of 3. The date/time at the origin is 26 July 91/1731Z.

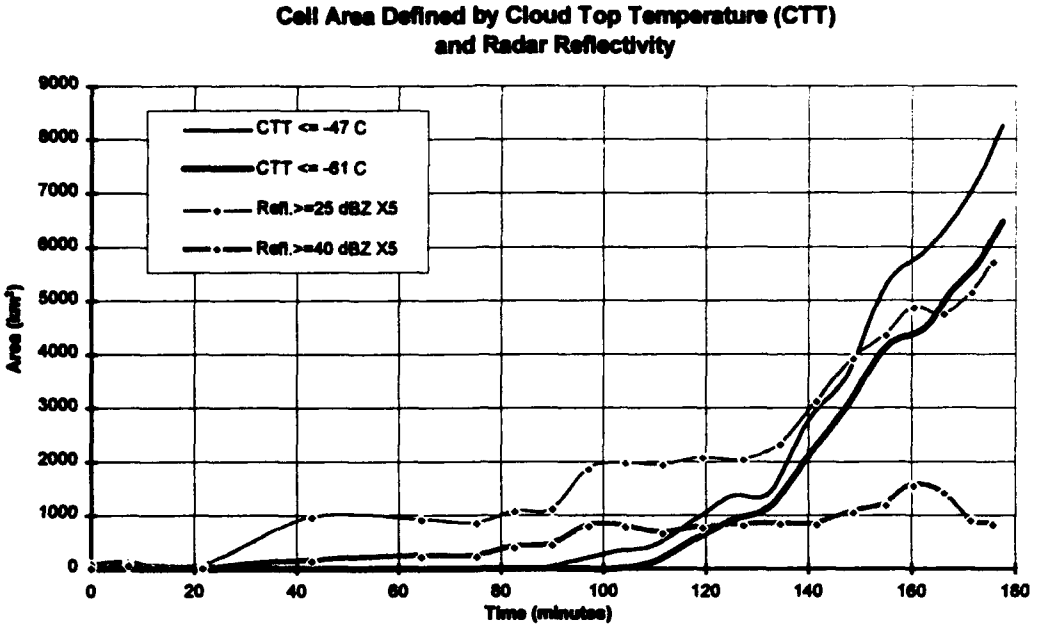

Figure 44a. Area of Cell #3 (Titusville) based on satellite derived cloud top temperature and radar reflectivity thresholded values versus time. The reflectivity values are multiplied by a factor of 5. The date/time at the origin is 26 July 91/1731Z.

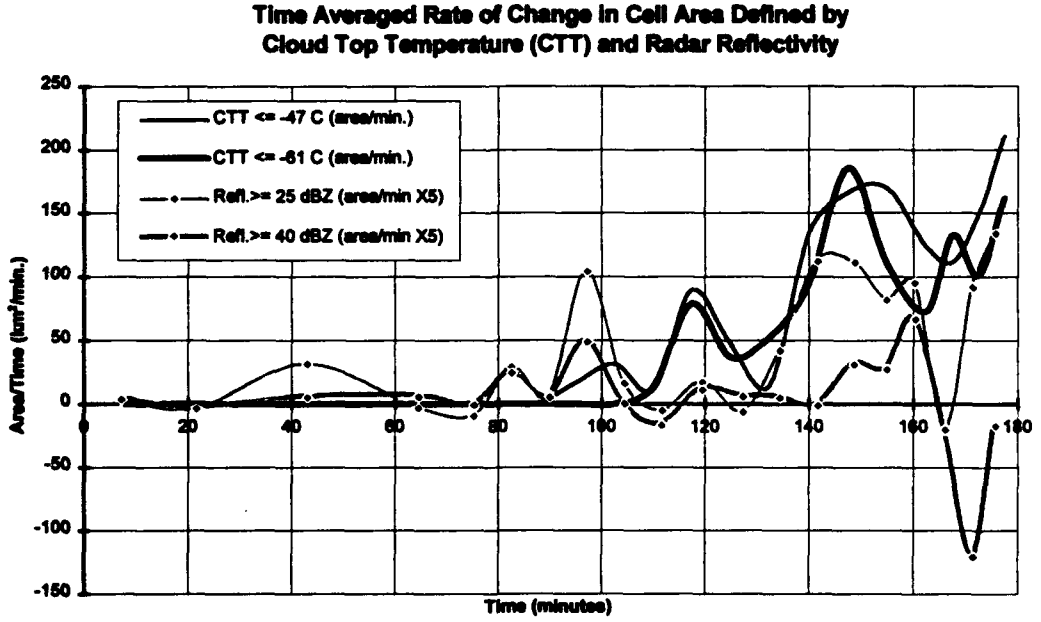

Figure 44b. Time averaged rate of change of the data in Figure 44a. The reflectivity values are multiplied by a factor of 5. The date/time at the origin is 26 July 91/1731Z.

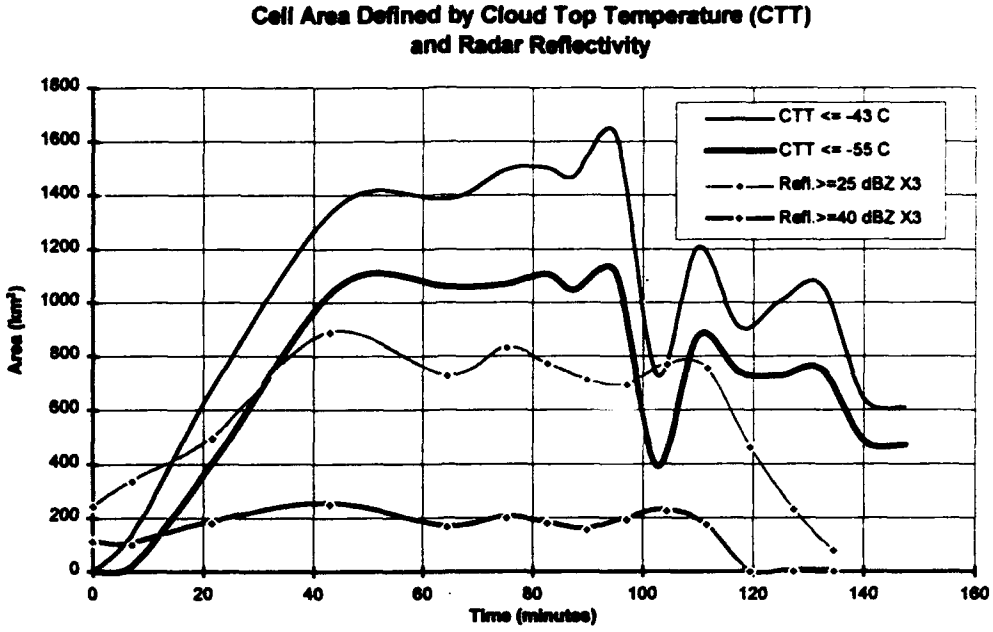

Figure 45a. Area of Cell #4 (Mosquito Lagoon) based on satellite derived cloud top temperature and radar reflectivity thresholded values versus time. The reflectivity values are multiplied by a factor of 3. The date/time at the origin is 26 July 91/1731Z.

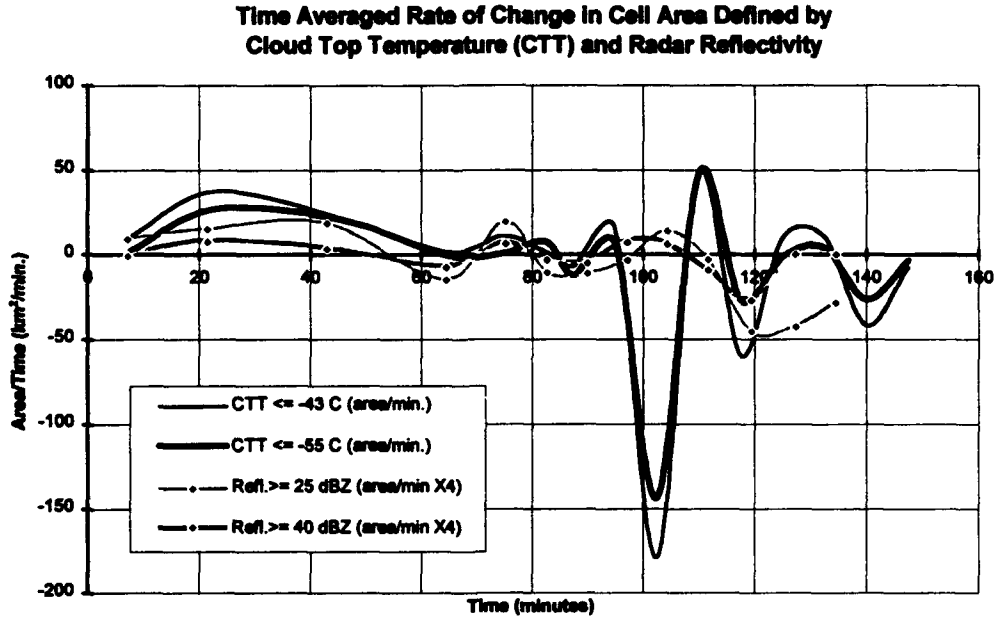

Figure 45b. Time averaged rate of change of the data in Figure 45a. The reflectivity values are multiplied by a factor of 4. The date/time at the origin is 26 July 91/1731Z.

3.4 Examples of Nowcasting Benefits Using the Combined Display

The satellite/radar combined display provides a forecaster with a useful nowcasting tool because the strengths of both sources can be utilized together to help determine convective potential. No time is wasted attempting to assimilate two different displays and therefore attention is quickly focused to the most active or potentially active regions. By late afternoon on the first case study day (24 July 91), cirrus and thunderstorm anvil clouds obscure much of the boundary-layer detail often observed in satellite imagery. Figures 46 and 47 reveal the important detail radar provides in such cases. Figure 46a shows a sea-breeze line labeled 'A' similar in shape to the east coast line. Although the northern half of this convergence line is observed on both satellite and radar, the southern portion is obscured on satellite and is only visible on radar. The same is true for outflow boundary-B (Figure 46a). Monitoring these boundaries is important since they both lead to intense convective cells with >50 dBZ reflectivity (Figures 46b-c).

Another example of cirrus masking is shown in Figures 47a-b. Outflow boundaries A and B (Figure 47a) are both difficult to detect on satellite imagery (Figure 47b). Knowing the outflow boundary-A is advancing to the northwest into unstable air enables a forecaster to predict the development of stronger thunderstorms (Figure 47c-d).

The second case study (25 July 91) provides examples of the detail offered by GOES imagery giving clues to the instability of the environment prior to similar indications on radar. The cloud streets labeled 'A' in Figure 48a indicate the atmosphere in this region is unstable enough to develop moderate cumulus clouds. A trigger mechanism such as the sea-breeze/convergent line B is needed to initiate deep

convection. Using radar alone (Figure 48b), a forecaster may not realize the convective potential of region A until rainshowers develop (Figure 48c). Ultimately, as a result of the collision of the sea-breeze/convergent line and the cloud streets, region A develops thunderstorms of >48 dBZ reflectivity (Figure 48d). An arc-cloud outflow boundary from a dissipating cell on this case study day can be observed on satellite propagating northward (Figure 49a) initiating moderate convection (Figure 49b). This feature is not detected on radar because the 3.0 degree elevation scan overshoots the shallow boundary.

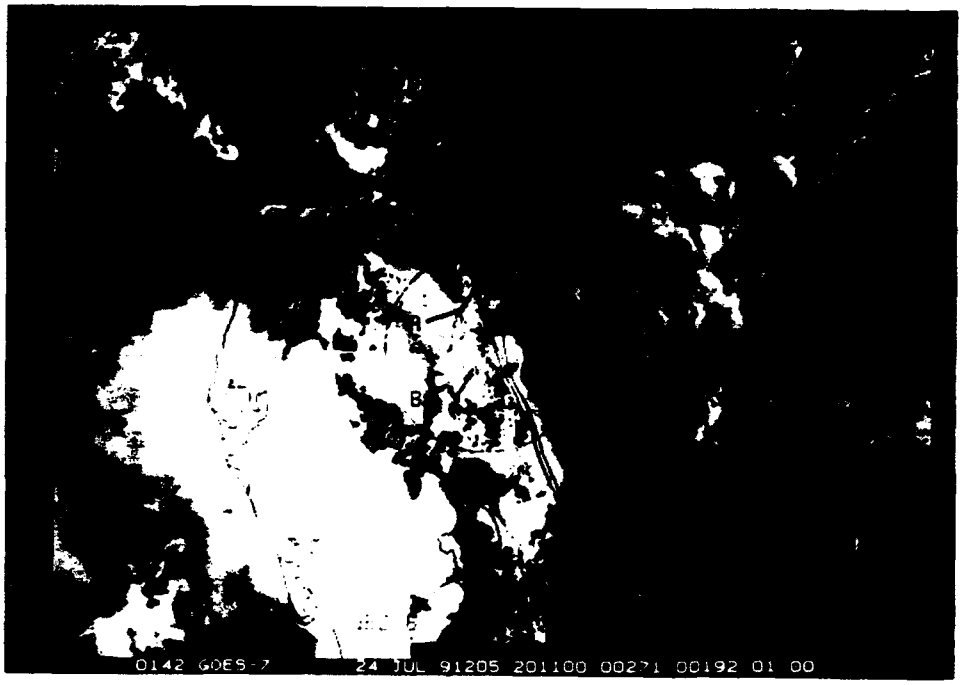

Figure 46a. GOES/visible image and CP-4 Doppler reflectivity scan combined display - 24 July 91/2011Z. A is the east-coast sea-breeze boundary; B is a radar-detected outflow boundary observed beneath a cirrus shield.

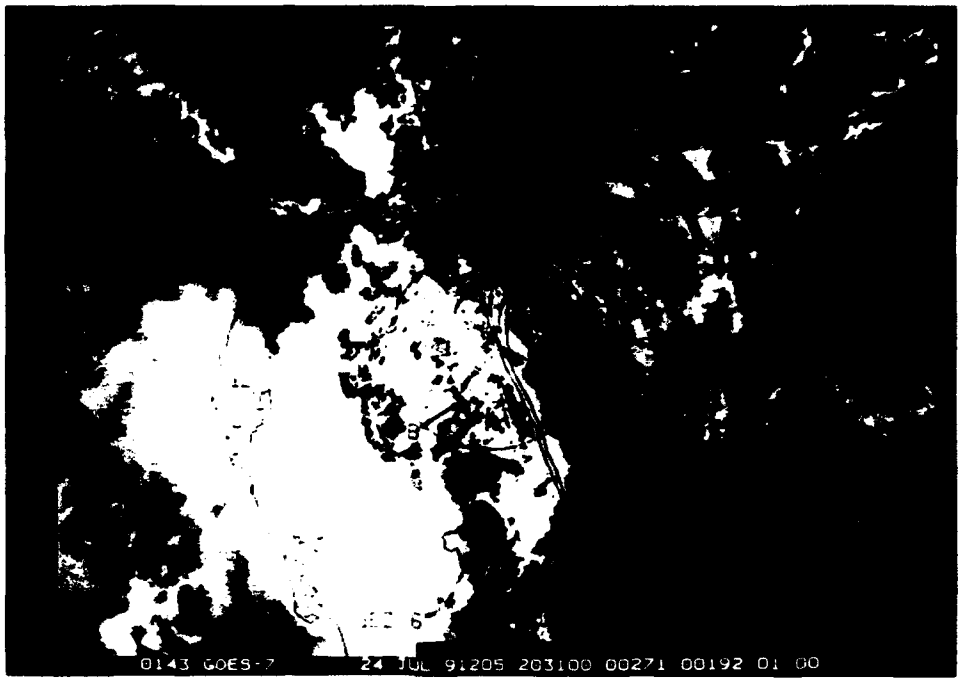

Figure 46b. GOES/visible image and CP-4 Doppler reflectivity scan combined display - 24 July 91/2031Z. The yellow circle indicates the region of probable convection due to the imminent collision of a convergence line and a developing cumulus cloud mass.

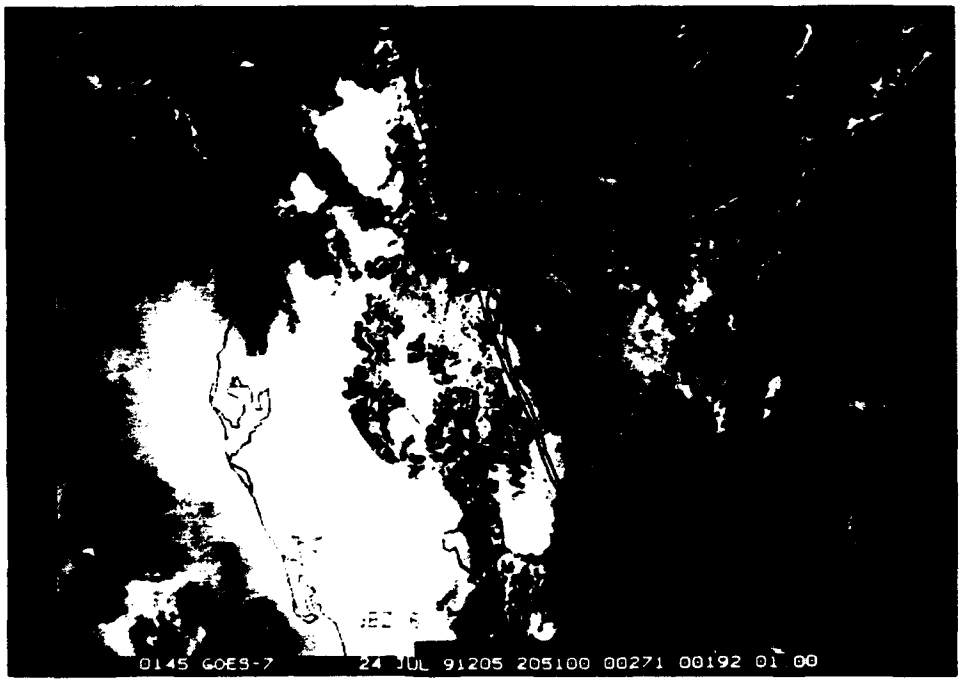

Figure 46c. Same as Figure 46b for 24 July 91/2051Z. Note the convection both in the circle and to its south. Signs of this development were apparent at least 40 minutes earlier on the combined display.

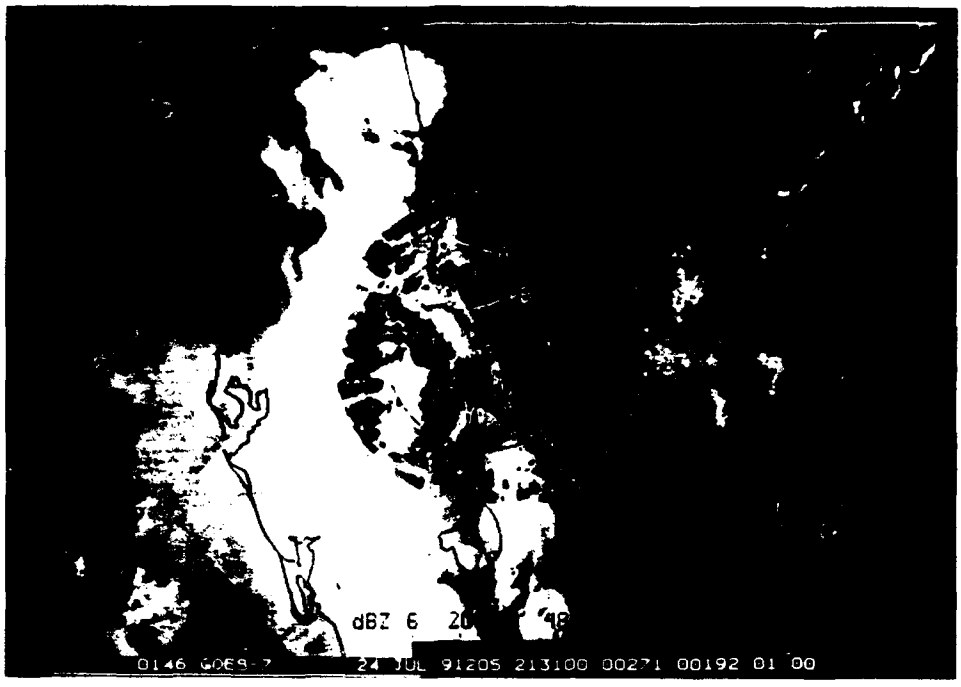

Figure 47a. GOES/visible image and CP-4 Doppler reflectivity scan combined display - 24 July 91/2131Z. The features labeled 'A' and 'B' are radar-detected outflow boundaries.

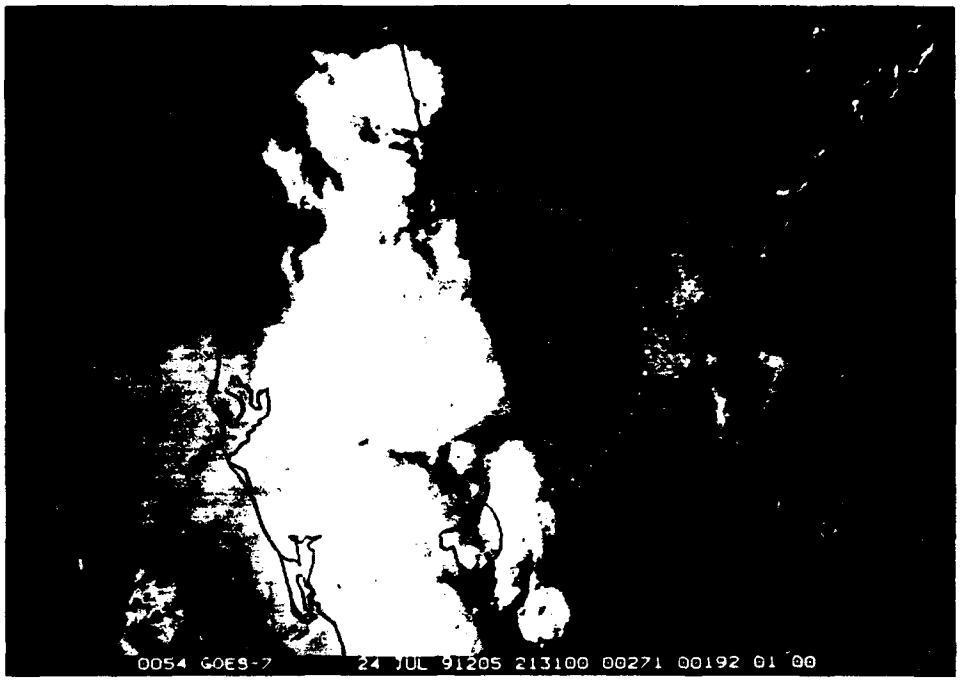

Figure 47b. GOES/visible image - 24 July 91/2131Z. Outflow boundaries A and B labeled in Figure 47a are not as obvious using only the satellite image.

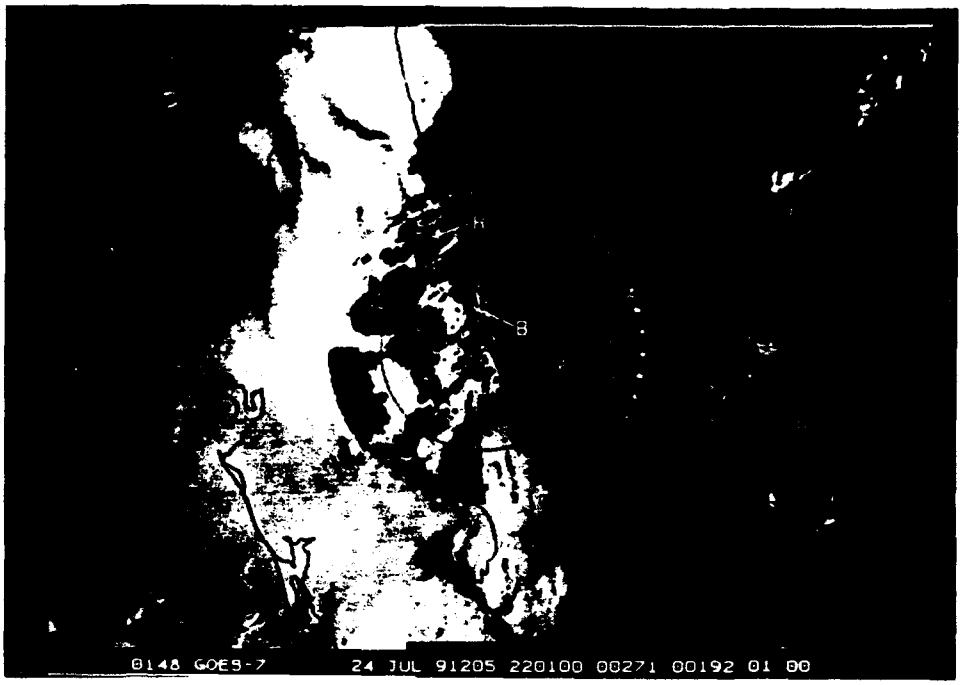

Figure 47c. GOES/visible image and CP-4 Doppler reflectivity scan combined display - 24 July 91/2201. Outflow-B continued to advance eastward while outflow-A generated a >50 dBZ thunderstorm cell.

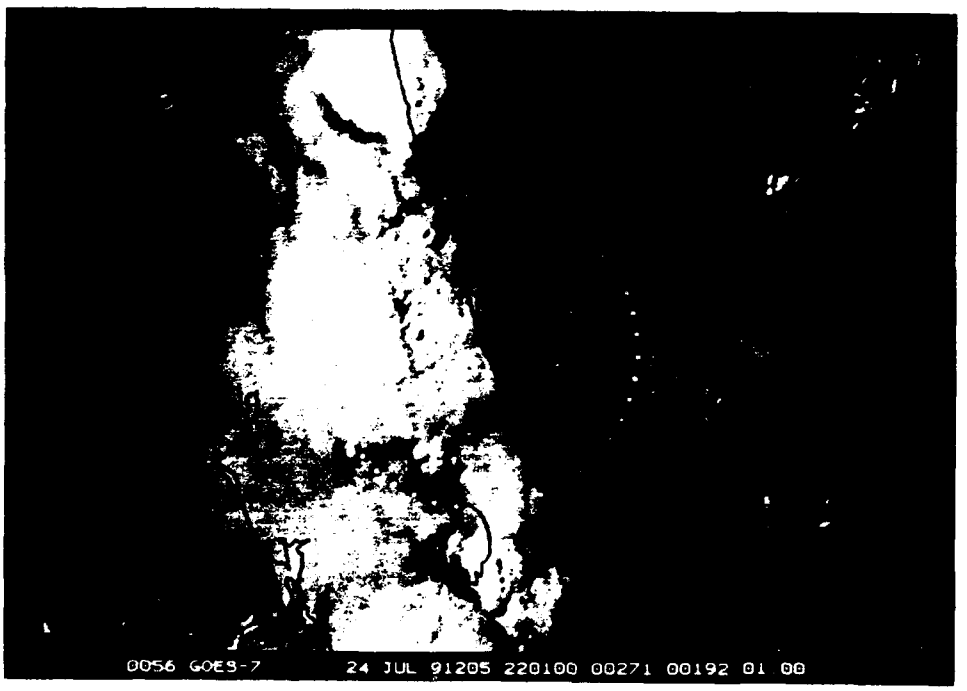

Figure 47d. GOES/visible image - 24 July 91/2201Z. Note the overshooting cloud top in the cell generated from outflow-A.

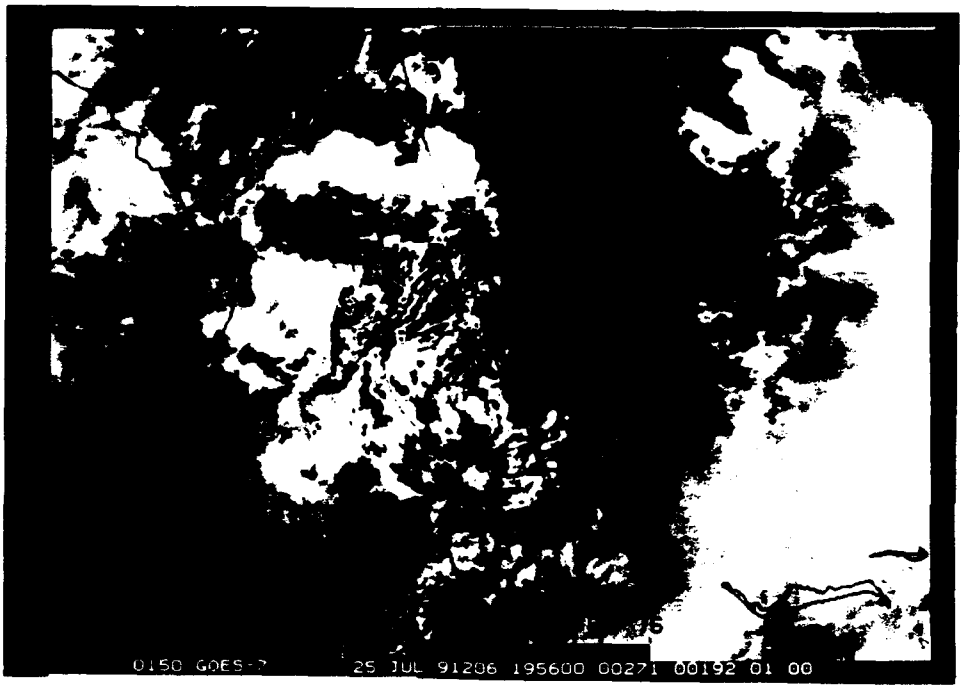

Figure 48a. GOES/visible image and CP-4 Doppler reflectivity scan combined display - 25 July 91/1956Z. The cloud streets in region-A indicate the atmosphere is moist and unstable, while the convergence boundary (B) could provide the necessary trigger for deep convective development.

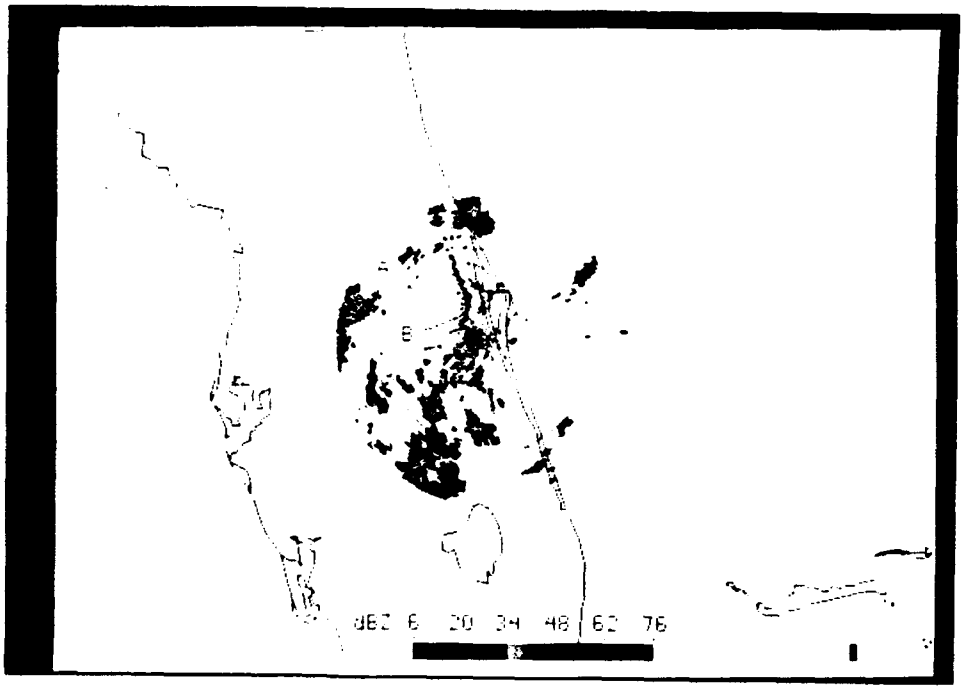

Figure 48b. CP-4 Doppler reflectivity scan - 25 July 91/1956Z. Used alone, not enough information is displayed to assess the convective potential of region-A.

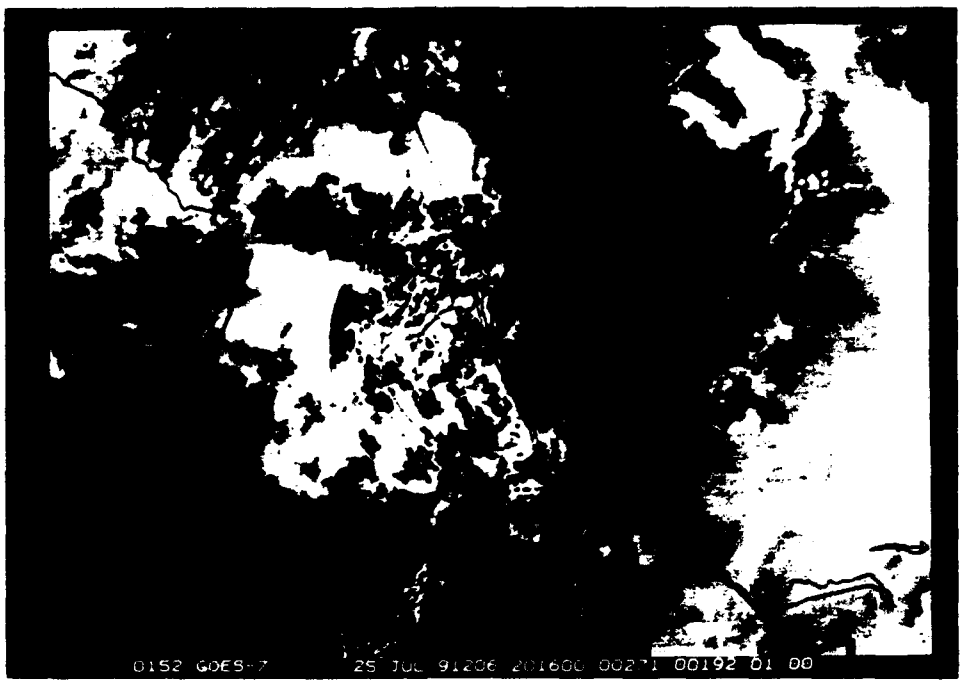

Figure 48c. GOES/visible image and CP-4 Doppler reflectivity scan combined display - 25 July 91/2016Z. Cloud streets in region-A are detected on radar at least 30 minutes after first observed on satellite.

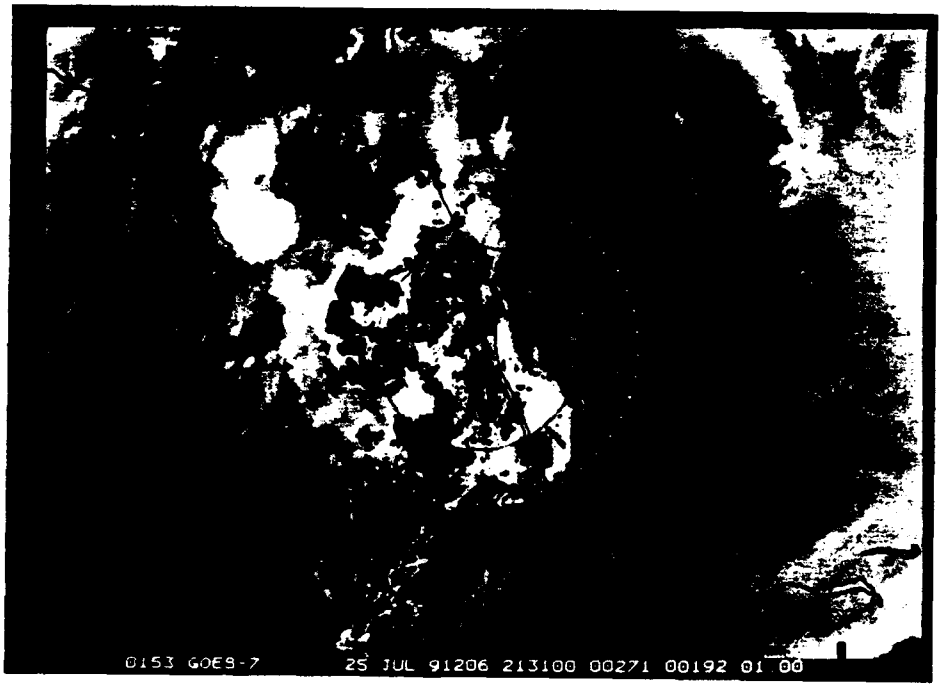

Figure 48d. GOES/visible image and CP-4 Doppler reflectivity scan combined display - 25 July 91/2131Z. The most intense convection within radar-range is occurring in the cloud street region-A (Figure 48a).

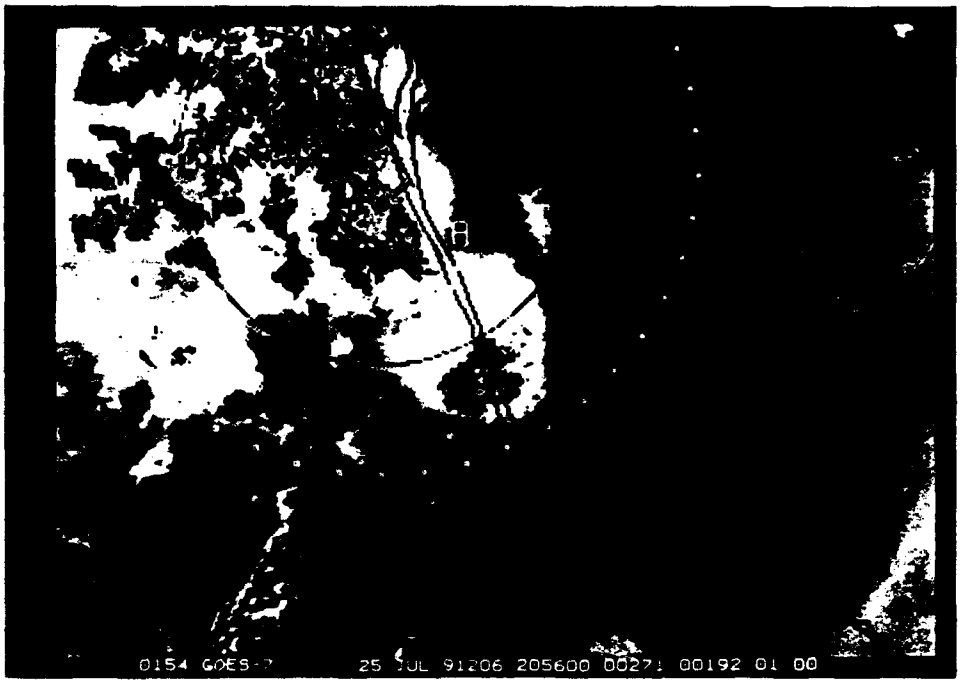

Figure 49a. GOES/visible image and CP-4 Doppler reflectivity scan combined display - 25 July 91/2056Z. An arc-cloud outflow boundary (A) seen on the satellite image is not detected on radar due to the 3.0° antenna elevation scan.

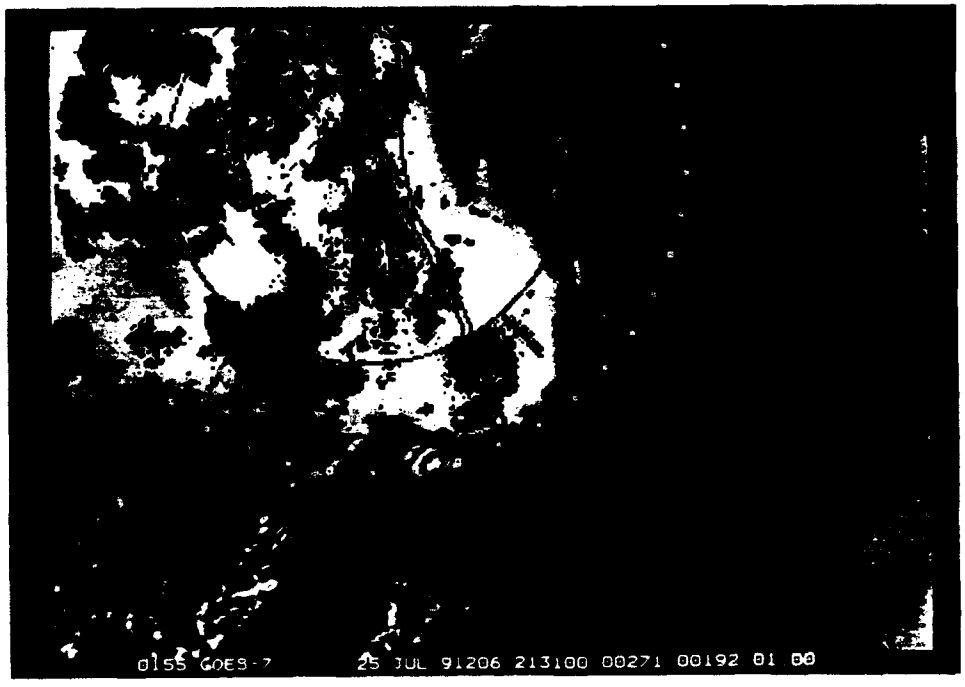

Figure 49b. GOES/visible image and CP-4 Doppler reflectivity scan combined display - 25 July 91/2131Z. The arc-cloud line in Figure 49a initiated new convection to the northwest of the outflow's dissipating parent cell.

Chapter 4

RESULTS

4.1 Conclusions

Conclusions from this study can best be described in two parts: 1) knowledge of convective storm evolution gained from the quantitative data analysis; and 2) nowcasting applications of the combined satellite/radar display.

Data analysis from the case studies reveal a time lag relationship between the maximum rate-of-change in cell area defined by radar echo and the rate-of-change in cell area defined by cloud top temperature. CTT area changes lag the cell's radar reflectivity area changes by 5-30 minutes in most cases. This relationship varies depending on the radar elevation angle and the reflectivity and temperature thresholds chosen to define the cell. This relationship is also dependent on location, therefore the results of this study are geographically bound to east-central Florida. For example, the evolution of a Florida thunderstorm as observed with satellite and radar may differ greatly from a storm in the central U.S.. Heavy rainshowers in Florida's subtropical humid environment often occur in cells with tops of only 10-12 Kft. A storm in the central plains, in contrast, may not yield a significant rainshower on radar until much higher cloud tops develop.

A cell may not exhibit this time lag relationship for many reasons. The complex interactions (sea breeze, outflow boundaries, collisions) seen in the case studies will disrupt a typical, expected relationship. The scale differences between the two sources

could also have a large impact on results. The changes in the radar echo, representing a much smaller area than the cloud top, may not always be reflected in the CTT changes.

No common pattern was observed by comparing the data during the early to mid-stages in the life cycle of the cells which could conclusively signal to a forecaster the approaching dissipation of the storm. The time rate-of-change of radar echo areas are very sporadic, oscillating frequently back and forth between positive and negative rates-of-change in cell area. The rate-of-change in cloud top temperature area, however was rarely negative until true dissipation when the "orphan" anvil slowly sublimates (Bluestein, 1993). The area defined by the cloud top temperature often steadily reaches a maximum peak, then steadily decreases. In four of the studied cells this occurred. Cloud top temperature changes are therefore a better indicator of convective storm dissipation than changes in radar reflectivity echo area. Knowing when the rate-of-change in the CTT area stops increasing (or the rate of increase begins to decrease) provides valuable information to a forecaster. For example, in Figure 35b, the point of inflection indicating the weakening of the cell (because of the decrease in the rate of area expansion) occurs 20 minutes before the maximum peak in CTT area growth in Figure 35a.

Tracking thunderstorm anvil growth and movement is very important in launch weather forecasting. Launch constraint 2.d. in Appendix A states that a launch cannot take place if the planned flight path will carry the vehicle "through or within 10 nautical miles of the nearest edge of any cumulonimbus or thunderstorm cloud, including its associated anvil." The monitoring of the rate-of-change of cloud top temperature in conjunction with other sources (upper level winds, satellite/radar imagery loop, surface

mesonet data) could help provide the launch weather forecaster with a thunderstorm and anvil dissipation nowcast.

Satellite rapid-scan imagery available in at least 10-minute intervals along with high temporal radar scan coverage (preferably synchronized with satellite image times) is essential to forecasting and the study of convective storm evolution. The high frequency images enable a more precise detection of the maximum rate-of-change in CTT area - shown to be a possible early signal of thunderstorm dissipation. Using the combined satellite/radar combined display, features observed to initiate or intensify convection often appeared only very briefly. Short time interval data allows for the detection and monitoring of these features.

Although it is difficult to present new positive findings from the quantitative relationship presented between the cloud top temperature and radar echo growth rates with a large degree of certainty, the qualitative aspects of the combined satellite/radar display for nowcasting are certain. This method of combined display allows a forecaster to take full advantage of the strengths in both sources of data. For example, the radar detects important boundary-layer convergence features masked by satellite observed cirrus or even in clear air, while monitoring approaching outflow boundaries using satellite can be done at greater ranges - well before they can be seen on the radar display. Often satellite can also provide a clearer picture of the convective potential in the atmosphere than what is observed on radar. Combination of these sources also increases the forecaster's efficiency by reducing the amount of data assimilation required when using satellite and radar data to produce a nowcast.

4.2 Overview

The research objectives in section 1.4 of this text were completed with varying degrees of success. A combined display of GOES imagery with Doppler radar scans was accomplished on a McIDAS/PC WIDE WORD workstation after converting the universal format radar data into image format. Many modifications to the conversion program were accomplished, most notably: 1) code added to extract and display velocity data; 2) a routine developed to filter out receiver noise from the display; 3) providing a means to display negative pixel values, representing negative reflectivity and velocity returns; and 4) a more efficient input routine was included to speed up the processing time of one scan from approximately 6 minutes to 1 minute. Although still not fast enough for use in an operational environment, it is now suitable for data processing in post analysis studies.

Available remapping and renavigating procedures (the RAMM branch landmark correlation re-navigating technique, for example) were used to prepare the images for graphic combination. The dual channel enhancement toggle function then merged the two data sources. Functions on McIDAS such as zoom and roam provide a useful means of easily manipulating the displayed product for better inspection. Color table enhancements and graphics for the radar images were designed for a more meaningful graphic display.

Unlike the development of the combined satellite/radar product, the application to show its usefulness in nowcasting convective storm evolution did not meet all expected goals. The qualitative use of the combined display was shown to benefit forecasting efforts, however the quantitative analysis of the compared satellite and radar data did not

reveal conclusive trends or relationships. The rate-of-change of a cell's cloud top temperature area does provide information pertaining to the dissipation phase of the thunderstorm. This information is important to forecasters and is especially applicable to launch weather forecasting.

4.3 Follow-on Research

Any further study of the relationship between satellite and radar data and the possible implications for benefits to nowcasting should include a larger sample of case studies. The sample used in this study was too small to produce conclusive results. Also required would be the use of more data sources in conjunction with the satellite and radar product to more thoroughly describe the mesoscale environment.

These steps could perhaps help to determine if the observed time lag between the rate-of-change in cell area defined by cloud top temperature and the associated radar reflectivity echo is related to the intensity of the storm or to the storm's rate of growth. Other possible areas of study with such a data set include: determining the average lifetime of convective cells or clusters in Florida or determining the average time it takes for the cells to reach peak intensity.

The use of soundings (rawinsonde or satellite) could be used in conjunction with the combined display to forecast the convective potential within an area of interest (see Purdom and Sinclair 1990). The CIRA/RAMM branch storm relative motion technique could be used for cells with a strong component of atmospheric motion to better locate the storm's vorticity center and perhaps the probability of further growth or dissipation.

Soon GOES-I data will be available and could greatly benefit studies of this type to improve nowcasting capability. Better image resolution will provide more detail. Improved cloud edge and cloud top feature detection capability will lead to improvements in severe storm identification. And with two views of a storm from the geostationary satellite network, better possibilities exist for making corrections for parallax. The amount of "hidden" data out of view behind the cloud top will be reduced by combining images from two viewing angles.

4.3.1 GOES-I/M System

The next generation of GOES satellites (GOES-I through GOES-M) will produce many new improvements over current geostationary satellite capabilities, providing exciting future research possibilities. The first of the series (GOES-8) was launched on April 13, 1994 (Figure 50).

Significant changes have been made by Ford Aerospace in its design and function. The first major change in design is that the new GOES series is no longer spin stabilized, but is three axis stabilized. This configuration permits the instrumentation to remain earth-oriented like current low altitude polar orbiters. This orientation also allows for more efficient duty cycles of imager and sounder which yield higher spatial resolution and improved signal-to-noise (Purdom et al., 1993). The second major design change is seen in the imager and sounder. In GOES-7, these instruments coexist in the VAS, or VISSR Atmospheric Sounder, and cannot each be fully utilized due to operational scheduling conflicts. This will no longer be a problem with GOES-I/M since these

instruments are separate and capable of independent, simultaneous operation (Kidder and Vonder Haar, 1992).

Figure 50. Drawing of GOES-I.

The improved multispectral imaging GOES-I features 5 imaging channels, all of which are scanned during every imager frame (Purdom et al., 1993):

1. 0.52-0.72 μm - visible
2. 3.78-4.03 μm - shortwave infrared window
3. 6.47-7.02 μm - upper level water vapor channel
4. 10.2-11.2 μm - longwave infrared window
5. 11.5-12.5 μm - infrared window with slightly different amounts of water vapor contamination than in the shortwave IR or longwave IR windows

The uses of these new channels include: nighttime fog identification, detection of liquid water clouds over snow during the daytime and low level moisture identification and sea surface temperature identification (Purdom, 1993). In addition to the types of information, most of the imager's channels have improved ground resolution and radiometric accuracy.

A simulation of GOES-I imagery from 10-bit NOAA AVHRR data shows GOES-I should provide significant improvements over the current geostationary system (Purdom, 1993). The anticipated improvements include: more accurate cloud drift wind measurements; development of new techniques for severe storm identification; low light visible imaging, highly accurate cloud height determination; and development of improved low level moisture and sea surface temperature products. In addition to these improvements, algorithms can be developed to combine and compare the various channels to produce new, advanced products benefiting areas as diverse as nowcasting and climate change (Purdom et al., 1993).

REFERENCES

Adler, R.F., and D.D. Fenn, 1979: Thunderstorm intensity as determined from satellite data. *J. Appl. Meteor.*, Vol. 18, 502-517.

Barnes, S.L., 1980: SESAME News: Report on a meeting to establish a common Doppler radar data exchange format. *Bull. Amer. Meteor. Soc.*, 61 (11), 1401-1404.

Bluestein, H.B., and C.R. Parks, 1983: A synoptic and photographic climatology of low-precipitation severe thunderstorms in the southern plains. *Mon. Wea. Rev.*, 111, 2034-46.

Bluestein, H.B., 1993: Synoptic-Dynamic Meteorology in Midlatitudes Vol. II, Observations and Theory of Weather Systems. Oxford University Press.

Brown, R.A., and V.T. Wood, 1987: A Guide for Interpreting Doppler Velocity Patterns. National Severe Storms Laboratory, NOAA, Norman, OK, Pub. *R400-DV-101*.

Browning, K.A., and C.G. Collier, 1990: Satellite and radar data are now combined to predict weather up to 2 hours ahead. *Earth in Space*, 2(6), 9-12.

Clark, J.D., 1983: The GOES User's Guide. U.S. Department of Commerce, National Oceanic and Atmospheric Administration, Washington, D.C.

Court, A., and J.F. Griffiths, 1986: Thunderstorm Climatology. In: Thunderstorms: A Social and Technological Documentary, Vol. II, E. Kessler, Ed., Univ. of Oklahoma Press, 11-52.

Foote, G.B., 1991: Convection and Precipitation/Electrification Experiment, Scientific Overview and Operations Plan, NCAR, Boulder, CO.

Fujita, T., 1982: Infrared, stereo-height, cloud-motion, and radar-echo analysis of SESAME-day thunderstorms. Preprints, 12th Conf. on Severe Local Storms, San Antonio, TX, 213-216.

Gould, K., 1992: The Zeb User's Manual, National Center for Atmospheric Research, Boulder, CO.

Green, R.N., and H.A. Parker, 1983: Application of satellite and radar data to severe thunderstorm analysis. 13th Conference on Severe Local Storms, Amer. Meteor. Soc., 190-195.

Kidder, S.Q., and T.H. Vonder Haar, 1992: Satellite Meteorology: An Introduction. To be published by Academic Press.

Madura, J., B. Boyd, N. Wyse, and M. Adams, 1992: An Assessment: Ability to Satisfy Weather Requirements in Support of America's Space and Missile Program.

McGinley, J.A., S.C. Albers, and P.A. Stamus, 1992: Local data assimilation and analysis for nowcasting. *Advances in Space Research*, Vol. 12, No. 7, 179.

Negri, A.J., and R.F. Adler, 1981: Relation of satellite-based thunderstorm intensity to radar-estimated rainfall. *J. of Appl. Meteor.*, Vol. 20, 288-300.

Purdom, J.F.W., 1976: Some uses of high-resolution GOES imagery in the mesoscale forecasting of convection and its behavior. *Mon. Wea. Rev.*, 104, 1474-1483.

Purdom, J.F.W., 1982: Subjective Interpretation of Geostationary Satellite Data for Nowcasting. Nowcasting, ed. K.A. Browning, Academic Press, 149-166.

Purdom, J.F.W., R.N. Green, and H.A. Parker, 1982: Integration of satellite and radar data for short range forecasting and storm diagnostic studies. Preprints, 9th Conference on Weather Forecasting and Analysis, Seattle, Amer. Meteor. Soc., 51-55.

Purdom, J.F.W., 1986: Satellite contributions to convective scale weather analysis and forecasting. Preprints 11th Conference on Weather Forecasting and Analysis, Amer. Meteor. Soc., 295-314.

Purdom, J.F.W., and P.C. Sinclair, 1988: Using satellite data to aid in diagnosing and forecasting convective development and intensity along arc cloud lines. Preprints Third Conference on Satellite meteorology and Oceanography, Boston, MA, Amer. Meteor. Soc., 166-171.

Purdom, J.F.W., and P.C. Sinclair, 1990: Convective scale interaction as observed using satellite data. Fifth Conference on Satellite Meteorology and Oceanography, London, England, Amer. Meteor. Soc., 378-383.

Purdom, J.F.W., and T.H. Vonder Haar, 1992: A Proposal for Investigations of Convective Development and Evolution Over Florida Using 1991 CaPE Experiment Satellite, Radar and Conventional Data, CIRA, Ft. Coilins, CO. (not yet submitted).

Purdom, J.F.W., 1993: Comparison of GOES-7 and simulated GOES-I imagery. Preprints, 13th Conference on Weather Analysis and Forecasting, Vienna, VA, 241-244.

Purdom, J.F.W., P.N. Dills, and K.E. Eis, 1993: Comparison of GOES-7 and Simulated GOES-I Imagery. CIRA Newsletter, Fort Collins, CO, Vol. 8, 3-8.

Reynolds, D.W., and E.A. Smith, 1979: Detailed analysis of composited digital radar and satellite data. *Bull. Amer. Meteor. Soc.*, Vol. 60, No. 9, 1024-1037.

Reynolds, D.W., and T.H. Vonder Haar, 1979: Satellite Support to HIPLEX. Final report to the Bureau of Reclaimation, Department of Atmospheric Science, Colorado State University, Fort Collins, CO.

Rinehart, R.E., 1991: Radar for Meteorologists. Knight Printing Company, Fargo, North Dakota.

Sinclair, P.C., and J.F.W. Purdom, 1982: Integration of research aircraft data and 3 minute interval GOES data to study the genesis and development of deep convective storms.

Smith, S.B., and J.F.W. Purdom, 1993: Improved meso-analysis for nowcasting using satellite data. Preprints 13th Conference on Weather Analysis and Forecasting, Vienna, VA, Amer. Meteor. Soc., 25-28.

USAF Document 009-HO-101: Technical Training for Doppler Weather Radar: WSR-88D Products. Chanute Technical Training Center (ATC), Chanute Air Force Base, IL.

Wakimoto, R.M., and N.T. Atkins, 1993: Observations of the sea-breeze front during CaPE. Part I: single-doppler, satellite and cloud photogrammetry analysis. Dept. of Atmospheric Sciences, UCLA. Submitted to *Mon. Wea. Rev.*, 1993.

Weems, J., 1994: Personal Communication with the Cape Canaveral Launch Weather Officer.

Wicklund, G., and G. Youngren, 1993: Operational impact and economic savings of a two-phase lightning warning system for the John F. Kennedy Space Center and Cape Canaveral Air Force Station. Preprints 13th Conference on Weather Analysis and Forecasting, Vienna, VA, Amer. Meteor. Soc., 92-95.

Williams, S.F., Caesar, K., and K. Southwick, 1992: The Convection and Precipitation Electrification (CaPE) Operations Summary and Data Inventory. NCAR/Office of Field Project Support, Boulder, CO.

Wilson, J.W., R. Carbone, H. Baynton, R. Serafin, 1980: Operational application of meteorological Doppler radar. *Bull. Amer. Meteor. Soc.*, Vol. 61, No. 10, 1154-1167.

Wilson, J.W., and K.E. Wilk, 1982: Nowcasting Applications of Doppler radar. Nowcasting, ed. K.A. Browning, Academic Press, 87-105.

Wilson, J.W., and R. Carbone, 1984: Nowcasting with Doppler radar: The Forecaster-Computer Relationship. Nowcasting II, ed. K.A. Browning, European Space Agency, 177-186.

Wilson, J.W., and W.E. Schreiber, 1986: Initiation of convective storms at radar-observed boundary-layer convergence lines. *Mon. Wea. Rev.*, 114, 2516-2536.

Wilson, J.W., and C.K. Mueller, 1993: Nowcasts of thunderstorm initiation and evolution. *Weather and Forecasting*, Vol. 8, 113-131.

Wyatt, D., and D. Kintigh, 1989: Internal U.S. Air Force study for manpower impact due to weather for Launch Complex 40/41.

APPENDIX A

CCAFS/KSC Launch Weather Natural/Triggered Lightning Constraints (courtesy of USAF 45th Weather Squadron)

1. Do not launch if any type of lightning is detected within 10 (ten) nautical miles of the launch site or planned flight path within 30 (thirty) minutes prior to launch, unless the meteorological condition that produced the lightning has moved more than 10 nautical miles away from the launch site or planned flight path.

2. Do not launch if the planned flight path will carry the vehicle:

a. through cumulus clouds with tops higher than the +5 degree Celsius level; or

b. through or within 5 nautical miles of cumulus clouds with tops higher than the -10 degree Celsius level; or

c. through or within 10 nautical miles of cumulus clouds with tops higher than the -20 degree Celsius level; or

d. through or within 10 nautical miles of the nearest edge of any cumulonimbus or thunderstorm cloud including its associated anvil.

3. Do not launch if, for Ranges equipped with a surface field mill network, at any time during the 15 minutes prior to launch time the one (1) minute average of absolute electric field intensity at the ground exceeds 1 kilovolt per meter (1kV/m) within 5 nautical miles of the launch site unless:

a. there are no clouds within 10 nautical miles of the launch site; and

b. smoke or ground fog is clearly causing abnormal reading.

NOTE: For confirmed instrumentation failures, continue countdown.

Relative to (1): The following clouds are acceptable if they have not been previously associated with a thunderstorm, or convective clouds with tops greater than the -10 degree Celsius temperature level within the last three hours:

(a) Thin fibrous (optically transparent) clouds;

(b) Less than or equal 2/8 cumulus/strato-cumulus/stratus (CU/SC/ST) clouds with tops below or equal to the +5 degree Celsius temperature level. For example, 3/8 CU/SC/ST is not acceptable regardless of cloud top level, nor is any CU/SC/ST cloud amount above the +5 degree Celsius temperature level.

Relative to (2): This also includes a maritime inversion with an onshore/alongshore wind present over the electric field mills, causing those mills located near the ocean to be elevated with a positive polarity between 1 kV/m and 1.5 kV/m inclusive.

4. Do not launch if the planned flight path is through a vertically continuous layer of clouds with an overall depth of 4,500 feet or greater where any part of the clouds is located between the zero (0) degree and -20 degree Celsius temperature levels.

5. Do not launch if the planned flight path is through any cloud types that extend to altitudes at or above the zero (0) degree Celsius temperature level and that are associated with disturbed weather within 5 nautical miles of the flight path.

6. Do not launch through thunderstorm debris clouds, or within 5 nautical miles of thunderstorm debris clouds not monitored by a field network or producing radar returns greater than or equal to 10 dbz.

7 Definitions:

a. Debris clouds: Any cloud layer other than a thin fibrous layer that has become detached from the parent cumulonimbus within 3 hours before launch.

b. Disturbed weather: Any meteorological phenomenon producing moderate or greater precipitation.

c. Cumulonimbus cloud: Any convective cloud that exceeds the -20 degree Celsius temperature level.

d. Cloud layer: Any cloud, broken or overcast layer, or layers connected by cloud elements, e.g., turrets from one cloud layer to another.

e. Planned flight path: The trajectory of the flight vehicle from the launch pad through its flight profile until it reaches the altitude of 100,000 feet.

f. Anvil: Stratiform or fibrous cloud produced by the upper-level outflow from thunderstorms or convective clouds. Anvil debris does not meet the definition if it is optically transparent.

NOTES:

1. Electrical charge regions can occur in clouds with altitudes at or above the zero degree Celsius isotherm. These charge regions can produce lightning discharges triggered by the proximity of long electrical conductors (launch vehicle plus conductive portion of plume).

2. The above constraints are for the avoidance of natural or triggered lightning, based on known cloud types that can produce discharges and the distances to the charge regions.

8. GOOD SENSE RULE:

If hazardous conditions exist that approach the launch constraint limits, or if hazardous conditions are believed to exist for any other reason, an assessment of the nature and severity of the threat shall be made and reported to the Launch Director.

APPENDIX C

USAF 45th Weather Squadron Weather Advisory/Warning Requirements (courtesy of USAF 45th Weather Squadron)

WEATHER ADVISORY REQUIREMENTS

LOCATION	CRITERIA	DD	DISSEMINATION
KSC	Lightning w/i 5 nm of any area	30 min	KSC/DO Hotline or 867-4910
	Wind SFC-300' > 18 kts	30 min	
	≥ 1" precipitation in ≤ 1 hr	30 min	
	Temperature ≤ 40F for ≥ 2 hrs	4 hours	
	Temperature ≤ 32F for ≥ 2 hrs	16 hours	
	Temperature ≤ 25F for ≥ 2 hrs	4 hours	
CCAFS	Thunderstorms w/i 25 nm of the RCC	1 hour	Support SRO (M-F 0730-1600L) Hotline or 853-2181 Cape Support Hotline or 853-5211 *(courtesy call to 45th SW/CP)* *After duty hours only Cape Support (courtesy call to 45th SW/CP)*
	Lightning w/i 5 nm of any area	30 min	
PORT	SFC Wind > 22 kts steady	30 min	*Same as CCAFS dissemination*
JDMTA	Lightning w/i 25 nm	30 min	*Same as CCAFS dissemination*
PATRICK	SFC Wind ≥ 25 kts	30 min	45 SW Command Post Hotline or 494-7001
	Thunderstorms w/i 10 nm	30 min	
	Lightning w/i 5 nm	Obsrvd	
	Gust spread ≥ 20 kts	Obsrvd	
	Wind shear below 020, ≥MDT TURBC SFC-100, ≥MDT Icing SFC-100	*Obsrvd, (only when Afld is open)*	
JOINT STARS MELBOURNE	Hurricane/Tropical Storm	30 min	951-5687 (back up 951-5000)
	Lightning w/i 5 nm	30 min	
	Hail (any size) w/i 25 nm	30 min	
	Wind ≥ 50 kt w/i 25 nm	30 min	
	Freezing precipitation	30 min	

KSC/CCAFS/PAFB WEATHER WARNING REQUIREMENTS

NOTE: ON ALL WARNINGS AND WATCHES, GIVE A COURTESY CALL TO THE FLT/CC

LOCATION	CRITERIA	DLT	DISSEMINATION
KSC	TORNADO	5 min	KSC/DO
	WATERSPOUT	5 min	Hotline or
	Wind SFC-300' ≥ 35 kts	30 min	867-4810
	Wind SFC-300' ≥ 50 kts	30 min	
	Wind SFC-300' ≥ 60 kts	30 min	
	Hail, (any size)	30 min	
CCAFS	TORNADO	5 min	Support ERO (M-F 0730-1600 Hotline or 853-2101
	WATERSPOUT	5 min	Cape Support Hotline or 853-5211
	Wind SFC-200' ≥ 35 kts but < 50 kts	60 min	After duty hours
	Wind SFC-200' ≥ 50 kts	30 min	only Cape Support
	Hail > 3/4"	30 min	
PAFB	TORNADO	5 min	45th SW Command Post
	WATERSPOUT	5 min	Hotline
	SFC Wind ≥ 35 kts	60 min	or 494-7001
	Hail ≥ 3/4"	30 min	
	≥ 2" Precip in 12 hrs or less	5 min	

APPENDIX D

CCAFS/KSC Range Weather Instrumentation
(Madura et al., 1992)

Weather Information Network Display System (WINDS): A network of 46 towers at heights ranging from 2 to 165 meters. Sensors provide wind and temperature measurements.

Ground based field mill network: Network of 34 sensors which measures electric potential near the surface to infer the electric charge aloft.

Lightning Detection System (LDS): A short baseline configuration of five Advanced Lightning Direction Finders (ALDF) used to detect cloud to ground lightning.

Modified WSR-74C radar: 5 cm radar modified to produce volumetric data sets of Constant Altitude Plan Position Indicator (CAPPI) scans from 24 elevation angles between 0.6 and 35.9 degrees over 5 minute intervals.

WSR-88D Doppler radar: Principle User Processor (PUP) of the NEXRAD located at Melbourne's National Weather Service Office. Displays many products using algorithms derived from reflectivity, velocity and spectrum width fields.

GOES satellite data: Real time display capability of GOES products received routinely every 30 minutes, updated every 5 minutes during final phases of launch countdowns.

Man Computer Interactive Data Display System (McIDAS): System used to ingest and display satellite imagery, sounding data, NWS bulletins and hourly observations, and NMC prognostic products.

Real Time Winds Aloft Processing System (RTWAPS): Used to receive, process, format, and transmit upper air wind speed and direction data from the weather balloon systems (rawinsondes and jimspheres).

Meteorological and Range Safety Support (MARSS): Inputs of wind, temperature and humidity data provided to this system to produce dispersion forecasts in the event of accidental fuel/hazardous material spills.

APPENDIX E

Common Doppler Radar Exchange Format
(from Barnes, 1980)

a. 1600 bpi, 9 track tapes
b. 16-bit words, signed integers, 2's complement
c. Physical records, length ≤ 4095 words
d. File marks between volume scans
e. ASCII words are left justified, blank filled

Mandatory header block

Word

1 UF (ASCII)
2 Record length (16-bit words)
3 Position of first word of nonmandatory header block. (If no nonmandatory header block exists, this points to the first existing header block following the mandatory. In this way, word(3) always gives 1+ the length of the mandatory header.)
4 Position of first word of local use header block. (If no local use headers exists, this points to the start of the data header block.)
5 Position of first word of data header block
6 Physical record number relative to beginning of file
7 Volume scan number relative to beginning of tape
8 Ray number within volume scan
9 Physical record number within the ray (one for the first physical record of each ray)
10 Sweep number within this volume scan
11–14 Radar name (8 ASCII characters. Includes processor ID.)
15–18 Site name (8 ASCII characters)
19 Degrees of latitude (North is positive, South is negative)
20 Minutes of latitude
21 Seconds (× 64) of latitude
22 Degrees of longitude (East is positive, West is negative)
23 Minutes of longitude
24 Seconds (× 64) of longitude (Note: minutes and seconds have same sign as degrees.)
25 Height of antenna above sea level (meters)
26 Year (of data) (last 2 digits)
27 Month
28 Day
29 Hour
30 Minute
31 Second
32 Time zone (2 ASCII—UT, CS, MS, etc.)
33 Azimuth (degrees × 64) to midpoint of sample
34 Elevation (degrees × 64)
35 Sweep mode: 0—Calibration
1—PPI (Constant elevation)
2—Coplane
3—RHI (Constant azimuth)
4—Vertical
5—Target (stationary)
6—Manual
7—Idle (out of control)
36 Fixed angle (degrees × 64) (e.g., elevation of PPI; azimuth of RHI; coplane angle)
37 Sweep rate ((degrees/second) × 64)
38 Generation date of common format—Year
39 Month
40 Day
41–44 8 char ASCII tape generator facility name
45 Deleted or missing data flag (Suggest 100000 octal)

Data header

Word

1 Total number of fields this ray
2 Total number of records this ray
3 Total number of fields this record
4 1st field name: e.g. VE = velocity (m/s)
SW = spectral width (m/s)
DM = reflected power dB(mW)
DZ = dB(Z)
etc.
5 Position of 1st word of 1st field header
6 2nd field name
7 Position of 1st word of 2nd field headers, etc.

Field header

Word

1 Position of first data word
2 Scale factor (meteorological units = tape value divided by scale factor)
3 Range to first gate (km)
4 Adjustment to center of first gate (m)
5 Sample volume spacing (m)
6 Number of sample volumes
7 Sample volume depth (m)
8 Horizontal beam width (degrees × 64)
9 Vertical beam width (degrees × 64)
10 Receiver bandwidth (MHz)
11 Polarization transmitted (0 = horizontal; 1 = vertical; 2 = circular; >2 = elliptical)
12 Wavelength (cm × 64)
13 Number of samples used in field estimate
14 Threshold field (e.g., DM) (2 ASCII)
15 Threshold value
16 Scale
17 Edit code (2 ASCII)
18 Pulse repetition time (microseconds)
19 Bits per sample volume (16 for exchanged tape)
20–? Words for individual fields, as follows

for VE

Word

20 Nyquist velocity (scaled)
21 FL (2 ASCII) If flagged in least significant bit with NCAR bad velocity flag (1 = good, 0 = bad)

for DM

Word

20 Radar constant = RC, such that dB(Z) = [(RC + DATA)/SCALE] + 20 log (range in km)
21 Noise power (dB(mW) × scale)
22 Receiver gain (dB × scale)
23 Peak power (dB(mW) × scale)
24 Antenna gain (dB × scale)
25 Pulse duration (μs × 64)

APPENDIX F

Universal Format Radar Data Header Block Information

```
**************************************************************************
Radar: CP4/   Site: DUDA  Lat:   28.229440  Lon:  -80.735560  Elev(m): 12
Date:  7/24/91   Time: 19:54.08   Time Zone: GMT
* * * * * * * * * * * * * * * * * * * * * * * * * * * * * * * * * * * * *
Format: UF
Number of words/record, temp(2):       1186
Pos. of 1st word of non-mand header block:         46
Pos. of 1st word of local use header block:         66
Position of 1st word of data header block:         82
Physical rec. # relative to beg. of file:          1
Volume scan # relative to beg. of tape:          21
Ray number within volume scan:          1
Physical record number within the ray:          1
Sweep number within this volume scan:          1
* * * * * * * * * * * * * * * * * * * * * * * * * * * * * * * * * * * * *
Azimuth(deg.):        104   Elevation(deg.):          0
Sweep mode:          8
Fixed angle(elev.-PPI;azimuth-RHI):          0
Sweep rate(degrees/second):          0
* * * * * * * * * * * * * * * * * * * * * * * * * * * * * * * * * * * * *
Field name: DZ   Num. of fields this rec.:          2
Scale factor:        100
Range to first gate (km):          0
Sample volume spacing(m):        200
Gatespace in X-direction:        200
Number of sample volumes:        511
**************************************************************************
```

Capt J. J. Baer, "Patient Education Brochures" (93-005D), Pacific University

Maj S. F. Barrett, "Digital Tracking and Control of Retinal Images" (93-010D), University of Texas

Maj R. C. Burk, "Full of Partial Multicommodity Cuts" (93-013D), University of North Carolina

Capt W. L. Craine, "Fuzzy Hypergraphs and Fuzzy Intersection Graphs" (93-018D), University of Idaho

Maj, D W. Cribb, "Stability Properties of Inclusive Connectivity for Graphs" (93-029D), Clemson University

Maj K. W. Currie, "An Empirical Study of Logistics Org Electrical Linkage and Performance" (93-026D), Texas A& M University

Capt R. E. Dueber, "Study of Uranium Oxide Insertion Compounds" (93-009D), Oxford University

Maj G. Elder, "Multi-Agent Coordination and Cooperation in a Distributed Dynamic Environment with Limited Resources Simulated Air Wars" (93-025D), Arizona State University

Maj J. M. Fernard, "Discrete Sliding Mode Control for Nonlinear Sampled Data System" (93-008D), University of Kansas

Capt J. M. Galbraith, "Interfacial Shear Behavior and Its Influence on Fiber Damage in Sapphire-Reinforced Gamma Titamium Aluminide Composites" (93-001D), Pennsylvania State University

Lt Col D. C. Herge, "Effects of Inspection Error on Optimal Inspection Policies and Software Fault Detection Models" (93-002D), Flordia State University

Capt J. A. Jacobson, "State Space Partitioning Methods for Solving a Class of Stochastic Network Problems" (93-006D), Georgia Institute of Technology

Capt B. L. Jones, "A Guidance and Navigation System for Two Spacecraft Rendezvous in Translunar Halo Orbit" (93-011D), University of Texas

Maj J. Lanicci, "A Synoptic Climatology of the Elevated Mixed Layer Inversion Over the Southern Great Plains in Spring" (93-016D), Pennsylvania State Univeristy

Capt L. J. Lehmkuhl, "A Polynomial Primae- Dval Interior Point Method for Convex Programming with Quadratic Contraints" (93-015D), George Washington University

Capt J. A. Lott, "Visible Vertical Cavity Surface Emetting Lasers" (93-023D), University of New Mexico

Capt J. L. Moler, "Synthesis, Reactivity, and Characterization of (*-Hexacarbocyclic) Manganese Dicarbonyl Complexes with Sulfur and Phosphorus Ligands" (93-012D), University of Iowa

Maj T. N. Mouch, "Computational Aerodynamics with Icing Effects" (93-007D), University of Kansas

Maj R. Nici, "Ultronic Wave Propagation Model for Mandestructive Evaluation of Solid Rocket Motor Propellant" (93-017D), University of Colorado

Maj T. L. Pohlen, "The Effect of Activity-Based Costing on Logistics Management" (93-019D), Ohio State University

Capt J. L. Putnam, "The Influence of Multiple Host Contacts on the Acquisition and Transmission of Dengue-2 Virus" (93-027D), University of Maryland

Capt T. J. Ravine, "*Legionella pneumophila*: *Virulent and Avirulent Interactions with Acanthamocba Castellanii*" (93-021D), Virginia Commonweath University

Capt D. L. Schneider, "Reliability and Maintainability of Modular Robot Systems: A Roadmap for Design" (93-004D), University of Texas

Maj T. Y. Schutz, "Evaluation of Monitoring Audiometry in the United States Air Force Hearing Conservation Program" (93-024D), Ohio State University

Maj M. Smith, "Reductive Dechlorination of Chlorophenols by Vitamin B12" (93-022D), Oregon State University

Capt G. M. Waltensperger, "Choice Bi-Manual Aiming with Unequal Indices of Difficulty" (93-003D), University of Oklahoma

Capt G. E. Yale, "Cooperative Control of Multiple Space Manipulators" (93-020D), Naval Postgraduate School

Maj D. M. Anderson, "Functional Properties of Nonhuman Primate Antibody to Porphyromonas Gingivals" (93-029), University of Texas

1st Lt J. J. Armentrout, "An Investigation of Stereopsis with AN/AVS-6 Night Vision Goggles at Varying Levels of Illuminance and Contrast" (93-160), Virginia Polytechnical Institute and State University

1st Lt C. L. Arnold, "Numerical Solution of a Second Order Boundary Problem for Two Dimensions Using Galerkin Approximations" (93-058), University of Central Florida

2nd Lt S. Barrows, "Air Force Pilot Retention: An Economic Analysis" (93-126), Pennsylvania State University

Capt L. C. Battle, "Regulation of Medical Waste in The United States" (93-144), George Washington University

Capt D. B. Bates, "Evaluation of Needlestick Prevention Devices" (93-055), University of Maryland

2nd Lt S. A. Baune, "Determination of Pressure Response Times for Gaseous Flow in a Tube" (93-170), Joint Institute Adv of Flight Sciences

1st Lt S. S. Brandt, "Search for Lunar Water Ice in Cometary Impact Craters" (93-138), University of Texas

Capt W. Brogan, Jr., "Pneumatically-Powered Orthosis and Electronic Control System for Stroke Patient Rehabilitation" (93-002), University of California

Maj A. L. Burman, "Marine Oil Spills: Prevention Methods & Enforcement Tools" (93-172), George Washington University

Capt W. B. Cade, "A Correlative Comparison of Geomagnetic Storms and Auroral Substorms Using Geomagnetic" (93-116), Utah State University

Capt B. Campbell, "Member's Perception of Service Quality at the Nellis Air Force Base Officers Open Mess" (93-100), University of Nevada

Capt W. Castillo, Analysis of Road Pricing Metering and the Priority Treatment of High Occupacy Vehicles Using System Dynamics" (93-009), Virginia Polytechnic Institute and State University

1st Lt R. C. Cecil, "Crowding Out in an Intergrated World Capitol Market" (93-047), Florida State University

Capt G. Chesley, "Decontamination Performance of Selected in Situ Technologies for Jet Fuel Contamination" (93-161), University of Iowa

2nd Lt M. K. Ciero, "Design of a Fluid Elastic Actuator with Application to Structural Control" (93-073), Massachusetts Institute of Technology

2nd Lt C. Clark, "Caring Practices of Clinical CRNA Instructors in Clinical Student Instruction" (93-159), Mercy College of Detroit

1st Lt D. S. Clark, "The Use of the Air Force Academy High Wind Alert System in Forecasting Moderate Intensity Wind Events for Military Bases in the Colorado Springs Area" (93-017), Pennsylvania State University

1st Lt J. M. Clark, "Flight Test Techniques for Aircraft Parameter Estimation" (93-145), Texas A&M University

Maj P. C. Clark, "Energy From the Sun-Evolution of Federal Support for Solar Energy" (93-030) George Washington University

Capt R. J. Clasen, "System Performance Modeling and Analysis of a Fault-Tolerant Real-Time Parallel Processor" (93-112), Northeastern University

Capt J. S. Cloutier, " The Effects of the Air Cast Sports Stirrup on Postural Sway in Normal Males" (93-036), University of Pittsburgh

Lt Col J. C. Collings, "Nursing Case Management: Adapting to the Challenges of Today's Healthcare Environment" (93-062), University of Maryland

Maj J. L. Conrad, "Buying "Green" Implemenation of Environment-Sound Purchasing Requirement In Department of Defense Procurements" (93-130), George Washington University

2nd Lt W. Cook, "A Teaching Tool for Linear Programming" (93-134), Texas A&M University

Capt J. C. Cornick, "A Comparison of Ceiling and Visibility Observations for NWS Manned Observation Sites and Asos Sites" (93-022), Colorado State University

Capt J. H. Davis, "Lunar Gravitational Field Estimation and the Effects of Mismodeling Upon Lunar Satellite Orbit Prediction" (93-171), Massachusetts Institute of Technology

Capt J. L. Davis, "Validation of the Thermospheric Vector Spherical Harmonic (VSH) Computer Model" (93-067), Arizona State Universtiy

Capt D. J. Della-Rose, "A Derivation of the Topside Heat Flux Using Incoherent Scatter Radar Observations" (93-124), Utah State University

1st Lt A. D Dembosky, "Meeting the Enduring Challenge: Unitied States Air Force Basic Doctrine Through 1992" (93-071), North Carolina State University

Lt Col H. S. Dickerson, "Recovery Following Orthoganic Surgery" (93-025), University of North Carolina

Capt G. M. Dunnavan, "Operations Plan for the Tropical Cyclone motion (TCM-92) Mini-Field Experiement" (93-007), Naval Postgraduate School

Capt B. I. Edwards II, "Prototype Terminal Aerodrome Forecast Using Mesoscale Model" (93-156), Colorado State Univerisity

Capt D. L. Echanis, "Parenting Attitudes of Expectant Couples Associated with the Air Force" (93-068), Indiana University School

Capt D. Ehrhard, "Application of Fourier - Based Features for Classification of Synthetic Aperture Radar Imagery" (93-108), Rochester Institute of Technology

1st Lt S. D. Eiken, "The Analysis of Low Profile, Broadband, Monopole, Vehicle Antennas and Matching Network Syrthesis" (93-051), University of Illinois

1st Lt M .D. Eliason, "Digital Fax's Role as an Automatic Call Distribution System, and Impact of Job Satisfaction" (93-101), Wright State University

Capt R. L. Elsberry, "Operations Plan for the Tropical Cyclone Motion (TCM-92) Mini-Field Experiement" (93-007), Naval Postgraduate School

1st Lt S. M. Farrell, "Organizational Cultures and Values as they Impact on Job Satisfaction and Organizational Commitment" (93-103), Wright State University

1st Lt J. Fancher, "A Blind Eye: The Consideration for Terrain and Environment in Air Force Doctrine" (93-043), Suny Stoneybrook

Capt M. S. Fincher, " Gender-Role Orientation of Female Cadets at the United States Air Force Academy" (93-075), Auburn University

1st Lt C. J. Finley, "Application of a Neptune Propulsion Concept to a Manned Mars Excursion" (93-111), Ohio State University

Capt S. Fiorino, "On the Origins of Low-Level Tornadic Circulations Within the Remnants of Hurricane Andrews" (93-148), Ohio State University

Capt R. P. Fleishauer, "Validation and Analysis of Microwave-Derived Rainfall Over the Tropics" (93-020), Saint Louis University

2nd Lt D. J. Fonte, "Implementing a 50x50 Gravity Field Model in an Orbit Determination System" (93-089), Massachusetts Institute of Technology

Capt K. Forman, "The Standardized Precipitation Index and its Use in the Western Contiguous United States" (93-097), Colorado State University

Maj G. L. Fronimos, "Responsibility Determinations of Department of Defense Enviorment Clean Up Contractors: Caveat Vendori" (93-105), George Washington University

Capt R. Gaslin, "A Study of the Career Paths of Female General Managers" (93-107), Purdue University

Capt A. M. Glaves, "Accuracy of the Peak TM Two and Three-Dimensional Videography Analysis for a Rearfoot Model" (93-061), University of North Carolina

Maj C. R. Glosson, "The Effects of NI-TI Hand Files, NI- TI Engine Files, and K-Flex Files on Root Canal Morphology" (93-031) University of Texas

Capt A. C. Gnann, "A Study of the Geographic Origin, Education, and Experience of Hotel General Managers" (93-045), Purdue University

Capt T. Guiden, "Defending America's Cambodian Incursion" (93-169), University of Virginia

2nd Lt C. M. Gyves, "An English Translation of General QI Jiguang's "Quanjing Jieyao Pian" (Chapter on the fist Canon & the Essentials of Nimbleness) From the Jixiao Xinshu (New Treatsie on Disciplined Service)" (93-082), University of Arizona

1St Lt W. P. Hallman, "Limitations to the Establishment of an Arms Supplier Regime" (93-131), Ohio State University

Maj R. H. Haller, " The Effect of NITI Hand and Rotary Canal Master "U" and K-Flex Instrumentation of Root Canal Morphology" (93-034), University of Texas

Capt M. J. Henneke, "Evaluation of Hybrid Reinforcement (Fiber-Reinforced-Plastic Rod with Steel Core)" (93-114), Pennsylvania State University

Capt M. M. Higgins, "Attitudes, Power, and Ability of Care Among U.S. Air Force Mental Health Nurses: A Descriptive Study" (93-035), University of Texas

Capt C. K. Hilsher, " Ventricular Assist Devices: Physiology Meets Technology" (93-064), University of Maryland

Capt L. K. Hogan, "Implications For Advanced Nursing Practice in the Use of Therapeutic Touch" (93-038), University of Maryland

Capt W. J. Holmes, "The Evolution of the Trust: A Creative Solution of Trustee Liability Under Cercla" (93-095), George Washington University

Capt B. J. Holmsted -Mark, "The Mental Health Nurse Role in the Near-Death Experience" (93-166), Southern Illoinis University

2dt Lt J. Jackson, "Experimental Evaluation of Fuzzy Logic Control of a Flexible Arm Manipulator" (93-167), University of Washington

Capt B. L. James, " Themes Presented and Source Diversity in Flite Newspaper Coverage of Operation Restore Hope" (93-081), Florida State University

Capt M. Joseph, "Computer-Human Interface Issues: Theory & Application" (93-117), Virginia Commonwealth University

Capt M. A. Kaster, "Mesoscale Precipitation Systems in Water Storms" (93-023), Saint Louis University

1st Lt K. Keever, "The Use of Music in Labor: Pain Perception" (93-004), George Washington University

Capt J. Kennedy, "Military Space Programs in the Press: An Analysis for Change" (93-057) California State University

Capt J. Kennedy, "The Effects of Postoperative Activity Tissue Oxygen Tension" (93-027), University of Washington

Capt R. J. Keppler, "A Multi-Attribute Evaluation Model for Air Force Engineering Projects" (93-059), University of Wisconsin

Maj Daniel Kirkpatrick, "Effect of Past Mentoring Experiences on Job Satisfaction of Nurses in Management Positions" (93-175), University of Texas

1st Lt Kelly Kleifges, "An Experimental Investigation of the Effects of Leading Edge Geometry on the Dynamics of Blunt Fin-Induced Shock Wave Turbulent Boundary Layer Interaction" (93-093), University of Texas

Capt J. B. Knowles, "The Influence of Forest Fire Induced Albedo Differences on the Generation of Mesoscale Circulations" (93-024), Colorado State University

Capt R.D. Krasner, "Further Development and Testing of a Second-Order Bulk Boundary Layer Model" (93-018), Colorado State University

Maj M. Kulpa, "The Relationship of Recent Tampon Use, Douching, Coitus, and Vaginal Medications to Reported Cervical Cytology Results" (93-044), University of Florida

Maj J. Larson, "Movement of the Epiglottis in Mammals" (93-133), University of Washington

Capt D. L. LaSalle, "The New Strategic Concept and NATO Crisis Management" (93-050), Tufts University

Capt W. A. Lavelle, "State Terrorism and the Death Squad: A Study of Phenomenon" (93-005), California State University

1st Lt S. E. Lavigne, "U.S. Foreign Policy Towards Latvia During the Inter-War period 1917-1941" (93-085), Arizona State University

Capt T. J. Lawrence, " Flow Instantly Tests for a Particle Bed Reactor Nuclear Thermal Rocket Fuel Element" (93-079), Massachusetts Institute of Technology

Maj B. J. Leddy, "Interpretation of Endodontic File Length Adjustment Using Radio Vision Graphy" (93-069), Indiana University

Capt F. A. Leute, "An Analysis of Simulated and Actual DMSP SSM/T-2 Brightness Temperatures" (93-016), Colorado State University

1st Lt W. A. Libby, "Neighboring Extremal Guidance for Systems with Piecewise Linear Control Using Time as the Reference Variable" (93-113), University of Texas

2nd Lt D. S. Linden, "A Modified Two-Fluid Model of Conductivity for Super conducting Surface Resistance Calculation" (93-077), Massachusetts Institute of Technology

Capt J. R. Linskens, "The Appearance of the Sun and Moon Seen Through Clouds" (93-147), Pennsylvania State University

Capt S. M. Loomans, " Flood Reconstruction in Southern Illinois Using Tree Rings" (93-015), University of Illinois

Capt M. J. Loveless, "Optimization of Satellite Coverage in Observing Cause and Effect Changes in the Inosphere, Magnetosphere, and Solar Wind" (93-118), Utah State University

Capt K. R. Lutz, "Vertical Profiles of Radar Reflectivity of Convection Cells in Tropical and Mid Latitude Mesoscale Convection Systems" (93-066), University of Michigan

Capt R. E. Ogle, "Testing a General Model on the Fear of Crime" (93-076), Florida State University

2nd Lt J. M. Olson, "Stealth Materials Technology: Part I Low Observable Technology and Background Part II: Sealth Composites and Their Applications Part III: Material Analysis Comparison and Testing Part IV: A Specific Analysis of Boron Nitride" (93-086), University of Illinois

1st Lt T. B. MacGregor, " Implications and Applications of New Communication Technologies in Air Force Public Affairs" (93-001), Wright State University

Capt L. Martin, "Fighters or Freighters U.S. Troop Carrier Aviation 1941-1945" (93-174), University of Nebraska

2nd Lt S. W. Martin, "The Evolution and Design of American Air Power After World War II: The Finletter Commission" (93-102), University of Georgia

Capt M. R. Martino, "Budget Studies of a Prefrontal Convective Rainband in Northern Taiwan Determined from Taxtex Data" (93-033), Saint Louis University

1st Lt C. Maes, "Aburated Point Spread Functions and Beam Quality for Optional System with Annular Pupils" (93-150), Pennsylvania State University

Capt R. L. Matta, "Determination of Free Available Chlorine in Dentrified Wastewater Effluent" (93-152), University of Florida

1st Lt T. B. McGregor, "Implications and Applications of New Communication Technologies in Air Force Affairs" (93-001), Florida State University

Capt P. D. McHugh, "The European Community Directive-An Alternative Environmental Impact Assessment Procedure After Massey" (93-149), George Washington University

Capt E. J. McKinley, "Operations Plan for the Tropoical Cyclone Motion (TCM-92) Mini-Field Experiement" (93-007), Naval Postgraduate School

Capt M. M. McNeil, " Von Hippel-Lindam Disease: A Rare Familiar Multi-System Disorder and the Impact of the Clinical Nurse Specialist" (93-039), University of Maryland

Capt S. N. McWhorter, "An Investigation into the Integration of Meter-Level Range and Millimeter-Level Phase Data Using a "Multimode Simulation for Optimal Filter Estimation" Software Package" (93-115), Ohio State University

Capt A. L. Miller, "Serum Levels of Two Immunological Makers the Soluble Low Affinity Receptor for ICE (SFCERII, SCD 23) and Soluble Inlerleuken 2 Receptor (SIL-2R) and their Correlation with Age, Gender and the Onset of Childhood Atopy" (93-132), University of Arizona

Capt N. S. Miller, "Remedial Investigation/Feasibility Study Analysis Asphalt Storage Area, Elmendorf AFB AK" (93-176), University of Texas

Capt B. D. Miner, "Opposing Mesocale Flows in a Broken Midlatitude Squall Line" (93-012), Colorado State University

2nd Lt A. M. Mitchell, "A Comparative Study of Analog and Digital Control Laws for the UWCSL" (93-008), University of Washington

Capt B. G. Mitchell, "Analysis of Global Radiation Budget's and Cloud Forcing Using Three Dimensional Cloud Nephanalysis Data Bases" (93-078), University of Utah

Capt N. R. Modlin, "Error Growth in Poor ECMWF Forecasts Over the Contiguous United States" (93-154), Texas A&M University

2nd Lt C. K. Moore, "Evaluation of the Zooplankton Community of Livingston Reservoir, Texas as related to Paddlefish Food Resources" (93-142), Texas A&M University

Maj D. A. Moore, "Maternal-Newborn and Surgical Nurses Perception of Professional Autonomy During the Development of Shared Governance" (93-165), Wright State University

Capt M. Murgan, "Solubilization of Pentanal by Cationic Surfactants and Binary Mixtures of Cationic Surfactants" (93-074), University of Oklahoma

Capt J. S. Murray, "Social Support for Siblings of Children with Cancer" (93-091), Boston College

Capt R. W. Nelson, "An Analysis of Changes in Threshold Limit Values Over Time" (93-041), Univeristy of North Carolina

Lt Col C. L. Nilsson, "Defense Contractor Recovery of Clean-up Costs at Contractor Owned and Operated Facilities" (93-139), George Washington University

2nd Lt S. R. Nowlin, "Correlation of Incoming Boundary Layer Pilot Pressure Fluctuations with the Unsteadiness of Fin-Induced Shock Wave Turbulent Boundary Layer" (93-143), University of Texas

Maj R. A. Noyes, "Laser Photoionization Time-Of-Flight Mass Spectrometry of Nitrated Polycyclic Aromatic Hydrocarbons and Nitrated Heterocyclic Compound" (93-070), University of California

Capt C. H. Pappas, "Propagation Characters of Mesoscale Convection Systems" (93-021), Saint Louis University

1st Lt A. C. Parker, "Development and Validation of the University of Texas System Entry-Level Police Examination" (93-042), University of Texas

1st Lt Brett A. Pauer, "Development of a Finite Element Method Program for the Analysis of Laminated Composite Plates Using First-Order Shear Deformation Theory" (93-146), Ohio State University

2nd Lt S. D. Pederson, "A Study of Opposition Movement in East Germany: Impact of American Foreign Policy During 1953 -1989" (93-106), University of Texas

Capt T. Phillips, "In the Wake of Somalia-Humanitarian Intervention as a Role for the United States Military" (93-168), University of Colorado

2nd Lt D. Platt, "The Flames of War and the Fire of the Homefront the Thomas L. Taylor Family and Gender Relationship During the American Civil War 1861-1864" (93-125), Ohio State University

Capt M. Raffensberger, "Numerical Simulations of a Mountain Thunderstorm: A Comparison with Doppler Radar observations" (93-155), Florida State University

2nd Lt C. Rate, "Map Dimensionality and Frame of Reference for Terminal Area Navigation Display: Where do we go from here?" (93-128), University of Illinois

Capt K. J. Reinecke-Richardson, "The Adult Diabetic Patient: An Education Challenge" (93-052), University of Maryland

Capt J. R. Rider, "Rights of the Criminally Accused Under International Law" (93-153), University of New Mexico

Capt J.C. Rix, "Beyond Guzman? The future of the Shining Path in Peru" (93-006), Naval Postgraduate School

Capt P. J. Reding, "The Central American Cold Surge: An Observational Analysis of the Deep Southward Penetration of North American Cold Fronts" (93-013), Texas A&M University

Capt J. I. Rosin, " The Relationship Between Decelerations with Late Components in the Second Stage of Labor and Umbilical Cord Artery PH" (93-032), University of Cincinnati

Capt S C. Ross, "The Gendered Narrator: The Voice of the God/Mother in Harriet Beecher Stowe's Dred" (93-087), University of Arlington

Capt S. A. Rugg, "An Investigation of the Group Based High Resolution Interferometer Sounder (GB-HIS) in a Costal Marine Environment" (93-054), Naval Postgraduate School

Capt D. J. Sandercrock, "The Incidence and Duration of Breastfeeding in Active Duty Military Women" (93-026), University of Cincinnati

Capt M. Satano, "Influence of Professional Nursing Practice On Nurse Satisfaction and Retention Among Active Duty United States Air Force Nurses" (93-060), University of Arizona

Capt L. K. Schuette, "Evaluation of the USDA's Food Guide Pyramid Using College Students' Dietary Intake Data" (93-040), Michigan State University

Capt Patricia Shepherd, "The Use of Music in Labor: Pain Perception" (93-004), George Washington University

1st Lt S. P. Simcox, "Forecasting the Ducting of Electromagnetic Waves on the Mesoscale" (93-122), Pennsylvania State University

Capt P. A. Sketton, "Implication for Advance Nursing Practice in the Patient with Heat Stress" (93-065), University of Maryland

Capt B. J. Smith, "An Object-Oriented Dynamic Software Process Model" (93-092), Boston College

1st Lt R. I. Smith, "Russia and Moldova: Developing Relations Between Two Countries" (93-049), Naval Postgraduate School

Capt J. S. Sorenson, "Minimizing Air Pollution During the Construction of Air Force Facilities" (93-162), University of Texas

Capt M. S. Sorrells, "Modeling the Minimum Energy State of the Earth's Magnetotail" (93-123), Utah State University

Capt W. J. Spendley, "Mesoscale Frontogenesis: An Analysis of Two Cold Front Case Studies" (93-037), North Carolina State University

Capt R. B. Stark, "Synthetic Image Generator Model: Application of View Angle Dependent Reflectivity Components and Performance Evaluation in the Visible Region" (93-158), Rochester Institute of Technology

Capt D. A. Steele, "A Comparison of Hobbes and Locke on Natural Law and Social Contract" (93-127), University of Texas

Capt D. L. Stewart, "Spin-Up in a Rectangular Cylinder" (93-163), Pennsylvania State University

Capt K. L. Stone, "Three-Dimensional Cloud Visualization Based on Satellite Imagery" (93-141), Naval Postgraduate School

Capt E. J. Struble, " Leukocyte Deformation and Endothelial Cell Contact Mechanics During Incipient Membrane Peeling and Cell Rolling" (93-063), Pennsylvania State University

2nd Lt D. E. Suzuki, "Development and Analysis of Startup Strategies for a Particle Bed Nuclear Rocket Engine" (93-088), Massachusetts Institute of Technology

1st Lt W. K. Sylla, "The Specific Heat of Titanium Disilicide" (93-094), State University of New York

2nd Lt S. Taijeron, "The Sea Breeze Convergence Zone and it's Relationship to Fair Weather Electricity in East Central Florida" (92-121), Ohio State University

Capt T. T. Tamura, "Development of a Field Method to Measure Out-of-Flatness of Structural Steel Plates" (93-028), University of Texas

2nd Lt R. Terrell, "Soviet Nationality Policy and National Identity in the Transcaucasian Republics: Drawing Together or Tearing Apart?" (93-136), Indiana University

Maj L. E. Thomas, "The Impact of New Electronic Imaging Systems on U.S. Air Force Visual Information Professionals" (93-046) Arizona State University

Lt Col R. Tobin, "The Role of States in Clean Up of Hazardous Waste at Federal Facilities" (93-129), George Washington University

Capt M. I. Trapp, "Fear of Crime in the Military Housing Community: A Look at Two Bases in the Southeasten U.S." (93-056), Florida State University

2nd Lt S. B. Treadwell, "Estimating Task Executive Delay in a Real-Time System via Static Source Code Analysis" (93-072), Massachusetts Institute of Technology

Capt C. M. T. Tuason, "Energy Potential Analysis of Zero Velocity Curves in the Restricted Three-Body Problem" (93-090), University of Texas

Capt Z. A. Tucker, " Orographic Microburts in a Severe Winter Windstorm" (93-019), North Carolina State University

Capt R. H. Turner, "The American Response to Fear of Crime" (93-048), University of South Carolina

Capt C. M. Vadnais, "Mesopause Winds and OH Intensities at Mid-Latitudes-Fabry Perot Interferometer Observations of the OH Emission at 8430 A From Bear Lake Observatory" (93-157), Utah State University

Capt B. H. VanAartsen, "Three-Dimensional Visualization of Goes Cloud Data Using Octress" (93-119), Colorado State University

2nd Lt D. Van Brunt, "Schemata Versus Dichotomous Constructs as Organizational Sytex in Memory" (93-098), Memphis State University

Capt W. Vandergrift-Moak, "Comparison of Predicted Ground-Level Airborne Radionuclide Concentrations to Measured Values Resulting From Operations of the Los Alamos Meson Physics Facility" (93-10), Texas A&M University

Capt D. R. Vecera, "The Old., the New, the States, the Evolution of t ation of Air Toxics" (93-003), George Washington University

Capt J. Vingar, "Aerobic Treatability of Waste Effluent the Leather Finishing" (93-151), University of Florida

1st Lt R. Waltz, "Backward Chaining Versus Whole Task Training in Simulated Aircraft Landing Instruction" (93-109), Florida State University

1st Lt D.A. Ward, "Turbine Blade Tip Film Cooling Measurements" (93-011), Arizona State University

Maj M. P. Weadon, "An Empirical Study of Tropical Cloud Clusters Using Special Sensor Microwave Imager Data" (93-120), Pennsylvania State University

Capt T. A. Weisenberger, "The Continuous Hub Concept" (93-137), Arizona State University

Maj B. C. Wells, "The Grin Without the Cat Claims for Damages From Toxic Exposure Without Present Injury" (93-173), George Washington University

2d Lt D. H. West, "Spatial and Temporal Variations of Satellite Microwave Measurements of Latent Heat Release in Tropical Cyclones Due to Environmental Forcing Obtained from a Numerical Model" (93-053), Ohio State University

Capt K.R. Weyenberg, " A Fuzzy Method for Preliminary Design Random Access Memory Failure Rate Predication" (93-014), University of Missouri

Maj S. Whyte, "A Flow Visualization Study of Acoustically Enhanced Hairpin Vortices" (93-164), University of Washington

Capt S. G. Zahn, "An Investigation of Warm Cloud Microphsics Using a Multi-Component Cloud Model: Interactive Effects of the Aerosol Spectrum" (93-140), Pennsylvania State University

Por

Maj D. M. Anderson, "Functional Properties of Non human Primate Antibody to Prophyromonas Gingivals" (93-029), University of Texas

1st Lt J. J. Armentrout, "An Investigation of Stereopsis with AN/AVS-6 Night Vision Goggles at Varying Levels of Illuminance and Contrast" (93-160), Virginia ~~Poly~~ Institute and State University

1st Lt C. L. Arnold, "Numerical Solution of a Second Order Boundary Problem for Two Dimensions Using Galenkin Approximations" (93-058), University of Central Florida

Galerkin Pilot

2nd Lt S. Barrows, "Air Force Polit Retention: An Economic Analysis" (93-126), Pennsylvania State University

Capt L. C. Battle, "Regulation of Medical Waste in The United States" (93-144), George Washington University

Capt D. B. Bates, "Evaluation of Needlestick Prevention Devices" (93-055), University of Maryland

2nd Lt S. A. Baune, "Determination of Pressure Response Times for Gaseous Flow in a Tube" (93-170), Joint Institute of Flight Sciences

1st Lt S. S. Brandt, "Search for Lunar Water Ice in Cometary Impact Craters" (93-138), University of Texas

Capt W. Brogan, Jr., "Pneumatically-Powered Orthosis and Electronic Control System for Stroke Patient Rehabilitation" (93-002), University of California

Marine Enforcement

Maj A. L. Burman, Maine Oil Spills: Prevention Methods & Inforcement Tools" (93-172), George Washington University

Capt W. B. Cade, "A Correlative Comparison of Geomagnetic Storms and Auroral Substorms Using Geomagnetic" (93-116), Utah State University

Capt B. Campbell, "Member's Perception of Service Quality at the Nellis Air Force Base Officers Open Mess" (93-100), University of ~~Nebraska~~ Nevada

1st Lt R. C. Cecil, "Crowding Out in an Intergrated World Capitol Market" (93-047), Florida State University

Capt G. Chesley, "Decontamination Performance of Selected in Situ Technologies for Jet Fuel Contamination" (93-161), University of Iowa

2nd Lt M. K. Ciero, "Design of a Fluid Elastic Actuator with Application to Structural Control" (93-073), Massachusetts Institute of Technology

2nd Lt C Clark, "Caring Practices of Clinical CRNA Intructors in Clinical Student Instruction" (93-158), University of Detroit Mercy College

159

1st Lt D. S. Clark, "The Use of the Air Force Academy High Wind Alert System in Forecasting Moderate Intensity Wind Events for Military Bases in the Colorado Springs Area" (93-017), Pennsylvania State University

1st Lt J. M. Clark, "Flight Test Techniques for Aircraft Parameter Estimation" (93-145), Texas A&M University

Maj P. C. Clark, "Energy From the Sun-Evolution of Federal Support for Solar Energy" (93-030) George Washington University

Capt R. J. Clasen, "System Performance Modeling and Analysis of a Fault-Tolerant Real-Time Parallel Processor" (93-112), Northeastern University

Capt J. S. Cloutier, " The Effects of the Air Cast Sports Stirrup on Postural Sway in Normal Males" (93-036), University of ~~New England~~ Pittsburgh

Lt Col J. C. Collings, "Nursing Case Management: Adapting to the Challenges of Today's Healthcare Environment" (93-062), University of Maryland

Maj J. L. Conrad, "Buying "Green" Implemenation of Environment-Sound Purchasing Requirement In Department of Defense Procurements" (93-130), George Washington University

2nd Lt W. Cook, "A Teaching Tool for Linear Programming" (93-134), Texas A&M University

Capt J. C. Cornick, "A Comparison of Ceiling and Visibility Observations for NWS Manned Observation Sites and Asos Sites" (93-022), Colorado State University

Capt J. H. Davis, "Lunar Gravitational Field Estimation and the Effects of Mismodeling Upon Lunar Satellite Orbit Prediction" (93-171), Massachusetts Institute of Technology

Capt J. L. Davis, "Validation of the Thermospheric Vector Spherical Harmonic (VSH) Computer Model" (93-067), Arizona State Universtiy

Capt D. J. Della-Rose, "A Derivation of the Topside Heat Flux Using Incoherent Scatter Radar Observations" (93-124), Utah State University

1st Lt A. D. Dembosky, "Meeting the Enduring Challenge: Unitied States Air Force Basic Doctrine Through 1992" (93-071), ~~Massachusetts Institute of Technology~~ North Carolina State University

Lt Col H. S. Dickerson, "Recovery Following Orthoganic Surgery" (93-025), ~~North Carolina University~~ Univ of North Carolina

Capt B. I. Edwards II, "Prototype Terminal Aerodrome Forecast Using Mesoscale Model" (93-156), Colorado State Univerisity

Capt D. L. Echanis, "Parenting Attitudes of Expectant Couples Associated with the Air Force" (93-068), Indiana University School

Capt D. Ehrhard, "Application of Fourier - Based Features for Classification of Synthetic Aperture Radar Imagery" (93-108), Rochester Institute of Technology

1st Lt S. D. Eiken, "The Analysis of Low Profile, Broadband, Monopole, Vehicle Antennas and Matching Network Syrthesis" (93-051), ~~United State Air Force Academy~~ Univ of Illinois

1st Lt M .D. Eliason, "Digital Fax's Role as an Automatic Call Distribution System, and Impact of Job Satisfaction" (93-101), Wright State University

1st Lt S. M. Farrell, "Organizational Cultures and Values as they Impact on Job Satisfaction and Organizational Commitment" (93-103), Wright State University

1st Lt J. Fancher, "A Blind Eye: The Consideration for Terrain and Environment in Air Force Doctrine" (93-043), Suny Stoneybrook

Capt M. S. Fincher, " Gender-Role Orientation of Female Cadets at the United States Air Force Academy" (93-075), ~~Hubern~~ Auburn University

1st Lt C. J. Finley, "Application of a Neptune Propulsion Concept to a Manned Mars Excursion" (93-111), Ohio State University

Capt S. Fiorino, "On the Origins of ~~Loc~~ Low Tornadic-Level ~~Form~~adic Circulations Within the Remnants of Hurricane Andrews" (93-148), Ohio State University

Capt R. P. Fleishauer, "Validation and Analysis of Microwave-Derived Rainfall Over the Tropics" (93-020), Saint Louis University

2nd Lt D. J. Fonte, "Implementing a 50x50 Gravity Field Model in an Orbit Determination System" (93-089), Massachusetts Institute of Technology

Capt K. Forman, "The Standardized Precipitation Index and its Use in the Western Contiguous United States" (93-097), Colorado State University

Maj G. L. Fronimos, "Responsibility Determinations of Department of Defense Environment Clean Up Contractors: Caveat Vendori" (93-105), George Washington University

Capt R. Gaslin, "A Study of the Career Paths of Female General Managers" (93-107), Purdue University

Capt A. M. Glaves, "Accuracy of the Peak TM Two and Three-Dimensional Videography Analysis for a Rearfoot Model" (93-061), University of North Carolina

Maj C. R. Glosson, "The Effects of NI-TI Hand Files, NI- TI Engine Files, and K-Flex Files on Root Canal Morphology" (93-031) ~~Temple University~~ Univ of Texas HSC

Capt A. C. Gnann, "A Study of the Geographic Origin, Education, and Experience of Hotel General Managers" (93-045), Purdue University

Capt T. Guiden, "Defending America's Cambodian Incursion" (93-169), University of Virginia

2nd Lt C. M. Gyves, "An English Translation of General QI Jiguang's "Quanjing Jieyao Pian" (Chapter on the fist Canon & the Essentials of Nimbleness) From the Jixiao Xinshu (New Treatsie on Disciplined Service)" (93-082), University of Arizona

1St Lt W. P. Hallman, "Limitations to the Establishment of an Arms Supplier Regime" (93-131), Ohio State University

Maj R. H. Haller, " The Effect of NITI Hand and Rotary Canal Master "U" and K-Flex Instrumentation of Root Canal Morphology" (93-034), ~~University of Maryland~~ Univ of Texas

Capt M. J. Henneke, "Evaluation of Hybrid Reinforcement (Fiber-Reinforced-Plastic Rod with Steel ~~Code~~ Core)" (93-114), Pennsylvania State University

Capt M. M. Higgins, "Attitudes, Power, and Ability of Care Among U.S. Air Force Mental Health Nurses: A Descriptive Study" (93-035), University of Texas

Capt C. K. Hilsher, " Ventricular Assist Devices: Physiology Meets Technology" (93-064), University of Maryland

Capt L. K. Hogan, "Implications For Advanced Nursing Practice in the Use of Therapeutic Touch" (93-038), University of Maryland

Capt W. J. Holmes, "The Evolution of the Trust: A Creative Solution of Trustee Liability Under Cercla" (93-095), George Washington University

Capt B. J. Holmsted -Mark, "The Mental Health Nurse Role in the Near-Death Experience" (93-166), Southern Illoinis University

2dt Lt J. Jackson, "Experimental Evaluation of Fuzzy Logic Control of a Flexible Arm Manipulator" (93-167), University of Washington

Capt B. L. James, " Themes Presented and Source Diversity in Flite Newspaper Coverage of Operation Restore Hope" (93-081), Florida State University

Capt M. Joseph, "Computer-Human Interface Issues: Theory & Application" (93-117), Virginia Commonwealth University

Capt M. A. Kaster, "Mesoscale Precipitation Systems in Water Storms" (93-023), Saint Louis University

Capt J. Kennedy, "Military Space Programs in the Press: An Analysis for Change" (93-057) California State University

Capt J. Kennedy, "The Effects of Postoperative Activity Tissue Oxygen Tension" (93-027), University of Washington

Capt R. J. Keppler, "A Multi-Attribute Evaluation Model for Air Force Engineering Projects" (93-059), University of Wisconsin

Maj Daniel Kirkpatrick, "Effects of Past Mentoring Experiences on Job Satisfaction of Nurses in Management Positions" (93-175), University of Texas

1st Lt Kelly Kleifges, "An Experimental Investigation of the Effects of Leading Edge Geometry on the Dynamics of Blunt Fin-Induced Shock Wave Turbulent Boundary Layer Interaction" (93-093), University of Texas

Capt J. B. Knowles, "The Influence of Forest Fire Induced Albedo Differences on the Generation of Mesoscale Circulations" (93-024), Colorado State University

Capt R.D. Krasner, "Further Development and Testing of a Second-Order Bulk Boundary Layer Model" (93-018), Colorado State University

Maj M. Kulpa, "The Relationship of Recent Tampon Use, Douching, Coitus, and Vaginal Medications to Reported Cervical Cytology Results" (93-044), University of Florida

Maj J. Larson, "Movement of the Epiglottis in Mammals" (93-133), University of Washington

Capt D. L. LaSalle, "The New Strategic Concept and Nato Crisis Management" (93-050), Tufts University

Capt W. A. Lavelle, "State Terrorism and the Death Squad: A Study of Phenomenon" (93-005), California State University

1st Lt S. E. Lavigne, "U.S. Foreign Policy Towards Latvia During the Inter-War period 1917-1941" (93-085), Arizona State University

Capt T. J. Lawrence, " Flow Instantly Tests for A Particle Bed Reactor Nuclear Thermal Rocket Fuel Element" (93-079), Massachusetts Institute of Technology

Maj B. J. Leddy, "Interpretation of Endodontic File Length Adjustment Using Radio Vision Graphy" (93-069), ~~University of California~~ - Indiana University

Capt F. A. Leute, "An Analysis of Simulated and Actual DMSP SSM/T-2 Brightness Temperatures" (93-016), Colorado State University

1st Lt W. A. Libby, "Neighboring ~~External~~ Extremal Guidance for Systems with Piecewise Linear Control Using Time as the Reference Variable" (93-113), University of Texas

2nd Lt D. S. Linden, "A Modified Two-Fluid Model of Conductivity for Superconducting Surface Resistance Calculation" (93-077), Massachusetts Institute of Technology

Capt J. R. ~~Linskes~~ Linsley, "The Appearance of the Sun and Moon Seen Through Clouds" (93-147), Pennsylvania State University

Capt S. M. Loomans, " Flood Reconstruction in Southern Illinois Using Tree Rings" (93-015), University of Illinois

Capt M. J. Loveless, "Optimization of Satellite Coverage in Observing Cause and Effect Changes in the Inosphere, Magnetosphere, and Solar Wind" (93-118), Utah State University

Capt K. R. Lutz, "Vertical Profiles of Radar Reflectivity of Convection Cells in Tropical and Mid Latitude Mesoscale Convection Systems" (93-066), University of Michigan

Capt R. E. Ogle, "Testing a General Model on the Fear of Crime" (93-076), Florida State University

2nd Lt J. M. Olson, "Stealth Materials Technology: Part I Low Observable Technology and Background Part II: Sealth Composites and Their Applications Part III: Material Analysis Comparison and Testing ~~PAR~~ Part IV: A Specific Analysis of Boron Nitride" (93-086), University of Illinois

1st Lt T. B. MacGregor, " Implications and Applications of ~~Computer Mediated~~ New Communication Technologies in Air Force Public Affairs" (93-[redacted]), Wright State University

Capt L. Martin, "Fighters or Freighters U.S. Troop Carrier Aviation 1941-1945" (93-174), University of Nebraska

2nd Lt S. W. Martin, "The Evolution and Design of American Air Power After World War II: The Finletter Commission" (93-102), [redacted] University of Georgia

Capt M. R. Martino, "Budget Studies of a Prefrontal Convective Rainband in Northern Taiwan Determined from Taxtex Data" (93-033), Saint Louis University

1st Lt C. Maes, "Aburated Point Spread Functions and Beam Quality for Optional System with Annular Pupils" (93-150), Pennsylvania State University

Capt R. L. Matta, "Determination of Free Available Chlorine in ~~Denitrified~~ Dentrified Wastewater Effluent" (93-152), ~~University of New Mexico~~

1st Lt T. B. McGregor, "~~Implications and Applications of New Communication Technologies~~ (insert) in Air Force Affairs" (93-001), Florida State University

Capt P. D. McHugh, "The European Community Directive/An Alternative Environmental Impact Assessment Procedure/ After Massey" (93-149), George Washington University

Capt M. M. McNeil, " Von Hippel-~~Linday~~ Lindau Disease: A Rare Familiar Multi-System Disorder and the Impact of the Clinical Nurse Specialist" (93-039), University of Maryland

Capt S. N. McWhorter, "An Investigation into the ~~Interfration~~ Integration of Meter-Level Range and Millimeter-Level Phase Data Using a "Multimode Simulation for Optimal Filter Estimation" Software Package" (93-115), Ohio State University

Capt A. L. Miller, "Serum Levels of Two Immunological Makers the Soluble Low Affinity Receptor for ICE (SFCERII, SCD 23) and Soluble Inlerleuken 2 Receptor (SIL-2R) and their Correlation with Age, Gender and the Onset of Childhood Atopy" (93-132), University of Arizona

Capt N. S. Miller, "Remedial Investigation/Feasibility Study Analysis Asphalt Storage Area, Elmendorf AFB AK" (93-176), University of Texas

Capt B. D. Miner, "Opposing Mesocale Flows in a Broken Midlatitude Squall Line" (93-012), Colorado State University

Capt B. G. Mitchell, "Analysis of Global Radiation Budget's and Cloud Forcing Using Three Dimensional Cloud Nephanalysis Data Bases" (93-078), University of Utah

Capt N. R. Modlin, "Error Growth in Poor ECMWF Forecasts Over the Contiguous United States" (93-154), Texas A&M University

2nd Lt C. K. Moore, "Evaluation of the Zooplankton Community of Livingston Reservoir, Texas as related to Paddlefish Food Resources" (93-142), Texas A&M University

Maj D. A. Moore, "Maternal-Newborn and Surgical Nurses Perception of Professional Autonomy During the Development of Shared Governance" (93-165), Wright State University

Capt M. Murgan, "Solubilization of Pentanal by Cationic Surfactants and Binary Mixtures of Cationic Surfactants" (93-074), University of Oklahoma

Capt J. S. Murray, "Social Support for Siblings of Children with Cancer" (93-091), Boston College

Capt R. W. Nelson, "An Analysis of Changes in Threshold Limit Values Over Time" (93-041) ~~North Carolina State~~ University of N C

Lt Col C. L. Nilsson, "Defense Contractor Recovery of Clean-up Costs at Contractor Owned and Operated Facilities" (93-139), George Washington University

2nd Lt S. R. Nowlin, "Correlation of Incoming Boundary Layer Pilot Pressure Fluctuations with the Unsteadiness of Fin-Induced Shock Wave Turbulent Boundary Layer" (93-143), University of Texas

Maj R. A. Noyes, "Laser Photo ionization Time-Of-Flight Mass Spectrometry of Nitrated Polycyclic Aromatic Hydrocarbons and Nitrated Heterocyclic Compound" (93-070), ~~North Carolina State University~~ Univ of California

Capt C. H. Pappas, "Propagation Characters of Mesoscale Convection Systems" (93-021), Saint Louis University

1st Lt A. C. Parker, "Development and Validation of the University of Texas System Entry-Level Police Examination" (93-042), University of Texas

1st Lt Brett A. Pauer, "Development of a Finite Element Method Program for the Analysis of Laminated Composite Plates Using First-Order Shear Deformation Theory" (93-146), Ohio State University

2nd Lt S. D. Pederson, "A Study of Opposition Movement in East Germany: Impact of American Foreign Policy During 1953 -1989" (93-106), University of Texas

Capt T. Phillips, "In the Wake of Somalia-Human Harian Intervention as a Role for the United States Military" (93-168), University of Colorado

2nd Lt D. Platt, "The Flames of War and the Fire of the Homefront the Thomas L. Taylor Family and Gender Relationship During the American ~~Civil~~ War 1861-1864" (93-125), Ohio State University

Capt M. Raffensberger, "Numerical Simulations of a Mountain Thunderstorm: A Comparison with Doppler Radar observations" (93-155), Florida State University

2nd Lt C. Rate, "Map Dimensionality and Frame of Reference for Terminal Area Navigation Display: Where do we go from here?" (93-128), University of Illinois

Capt K. J. Reinecke-Richardson, "The Adult Diabetic Patient: An Education Challenge" (93-052), University of Maryland

Capt J. R. Rider, "Rights of the Criminally Accused Under International Law" (93-153),

Capt J.C. Rix, "Beyond Guzman? The future of the Shining Path in Peru" (93-006), Naval Postgraduate School

Capt P. J. Reding, "The Central American Cold Surge: An Observational Analysis of the Deep Southward Penetration of North American Cold Fronts" (93-013), Texas A&M University

Capt J. I. Rosin, " The Relationship Between Decelerations with Late Components in the Second Stage of Labor and Umbilical Cord PH" (93-032), University of Cincinnati

Capt S.C. Ross, "The Genered Narrator: The Voice of the God/Mother in Harriet Beecher Stowe's Dred" (93-087), University of Arlington

Capt S. A. Rugg, "An Investigation of the Group Based High Resolution Interferometer Sounder (GB-HIS) in a Costal Marine Environment" (93-054), Naval Postgraduate School

Capt D. J. Sandercrock, "The Incidence and Duration of Breastfeeding in Active Duty Military Women" (93-026), University of Cincinnati

Capt M. Satano, "Influence of Professional Nursing Practice On Nurse Satisfaction and Retention Among Active Duty United States Air Force Nurses" (93-060), University of Arizona

Capt L. K. Schuette, "Evaluation of the USDA's Food Guide Pyramid Using College Students' Dietary Intake Data" (93-040), Michigan State University

1st Lt S. P. Simcox, "Forecasting the Ducting of Electromagnetic Waves on the Mesoscale" (93-122), Pennsylvania State University

Capt P. A. Sketton, "Implication for Advance Nursing Practice in the Patient with Heat Stress" (93-065), University of Maryland

Capt B. J. Smith, "An Object-Oriented Dynamics Software Process Model" (93-092), Boston College

1st Lt R. I. Smith, "Russia and Moldova: Developing Relations Between Two Countries" (93-049), Naval Postgraduate School

Capt J. S. Sorenson, "Minimizing Air Pollution During the Construction of Air Force Facilities" (93-162), University of Texas

Capt M. S. Sorrells, "Modeling the Minimum Energy State of the Earth's Magnetotail" (93-123), Utah State University

Capt W. J. Spendley, "Mesoscale Frontogenesis: An Analysis of Two Cold Front Case Study" (93-037), North Carolina State University

Capt R. B. Stark, "Synthetic Image Generator Model: Application of View Angle Dependent Reflectivity Components and Performance Evaluation in the Visible Region" (93-158), Rochester Institute of Technology

Capt D. A. Steele, "A Comparison of Hobbes and Locke on Natural Law and Social Contract" (93-127), University of Texas

Capt D. L. Stewart, "Spin-Up in a Rectangular Cylinder" (93-163), Pennsylvania State University

Capt K. L. Stone, "Three-Dimensional Cloud Visualization Based on Satellite Imagery" (93-141), Naval Postgraduate School

Capt E. J. Struble, " Leukocyte Deformation and Endothelial Cell Contact Mechanics During Incipient Membrane Peeling and Cell Rolling" (93-063), Pennsylvania State University

2nd Lt D. E. Suzuki, "Development and Analysis of Startup Strategies for a Particle Bed Nuclear Rocket Engine" (93-088), Massachusetts Institute of Technology

1st Lt W. K. Sylla, "The Specific Heat of Titanium Disilicide" (93-094), State University of New York

2nd Lt S. Taijeron, "The Sea Breeze Convergence Zone and it's Relationship to Fair Weather Electricity in East Central Florida" (92-121), Ohio State University

Capt T. T. Tamura, "Development of a Field Method to Measure Out-of-Flatness of Structural Steel Plates" (93-~~029~~ 028), University of Texas

2nd Lt R. Terrell, "Soviet Nationality Policy and National Identity in the Transcaucasian Republics: Drawing Together or Tearing Apart?" (93-136), Indiana University

Maj L. E. Thomas, "The Impact of New Electronic Imaging Systems on U.S. Air Force Visual Information Professionals" (93-046) Arizona State University

Lt Col R. Tobin, "The Role of States in Clean Up of Hazardous Waste at Federal Facilities" (93-129), George Washington University

Capt M. ~~K~~ Trapp, "Fear of Crime in the Military Housing Community: A Look at Two Bases in the Southeaster U.S." (93-056), Florida State University

2nd Lt S. B. Treadwell, "Estimating Task Executive ~~Dealy~~ Delay in a Real-Time System via Static Source Code Analysis" (93-072), Massachusetts Institute of Technology

Capt C. M. T. Tuason, "Energy Potential Analysis of Zero Velocity Curves in the Restricted Three-Body Problem" (93-090), University of Texas

Capt Z. A. Tucker, " Orographic Microburts in a Severe Winter Windstorm" (93-019), North Carolina State University

Capt R. H. Turner, "The American Response to Fear of Crime" (93-048), University of South Carolina

Capt C. M. Vadnais, "Mesopause Winds and OH Intensities at ~~Nidc~~ mid Latitudes-Fabry Perot Interferometer Observations of the OH Emission at ~~9430~~ 8430 A From Bear Lake Observatory" (93-157), Utah State University

Capt B. H. VanAartsen, "Three-Dimensional Visualization of Goes Cloud Data Using Octress" (93-19), Colorado State University

2nd Lt D. Van Brunt, "Schemata Versus Dichotomous Constructs as Organizational Sytex in Memory" (93-098), Memphis State University

Capt W. Vandergrift, "Comparison of Predicted Ground-Level Airborne Radionuclide Concentrations ~~of~~ to Measured ~~Cal~~ Values Resulting From Operations of the Los Alamos Meson Physics Facility (93-10), Texas A&M Univ

Capt D. R. Vecera, "The Old., the New, the States, the ~~Education~~ Evolution of the Regulation of Air Toxics" (93-003), George Washington University

Capt J. Vingar, "Aerobic Treatability of Waste Effluent the Leather Finishing" (93-151), University of Florida

1st Lt R. Waltz, "Backward ~~Challenging~~ Chaining Versus Whole Task Training in Simulated Aircraft Landing Instruction" (93-109), Florida State University

1st Lt D A. Ward, "Turbine Blade Tip Film Cooling Measurement" (93-011), Arizona State University

Maj M. P. Weadon, "An Empirical Study of Tropical Cloud Clusters Using Special Sensor Microwave Imager Data" (93-120), Pennsylvania State University

Capt T. A. Weisenberger, "The Continuous Hub Concept" (93-137), Arizona State University

Maj B. C. Wells, "The Grin Without the Cat Claims for Damages From Toxic Exposure Without Present Injury" (93-173), George Washington University

2d Lt D. H. West, "Spatial and Temporal Variations of Satellite Microwave Measurements of Latent Heat Release in Tropical Cyclones ~~Due to~~ Environmental Forcing Obtained from a Numerical Model" (93-053), Ohio State University

Capt K.R. Weyenberg, " A Fuzzy Method for Preliminary Design Random Access Memory Failure Rate Predication" (93-014), University of Missouri

Maj S. Whyte, "A Flow Visualization Study of Acoustically Enhanced Hairpin Vortices" (93-164), University of Washington

Capt S. G. Zahn, "An Investigation of Warm Cloud Microphsics Using a Multi-Component Cloud Model: Interactive Effects of the Aerosol Spectrum" (93-140), Pennsylvania State University

Capt J. J. Baer, "Patient Education Brochures" (93-005D), Pacific University

Maj S. F. Barrett, "Digital Tracking and Control of Retinal Images" (93-010D), University of Texas

Maj R. C. Burk, "Full of Partial Multicommodity Cuts" (93-013D), University of North Carolina

Maj W. L. Craine, "Fuzzy Hypergraphs and Fuzzy Intersection Graphs" (93-018D), University of Idaho

Maj, D W. Cribb, "Stability Properties of Inclusive Connectivity for Graphs" (93-029D), Clemson University

Maj K. W. Currie, "An Empirical Study of Logistics Org Electrical Linkage and Performance" (93-026D), Texas A& M University

Capt R. E. Dueber, "Study of Uranium Oxide Insertion Compounds" (93-009D), ~~Merton College~~ Oxford University

Maj G. Elder, "Multi-Agent Coordination and Cooperation in a Distributed Dynamic Environment with Limited Resources Simulated Air Wars" (93-025D), Arizona State University

Maj J. M. Fernard, "Discrete Sliding Mode Control for Nonlinear Sampled Data System" (93-008D), University of Kansas

Capt J. M. Galbraith, "Interfacial Shear Behavior and Its Influence on Fiber Damage in Sapphire-Reinforced Gamma Titamium Aluminide Composites" (93-001D), Pennsylvania State University

Lt Col D. C. Herge, "Effects of Inspection Error on Optimal Inspection Policies and Software Fault Detective Models" (93-002D), Flordia State University

Capt J. A. Jacobson, "State Space Partitioning Methods for Solving a Class of Stochastic Network Problems" (93-006D), Georgia Institute of Technology

Maj B. L. Jones, "A Guidance and Navigation System for Two Spacecraft Rendezvous in Translunar Halo Orbit" (93-011D), University of Texas

Maj J. Lanicci, "A Synoptic Climatology of the Elevated Mixed Layar ~~in Version~~ Over the Southern Great Plains in Spring" (93-016D), Pennsylvania State Univeristy

Maj Capt L. J. Lehmkuhl, "A Polynomial Primae-Oval Interior Point Method for Convex Programming with Quadratic Contracts" (93-015D), George Washington Univ

Capt J. A. Lott, "Visible Vertical Cavity Surface Emetting Lasers" (93-023D), University of New Mexico

Capt J. L. Moler, "Synthesis, Reactivity, and Characterization of (*-Hexacarbocyclic) Manganese Dicarbonyl Complexes with Sulfur and Phosphorus Ligands" (93-012D), University of Iowa

Maj T. N. Mouch, "Computational Aerodynamics with Icing Effects" (93-007D), University of Kansas

Maj R. Nici, "Ultronic Wave Propagation Model for Mandestructive Evaluation of Solid Rocket Motor Propellant" (93-017D), University of Colorado

Maj T. L. Pohlen, "The Effect of Activity-Based Costing on Logistics Management" (93-019D), Ohio State University

Capt J. L. Putnam, "The Influence of Multiple Host Contacts on the Acquisition and Transmission of Dengue-2 Virus" (93-027D), University of Maryland

Capt T. J. Ravine, "Legionella pneumophila: Virulent and Avirulent Interactions with Acanthamocba Castellanii" (93-021D), Virginia Commonweath University

Capt D. L. Schneider, "Reliability and Maintainability of Modular Robot Systems: A Roadmap for Design" (93-004D), Univ of Texas

Maj T. Y. Schutz, "Evaluation of Monitoring Audiometry in the United States Air Force Hearing Conservation Program" (93-024D), Ohio State University ←

Maj M. Smith, "Reductive Dechlorination of Chlorophenols by Vitiam B12" (93-022D), Oregon State University. ←

Capt G. M. Waltensperger, "Choice Bi-Manual Aiming with Unequal Indices of Difficulty" (93-003D), University of Oklahoma

Capt G. E. Yale, "Cooperative Control of Multiple Space Manipulators" (93-20D), Naval Postgraduate ← Postgraduate Sch